Annika Grafschafter, Dipl.-Ing. BSc.

Simple and Effective:
The Taylor-Couette Disc Contactor for liquid-liquid extraction (Design and Performance)

DOCTORAL THESIS

to achieve the university degree of

Doktorin der technischen Wissenschaften

submitted to

Graz University of Technology

Supervisor

Univ.-Prof. Dipl.-Ing. Dr.techn. Matthäus Siebenhofer

Institute of Chemical Engineering and Environmental Technology

Graz, Juni 2019

AFFIDAVIT

I declare that I have authored this thesis independently, that I have not used other than the declared sources/resources, and that I have explicitly indicated all material which has been quoted either literally or by content from the sources used. The text document uploaded to TUGRAZonline is identical to the present doctoral thesis.

18.06.2019

Date

Signature

„Man sieht nur mit dem Herzen gut,
das Wesentliche ist für das Auge unsichtbar.“

Antoine de Saint-Exupéry

ACKNOWLEDGEMENT

I would like to thank all the people who have accompanied me on my way to the finalization of my theses and who have, not always aware, contributed their part. My deep appreciation goes to:

Matthäus Siebenhofer	for being the best doctoral father on earth, for having plenty of time for all the "sieges", for your inexhaustible knowledge in all areas of engineering and life and for challenging me over the years, by what it never got boring even though the number of my gray hairs rose up to an uncountable quantity. Most of all, I would like to thank for all the opportunities to present and defend the results of my work, all around the world. Thank you for becoming a friend of mine.
Draxler Sepp	for reviewing and assessing my PhD-thesis, as well as for taking the time to arrive to Graz.
Laboratory Team	for all the support and funny crazy time together. Special thanks goes to Georg Rudelstorfer for his relentless attitude to say: it is still possible.
Office colleges	for a great time spent on conferences and all the beer we shared together.
All Master- and Bachelor students	for the laboratory work.
My big and unique family, Especially my father	for having infinite trust in what I am doing, for supporting me with life lessons and for admiring my work.
Anatol	for tolerating my idiosyncrasies.

ABSTRACT

Liquid-liquid extraction is a leading technology in separations, raising the economic feasibility of separation processes, and is widely applied in the industry. Although plenty of different extraction devices are available on the market, equipment design and optimization is still on the research agenda since feedstocks have been changing from fossil to biogenic raw materials in the last decades. Applications in biotechnology demand simple design of robust equipment with stable operation under harsh operation conditions. The novel Taylor-Couette Disc Contactor design, a hybrid solution combining the advantages of a Rotating Disc Contactor and a Taylor-Couette Reactor in one apparatus, contrives these needs.

This thesis deals with the hydrodynamics of different design of internals, operation flexibility and performance of the novel extraction device. At the very beginning, the effect of different shaft diameters on the hydraulics of a Taylor-Couette Reactor column was examined with the aim to improve the hydraulic capacity. The hydraulic capacity could be increased by reducing the shaft diameter, which led to higher axial dispersion and lower residence time of the dispersed phase, though. For this reason, rotor discs where fixed along the shaft. An increase of the rotor disc diameter led to lower axial dispersion, higher holdup values and residence time of the dispersed phase. With these experiments, the optimum shaft and rotor diameter for the Taylor-Couette Disc Contactor, already suggested by CFD simulations [1], was confirmed. To acquire design rules for the Taylor-Couette Disc Contactor, the effect of hydraulic load, rotational speed and liquid phase ratio on residence time distribution, dispersed phase holdup and drop size distribution were investigated for 50 mm, 100 mm and 300 mm column diameter. Hydrodynamic correlations were thus developed via dimensional analysis for the binary test system kerosene/water. Analysis of the residence time distribution of the continuous phase and mass transfer experiments suggest application of the continuous stirred tank reactor cascade for reactor design. Finally, continuous multiphase flow (liquid-liquid-solid) for heterogeneous catalyzed reactions with simultaneous liquid-liquid extraction was successfully implemented in the Taylor-Couette Disc Contactor with 50 mm column diameter. The outcome of this thesis provides a simple tool for the hydrodynamic design of the Taylor-Couette Disc Contactor and shows the potential for versatile applications of the novel column.

KURZFASSUNG

Die Flüssig-Flüssig Extraktion zählt dank ihrer Wirtschaftlichkeit zu den führenden Trenntechnologien die industriell weit verbreitet Anwendung findet. Obwohl eine große Anzahl an Extraktionsapparaten am Markt angeboten werden, steht die Auslegung und Optimierung der Anlagen nach wie vor auf der Forschungsagenda, vor allem durch den zunehmenden Wechsel von fossilen hin zu biogenen Rohstoffen in den letzten Jahrzehnten. Anwendungen in der Biotechnologie fordern ein einfaches und robustes Apparatedesign, welches einen stabilen Betrieb auch bei harschen Betriebsbedingungen garantiert. Das neuartige Taylor-Couette Disc Contactor Design erfüllt diese Anforderungen in Form einer Hybridlösung, welche die Vorteile eines Rotating Disc Contactors und Taylor-Couette Reaktors in einer Extraktionskolonne miteinander vereint.

Im Rahmen dieser Dissertation wurden hydrodynamische Parameter unterschiedlicher Rührerdesigns der neuen Extraktionskolonne, sowie deren Betriebsflexibilität und Betriebsgrenzen untersucht. Zu Beginn wurde der Einfluss verschiedener Wellendurchmesser auf die Hydrodynamik eines Taylor-Couette Reaktors untersucht, mit dem Ziel dessen hydraulische Belastung zu erhöhen. Mit kleiner werdendem Wellendurchmesser konnte die hydraulische Belastung des Reaktors signifikant verbessert werden, was jedoch zu erhöhter axialer Rückvermischung und geringer Verweilzeit der dispersen Phase führte. Um die axiale Rückvermischung zu reduzieren und die Verweilzeit zu erhöhen wurden entlang der Welle zusätzlich Rotorscheiben angebracht. Größere Rotorscheibendurchmesser führten zur Verringerung der axialen Rückvermischung, Erhöhung des dispersen Holdup und zur Erhöhung der Verweilzeit der dispersen Phase. Aus diesen Experimenten konnte ein optimaler Wellen- und Rotorscheibendurchmesser für den Taylor-Couette Disc Contactor, welche bereits mittels CFD Simulation vorgeschlagen wurden, bestätigt werden. Um Designregeln zur Auslegung des Taylor-Couette Disc Contactors zu erhalten, wurde der Einfluss der hydraulischen Belastung, der Rotationsgeschwindigkeit und des Phasenverhältnisses auf die Verweilzeitverteilung, des dispersphasen Holdup und der Tropfengrößenverteilung in Kolonnen mit 50 mm, 100 mm und 300 mm Durchmesser untersucht. Mit Hilfe der Dimensionsanalyse wurden hydrodynamische Korrelationen zur Bestimmung der Tropfengrößenverteilung, des Sauterdurchmessers und des Holdup für das binäre

System Kerosin/Wasser abgeleitet. Durch die Auswertung von Verweilzeitverteilungsmessungen der kontinuierlichen Phase sowie durch Stoffaustauschexperimente konnte gezeigt werden, dass zur Modellierung des Taylor-Couette Disc Contactors eine kontinuierliche Rührkesselkaskade am besten geeignet ist. Abschließend konnte kontinuierliche Mehrphasenströmung (flüssig-flüssig-fest) zur heterogen katalysierten Veresterung bei gleichzeitiger Flüssig-Flüssig Extraktion erfolgreich in einem Taylor-Couette Disc Contactor implementiert werden. Das Ergebnis dieser Arbeit liefert einen einfachen Ansatz für die hydrodynamischen Auslegung des Taylor-Couette Disc Contactors und zeigt dessen Potenzial für die vielseitigen Anwendungsmöglichkeiten auf.

Table of Contents

Chapter 1

Introduction & Motivation

1. Introduction & Motivation

Going back in history, it can be assumed that the production of perfumes and medicines by extraction from flowers and leaves with the aid of the solvent water is one of the humankind's oldest separation technology [2]. Pioneers in this field were the Egyptians, denoted as the first true chemists. Although extraction, previously summarized under the term alchemy, was practiced during subsequent centuries, it found widespread dissemination in Europe only 500 years ago. The big breakthrough of liquid-liquid extraction came in the 20th century, when liquid-liquid extraction found its first industrial application for uranium production in the 1940s, after recognizing the power of new organic solvents. Independent of the long history of liquid-liquid extraction it is classified as new technology among separation techniques from an engineering perspective, since research on potential solvents beside water, alcohols and oils, is relatively new. [3] Nowadays, a great variety of highly selective solvents is available, enabling extraction processes to be much more effective. Apart from the challenges of choosing the best solvent for a specific separation task, engineers have ever since been investigating the performance of extraction devices, dealing with two governing questions:

"What is the ideal extraction device and how can it be designed?"

To answer the first part of the question, there is no ideal extraction device since the best-suited type of contactor solely depends on the separation task and the properties of the liquids. Understanding the hydrodynamic behavior and mass transfer of a two-phase liquid system is still far from complete, and so umpteen types of extraction devices are offered on the market with the aim to find the best performance for a given application [4]. However, all extraction devices are designed for a specific purpose, namely to show high separation performance and high hydraulic capacity, which is closely related to a high mass transfer area between the two liquid phases. High mass transfer area is provided by dispersing a liquid in a second immiscible liquid, either with or without energy input. The easiest extraction device for liquid-liquid extraction with energy input is a stirred batch tank reactor. Though industry does prefer continuous operation, as it is simpler to control automatically, tank reactors are avoided if possible [3, 5]. The simplest continuous liquid-liquid extraction unit is the mixer-settler type extractor, a

combination of a stirred tank and a settler, corresponding to an extraction efficiency of one theoretical stage. Industrial mixer-settler devices are used to obtain very high throughputs when a small number of stages are needed [6]. They provide stable and easy to control operation. For higher separation efficiency, several mixer-settlers can be connected in series to form a mixer-settler cascade [7]. However, apart from high investment cost and solvent cost, the main problem of mixer-settler batteries is the horizontal arrangement, resulting in a large area requirement for the equipment [7 - 9]. In order to avoid waste of area, mixer-settler apparatuses were designed as a tower, but the mode of operation is very complex and increases process control cost. Simple process operation and minimum space requirement can be realized with column type extraction devices, which primarily work in countercurrent operation mode to make use of the sedimentation forces by different density of the two liquids. Column type devices basically allow free choice of mass transfer direction, just depending on the decision which phase is dispersed in the second phase of an immiscible binary system [10]. In general, column type devices can be categorized into columns without energy input (static devices), pulsed columns or columns with agitated internals. Agitated columns have to be highlighted since they are very suitable for a wide range of application due to their flexible operation mode and reasonable capacity. Droplet size and thus the degree of mixing can easily be adjusted by the rotational speed of the rotating internals. For mixing liquid systems that tend towards emulsification, for highly viscous or particle-laden liquids or liquids that are sensitive to mechanical stress, the most suitable energy input can be realized with Taylor-Couette Reactors (TCR) or Rotating Disc Contactors (RDC). A TCR consists of two concentrically arranged rotating cylinders and forms banded two-phase flow due to formation of Taylor-Couette vortexes. Although the benefits of banded two-phase flow as well as the benefits of the simple design are known since many years, this extraction device could not establish in industrial scale. Because of a suggested minimum ratio of the diameter of the rotating shaft (d_{Sh}) to the diameter of the column (D) of $d_{Sh}/D > 0.75$, the hydraulic capacity of a Taylor-Couette reactor is very limited [11]. A similar flow pattern to banded two-phase flow is obtained in RDC columns, whereby the flow pattern is induced by rotor discs and stabilized by stator rings in order to increase residence time and decrease axial backmixing. The RDC design is well established in industrial scale, nevertheless the design suffers from some uncertainties regarding the optimum ratio of the shaft diameter to the column

diameter [12]. The shaft diameter is sized as small as possible because of fearing loss of active cross section area [9]. As a consequence of this design weakness the dispersed phase tends to form stable coalesced layers at the shaft since limited vortex strength cannot keep the solvent phase dispersed in the toroidal vortexes [1]. Hydrodynamic dead zones at stator rings cannot be avoided, resulting in crud accumulation and fouling. A schematic drawing of the TCR, RDC as well as several different extraction devices established in industry are shown in Fig. 1.

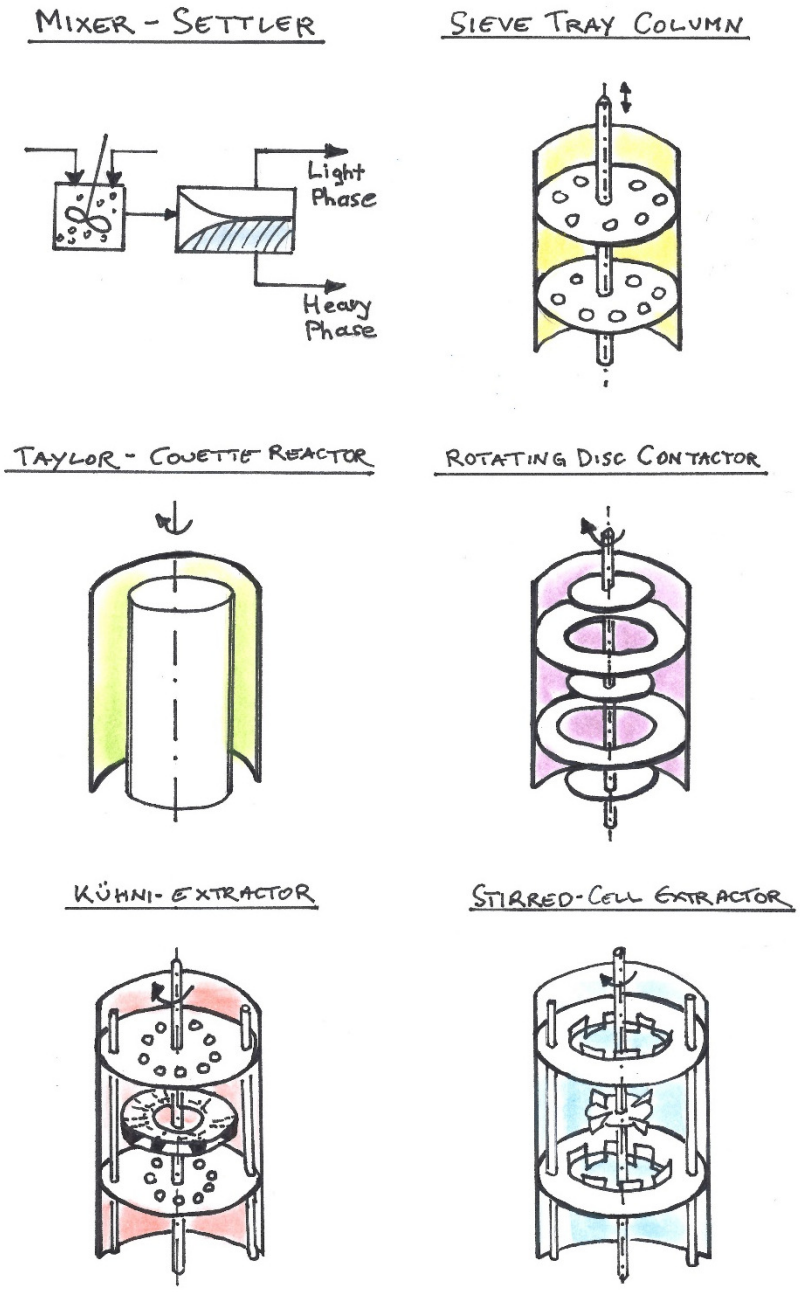

Figure 1 – Schematic drawing of different types of extraction devices (modified from [9, 13-14])

Due to the variety of different extraction equipment, the question arises whether it is necessary to spend money and time on new equipment design, or if existing devices may suffice the needed requirements of stable operation at high capacity and separation efficiency. Even though the commercial launch of new equipment can be cost- and time intensive, the answer is considered to be yes, since there are still engineering challenges waiting for appropriate solutions. For example, the complexity of internals of many devices is not attractive and may lead to problems in operation and maintenance and limit the hydraulic capacity [15]. Maintenance and investment costs increase with increasing complexity of internals. Furthermore, the global change of raw materials from fossil to biogenic raw materials has become inevitable in the last decades. The change of feedstock needs adjustment of equipment design since biogenic raw materials evidently show different properties in comparison with fossil raw materials. They can be highly viscous, suffer from bad interface properties, suffer from deficiency in chemical and thermal stability, may be sensitive to mechanical stress or contain high amount of solids. The varying quality of fermentation broth requires robust device for harsh operation conditions and flexible operation.

Based on the intention to develop a novel liquid-liquid extraction column that addresses the mentioned problems of crud accumulation and sensitivity to particle laden feed in principle, the TCR was modified and improved by reducing the diameter of the rotary shaft to allow higher hydraulic capacity. Although higher hydraulic capacity of the TCR could be achieved, the lack of reasonable residence time of the dispersed phase and high axial dispersion demanded improvement of the design. The shaft diameter d_{Sh} was fixed with 50 % of the column diameter and rotor discs were placed along the shaft in appropriate distance. The distance between the rotor discs was deduced from CFD analysis. Hydraulics were investigated for varying rotor disc diameter d_R and varying operation conditions. The investigation ended up by an optimized rotor disc diameter (d_R) and shaft diameter (d_{Sh}), which was already deduced from CFD analysis [1]. A novel two-phase extractor design, called the Taylor-Couette Disc Contactor (TCDC) was established, which in accordance to the history of design, is a hybrid solution combining the advantages of the RDC and the TCR in one apparatus, as shown in Fig. 2.

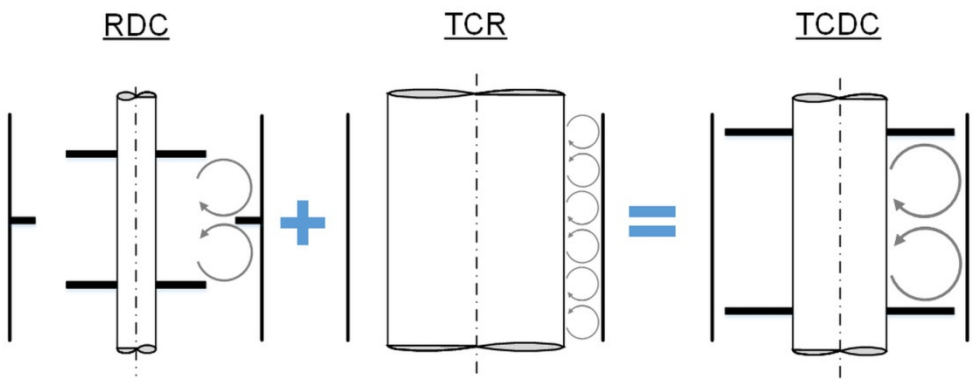

Figure 2 - TCDC design history

To consider the second question as mentioned above, engineers have been dealing with the question how extraction devices can be designed reasonably. In general, reactors with continuous feed can be designed with the ideal plug flow reactor (PFR) model or the continuous stirred tank reactor (CSTR) cascade, as shown in equation (1) and (2). Within these equations, the index A denotes the transferring component, F_A the molar flow rate and F_V the volume flow rate. V_R is the volume available for reaction (mass transfer) and A_R is the cross-section area of plug flow.

$$mass\ balance\ (CSTR):\ \ F_{A,0} = F_A - r_A * V_R + \frac{dNA}{dt}$$
$$With:\ F_{A,0} = F_V * c_{A,0} \tag{1}$$

$$mass\ balance\ (PFR):\ \ F_A = F_A + dF_A - r_A * dV_R + \frac{dNA}{dt}$$
$$With: dV_R = A_R * dH\ and\ dF_A = F_V * dc_A \tag{2}$$

The rate of reaction $-r_A$ is the change in concentration (depletion) of component A over time, as for instance is the mass transfer $\dot{n}_A$ as shown in equation (3). Mass transfer $\dot{n}_A$ between the two liquid phases can be approximated with the two-film theory, as shown in equation (4).

$$-r_A = -\frac{dc_A}{dt} = \dot{n}_A \tag{3}$$

$$\dot{n}_A = a * k_L * (c_A - c_A{}^*) \tag{4}$$

In this equation, a is the specific mass transfer area, k_L the overall liquid-phase mass transfer coefficient and (c_A-c_A*) the driving force, whereby c_A represents the actual concentration in the raffinate phase and c_A* the corresponding concentration in equilibrium. The film theory is based on the theory of linear molecular diffusion through two stagnant thin films at the interface of two liquids. Local fluid velocities caused from turbulences in the bulk phase of each fluid, approach zero at the phase interface and molecular diffusion controls mass transfer [16]. Equilibrium is expressed in terms of the Nernst distribution coefficient K for liquid-liquid equilibrium [17, 18].
However, the initial point for these calculations is given by the information about the hydrodynamic characteristics of the reactor, defined as the specific mass transfer area a. It provides information about the area available for mass transfer and has a direct effect on the rate of extraction $-r_A$. The specific mass transfer area can be calculated with the dispersed phase holdup φ and the Sauter mean diameter d_{32} as shown in equation (5). The shape of droplet is assumed to be spherical.

$$a = \frac{A_{Phase\ boundary}}{V_{Reaction}} = \frac{d_{32}^2\,\pi}{d_{32}^3\,\frac{\pi}{6}}\,\varphi = 6\,\frac{\varphi}{d_{32}} \tag{5}$$

So far, liquid-liquid extraction columns are designed using the HTU-NTU concept as derived from the ideal PFR balance, according to equation (6).

$$H_{column} = HTU * NTU = \frac{F_V}{A_R\,k_L\,a}\int_{c_{A0}}^{c_A}\frac{dc_A}{c_A - c_A{}^*} \tag{6}$$

Ideal plug flow assumes an axial flow pattern without axial dispersion. However, stirred liquid-liquid extraction columns show distinct axial backmixing, which is a big issue in column design and scale-up [7, 14]. The HTU-NTU concept is therefore extended by using the height of dispersion unit (HDU) value that considers axial backmixing of the dispersed and continuous phase, as shown in equation (7) and (8). With the dispersion model, that explains the deviation of the real flow profile from the ideal plug flow profile due to dispersion analogously to molecular diffusion, the HDU value can be calculated with the aid of the axial dispersion coefficient D_{ax}, as shown in equation (9) [14].

$$H_{column} = \overline{HTU} * NTU \tag{7}$$

$$\overline{HTU} = HTU + HDU \tag{8}$$

$$HDU = \frac{D_{ax,c}}{v_c} + \frac{D_{ax,d}}{v_d} \tag{9}$$

By measuring the residence time distribution of the dispersed phase and the continuous phase, the axial dispersion coefficient can be determined with the aid of the Bodenstein number Bo, as shown in equation (10) [14]. In this equation u is the flow velocity, L a characteristic length and D_{ax} the axial dispersion coefficient.

$$Bo_c = \frac{u_c * L}{D_{ax,c}}; \quad Bo_d = \frac{u_d * L}{D_{ax,d}} \tag{10}$$

However, radial and axial mixing, as well as the Sauter mean diameter and the dispersed phase holdup are not readily quantified. The scale-up of agitated columns is often not based on fundamentals, but based on empirical correlations [5, 19]. The separation efficiency of columns decreases with increasing column diameter because of increasing residence time distribution [7]. Experimental results of the laboratory column need to be corrected by empirical scale-up equations deduced from pilot-plant experiments to be applicable for industrial scale [6, 9]. Intensive investigation of the hydraulics of a particular column design at different operation points in laboratory and pilot scale is thus indispensable.

1.1 FRAMEWORK

For the reasons mentioned, this thesis focuses on the hydraulic investigation of TCDC design and performance. Hydrodynamics of 50 mm, 100 mm and 300 mm column diameter of the TCDC was investigated for varying rotational speed, hydraulic load and phase ratio of the liquid phases. Since the TCDC design is an improved modification of the TCR with rotor shaft diameter $d_{Sh} < 0.75*D$ to provide higher hydraulic capacity, the effect of varying shaft diameter on the hydraulics of a TCR column is summarized in Chapter 2. Although the hydraulic capacity of the TCR could be increased, low residence time of the dispersed phase and high axial backmixing led to the installation of rotor

discs along the shaft. The effect of varying rotor disc diameter on hydraulics was investigated and results are summarized in Chapter 3. This study ended up by an optimized TCDC design, which was used for all subsequent experiments. Since design rules for the TCDC were not available, the question raised whether existing empirical correlations, originally developed for RDC column design, are suitable for prediction of hydrodynamics in the TCDC column. Chapter 4 presents experimental data of the Sauter mean diameter and dispersed phase holdup, which were compared with RDC correlations. Chapter 4 also contains experimental results of mass transfer experiments compared with the basic design models PFR and CSTR cascade. In Chapter 5, empirical correlations for the prediction of the hydrodynamics of TCDC columns were developed by dimensional analysis. Dispersed phase holdup, drop size distribution as well as the residence time distribution of an up-scaled TCDC with 300 mm column diameter are summarized in Chapter 6. The results are compared with results of hydraulic analysis of a 100 mm diameter column. This chapter also shows the applicability of the empirical correlation for the prediction of the dispersed phase holdup and Sauter mean diameter as well as the effect of varying phase ratio on hydraulics. Chapter 7 is intended for publication. This chapter deals with the implementation of continuous multiphase flow (liquid-liquid-solid) in a TCDC column with 50 mm column diameter. Multiphase flow may be needed in combinations of liquid-phase catalysed reaction with product separation by liquid-liquid extraction. To proof this concept, heterogeneously catalysed esterification of acetic acid with methanol with simultaneous extraction of the product methyl acetate with biodiesel was successfully performed in batch experiments. The experiments may serve as a first example for the demonstration of industrially relevant multiphase flow applications. Continuous multiphase flow was thus implemented in the TCDC and results of the hydrodynamic investigation are presented in this chapter as well. Chapter 8 provides a summary as well as future prospects, followed by an appendix with a list of publications and supervised theses.

1.2 REFERENCES

[1] E. Aksamija, "Der Taylor-Couette Disc Contactor (TCDC); ein vereinfachtes und optimiertes Design von Drehscheibenextraktoren," Ph.D. Thesis, Graz University of Technology, 2015.

[2] M. Blass, E. Liebl, T. Häberl, "Solvent Extraction - A Historical Review," in Value adding through solvent extraction - Volume 1, 1996.

[3] P. J. D. Lloyd, "Principles of Industrial Solvent Extraction," in Solvent Extraction Principles and Practice, New York, Basel: New York: M. Dekker, 2004.

[4] S. Geoff, "Value adding through solvent extraction."

[5] V. S. Kislik, "Engineering Development of Solvent Extraction Processes," in Solvent Extraction: Classical and Novel Approaches, Elsevier, 2012, pp. 157–184.

[6] P. C. Wankat, "Liquid-Liquid Extraction," in Separation Process Engineering: Includes Mass Transfer Analysis, Third Edit., Upper Saddle River: Pearson, 2012.

[7] E. Blass, "Engineering Design and Calculation of Extractors for Liquid-Liquid Systems," in Solvent Extraction Principles and Practice, New York, Basel: New York: M. Dekker, 2004.

[8] C. Lo, C. T. Baird, M. H. I. Hanson, Handbook of Solvent Extraction. New York: John Wiley & Sons, 1983.

[9] E. Müller, R. Berger, E. Blass, D. Sluyts, and A. Pfennig, "Liquid-Liquid Extraction," in Ullmann's Encyclopedia of Industrial Chemistry, Weinheim, Germany: Wiley-VCH Verlag GmbH & Co. KGaA, 2008, pp. 250–300.

[10] A. Pfennig, T. Pillhofer, and J. Schröter, "Flüssig-Flüssig Extraktion," in Fluidverfahrenstechnik: Grundlagen, Methodik, Technik, Praxis, Wiley-VCH Verlag GmbH & Co. KGaA, 2008.

[11] C. A. Jones, "Nonlinear Taylor vortices and their stability," J. Fluid Mech., vol.

102, no. 5, pp. 249–261, 1981.

[12] W. C. G. Kosters, “Rotating-Disk Contactor,” in Handbook of Solvent Extraction, New York: Wiley: New York, 1983, pp. 391–405.

[13] P. C. Wankat, “Liquid-Liquid Extraction,” in Separation Process Engineering: Includes Mass Transfer Analysis, Third Edit., Upper Saddle River: Person, 2012.

[14] K. Sattler and H. J. Feindt, “Extraction,” in Thermal Separation Processes, Weinheim, Germany: Wiley-VCH Verlag GmbH, 1995, pp. 458–463.

[15] M. J. Slater, “On the invention of new liquid-liquid extraction columns,” in Value adding through solvent extraction - Volume 2, 1996.

[16] P. C. Wankat, “Introduction to Separation Process Engineering,” in Separation Process Engineering: Includes Mass Transfer Analysis, Upper Saddle River: Pearson, 2012.

[17] P. M. Doran, “Mass transfer,” in Bioprocess Engineering Principles, Second Edi., Elsevier, 2013, p. i.

[18] A. Pfennig, “Verfahrenstechnische Grundlagen zu Stoffaustuasch und Wärmeübertragung,” in Fluidverfahrenstechnik: Grundlagen, Methodik, Technik, Praxis, Wiley-VCH Verlag GmbH & Co. KGaA, 2008.

[19] V. S. Kislik, “Engineering Development of Solvent Extraction Processes,” in Solvent Extraction: Classical and Novel Approaches, Elsevier, 2012.

Chapter 2

Two-Phase Taylor-Couette Contactors: Holdup, Axial Dispersion and Droplet Size

SEPARATION SCIENCE AND TECHNOLOGY
https://doi.org/10.1080/01496395.2019.1595650

Taylor & Francis
Taylor & Francis Group

Two-phase Taylor–Couette contactors: Holdup, axial dispersion, and droplet size

Annika Grafschafter and Matthäus Siebenhofer

Institute of Chemical Engineering and Environmental Technology, Graz University of Technology, Graz, Austria

ABSTRACT

The simple and robust design of Taylor–Couette contactors has been attracting interests of research and industry since it was invented in the nineteenth century. Taylor–Couette contactors provide flexible operation under harsh operation conditions, as needed in liquid–liquid extraction. Nevertheless, industrial application is rather scarce, probably dating back to the historical limitation of Taylor–Couette flow being a gap phenomenon with limited hydraulic performance.

In order to improve the hydraulic performance of two-phase Taylor–Couette contactors, a research program was performed in pilot scale. Therefore, various parameters like dispersed phase holdup, residence time distribution as well as mean droplet size for varying radius ratio were related to the shaft centrifugation number.

ARTICLE HISTORY
Received 29 November 2018
Accepted 12 March 2019

KEYWORDS
Taylor–Couette; hydrodynamics; holdup; axial dispersion; droplet size

Introduction

At the end of the nineteenth century, Maurice Couette constructed the first rotational viscometer, using laminar flow between two concentrical cylinders. The flow in the gap of the cylinders is thus called Couette flow.[1] Subsequently, G. I. Taylor studied the instabilities of Couette flow when increasing the rate of rotation of the inner cylinder and he explained these instabilities theoretically and established the definition of Taylor–Couette flow patterns.[2] The pioneering work of G. I. Taylor attracted attention of many researchers due to the structured flow pattern of Taylor–Couette vortexes and their simple geometry for mathematical modeling.[3] Depending on the rate of rotation of the outer or inner cylinder, up to 74 different flow patterns have been identified so far, with several flow patterns attracting applied research in chemical process engineering.[4] Although the benefits of Taylor–Couette flow have been discussed for many decades, the industrial application is rather scarce and has just been implemented in photochemistry, precipitation reactions, metallurgy, and nuclear industry, with limitation to laboratory scale in many applications. Especially, two-phase Taylor–Couette flow has not been investigated yet in detail. To the best of our knowledge, only a few published papers are available today.[5–7] The reason for the limited application may be explained by the historical definition and probably limitation of Taylor–Couette flow being classified as gap phenomenon[8] with limited free cross-sectional area, and as a consequence limited hydraulic performance. Due to the recommended minimum radius ratio η of the inner cylinder radius R_i to the outer column cylinder radius R of $\eta > 0.75$ for achieving stable toroidal vortices, [9,10] the free cross-sectional area is limited to a fraction of less than 44% of the overall cross-sectional area, excluding any industrial scale application.

Liquid–liquid extraction is a leading technology in separations, raising the economic feasibility of separation processes, and it is widely applied in the industry. Although plenty of different extraction devices are offered on the market, either providing stagewise or continuous phase contact, equipment design and optimization is still on the research agenda. Applications in the nuclear industry and in biotechnology demand simple design of robust equipment with stable operation under harsh operation conditions. Two-phase Taylor–Couette contactors, just constructed of a rotating shaft in a cylinder, would address these needs. Although liquid–liquid extraction in Taylor–Couette contactors is not a new idea, just a few papers have been published.[3,5–7] Latest investigations cover separation of metal ions from high-level nuclear waste by liquid–liquid extraction via Taylor–Couette vortexes[11] and optimization of extraction performance of Taylor–Couette extractors by modification of the flow geometry.[12] Taylor–Couette contactors have mainly been used in laboratory scale with limited hydraulic load due to the low free cross-sectional area. To the

CONTACT Annika Grafschafter a.grafschafter@tugraz.at Institute of Chemical Engineering and Environmental Technology, Inffeldgasse 25C, Graz 8010, Austria

Color versions of one or more of the figures in the article can be found online at www.tandfonline.com/lsst.
Supplemental data for this article can be accessed here.

best of our knowledge, the effect of different radius ratios on two-phase Taylor–Couette flow has not been published so far, particularly in pilot scale. This paper reports the experimental investigation of two-phase Taylor–Couette contactors with small radius ratio of η = 0.5, 0.6, 0.7, and 0.8. Computational fluid dynamics simulations predicted formation of toroidal Taylor vortices in spiral flow without formation of hydrodynamic dead zones even for small radius ratio of η = 0.5. Consequently, the idea of increasing the hydraulic performance of Taylor–Couette contactors for two-phase operation was investigated in pilot scale by decreasing the shaft diameter. Several experiments were performed with the aim of collecting experience in operation of two-phase Taylor–Couette contactors with radius ratios $\eta \leq 0.8$, and the results were compared with two-phase Taylor–Couette contactors with radius ratios η = 0.8.

Experimental setup and measurement procedure

The effect of varying radius ratio (η) on the hydraulics of two-phase Taylor–Couette flow was investigated in terms of dispersed phase holdup (φ) measurements, residence time distribution (RTD) measurements, and mean droplet size measurements in a pilot plant with 1 m active column height and 0.1 m diameter. The experimental setup consists of two concentrically arranged cylinders. The outer column cylinder is fixed and the inner shaft cylinder is stabilized at both ends with shaft bearings. The fixed column is made of glass to enable visual control of two-phase flow. The inner shaft cylinder is made of stainless steel. To determine the effect of the radius ratio on hydrodynamics, four different shaft diameters (d_{Sh}) were investigated in this study. A schematic drawing of the column is shown in Fig. 1, and the design specifications of the shaft geometries and characteristic dimensionless design parameters are listed in Table 1. For two-phase operation, ShellSol-T was used as dispersed phase and deionized water was used as continuous phase. The setup was operated in counter current mode; therefore, the solvent phase was fed at the bottom of the column and water was fed at the top. The physical properties of the test system are summarized in Table 2. For the hydrodynamic investigation, the rate of rotation n (s^{-1}) of the shaft as well as the total hydraulic load B ($m^3\ m^{-2}h^{-1}$) of the column were varied. The phase ratio of the dispersed phase and the continuous phase was kept constant at 1 throughout all experiments. The volumetric flow rate of the continuous and dispersed phase was adjusted to ensure same total hydraulic load related to the free net cross-sectional area of the column. RTD with salt tracer was recorded in single phase as well as two-phase operation.

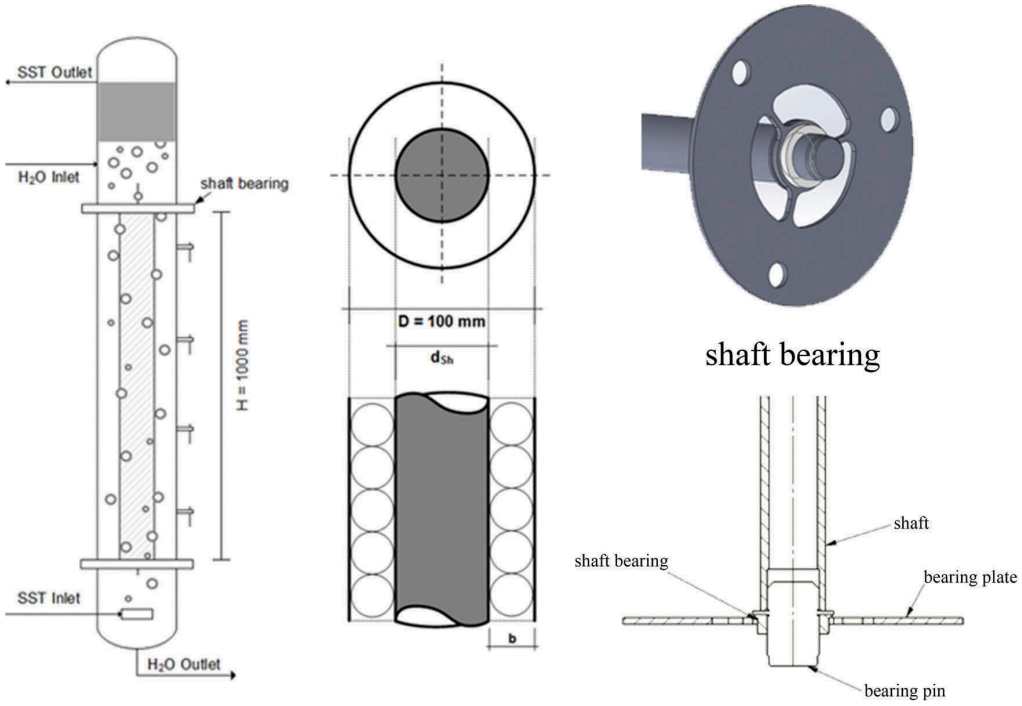

Figure 1. Schematic drawing of the Taylor–Couette contactor and a sketch of the shaft bearing.

Table 1. Design specifications of the investigated shaft geometries and dimensionless parameters.

	Abbreviation	Value	Unit
Column diameter (outer diameter)	D	100	mm
Shaft diameter (inner diameter)	d_{Sh}	50, 60, 70, and 80	mm
Active column height	H	1000	mm
Gap width	b	25, 20, 15, and 10	mm
Radius ratio/diameter ratio	$\eta = d_{Sh}/D$	0.5, 0.6, 0.7, and 0.8	-
Column aspect ratio	$\Gamma = H/b$	20, 25, 33.3, and 50	-
Gap ratio	$\zeta = b/d_{Sh}$	1, 0.67, 0.43, and 0.25	-
Number of revolutions	n	355–925	rpm
Centrifugation number	Z	5.6–24	-
Total hydraulic load	B	20, 30, and 40	$m^3\ m^{-2}h^{-1}$

Table 2. Physical properties of the liquid phases.

	Density ($kg\ m^{-3}$)	Kinematic viscosity ($m^2\ s^{-1}$)
ShellSol-T (dispersed)	756.8	1.85×10^{-6}
Deionized water (continuous)	998.1	1.102×10^{-6}

The dimensionless centrifugation number Z[13] provides comparability of energy input for different shaft diameters. The rate of rotation n for a given centrifugation number Z is calculated according to Eq. (1), based on the shaft diameter d_{Sh}, the angular velocity w, and gravity g.

$$Z = \frac{w^2 * d_{Sh}}{2 * g} = \frac{(2 * \pi * n)^2 * d_{Sh}}{2 * g} \quad (1)$$

Dispersed phase holdup

According to Eq. (2), the mean dispersed phase holdup φ is defined as the ratio of the volume of the dispersed phase V_d and the total volume consisting of the dispersed phase volume and the volume of the continuous phase V_c:

$$\varphi = \frac{V_d}{V_d + V_c} \quad (2)$$

The dispersed phase holdup was calculated with Eq. (5) according to the hydrostatic equilibrium method after reaching steady state operation. Therefore, the height of the continuous phase h_1 in a separate Y-branch, the height of the phase interphase h_2 (mixed phase), and the overall height h_3 of both liquids were measured. Via the definition of the mean density with Eq. (3)

$$\rho_{mix} = \frac{V_c * \rho_c + V_d * \rho_c}{V_c + V_d} \quad (3)$$

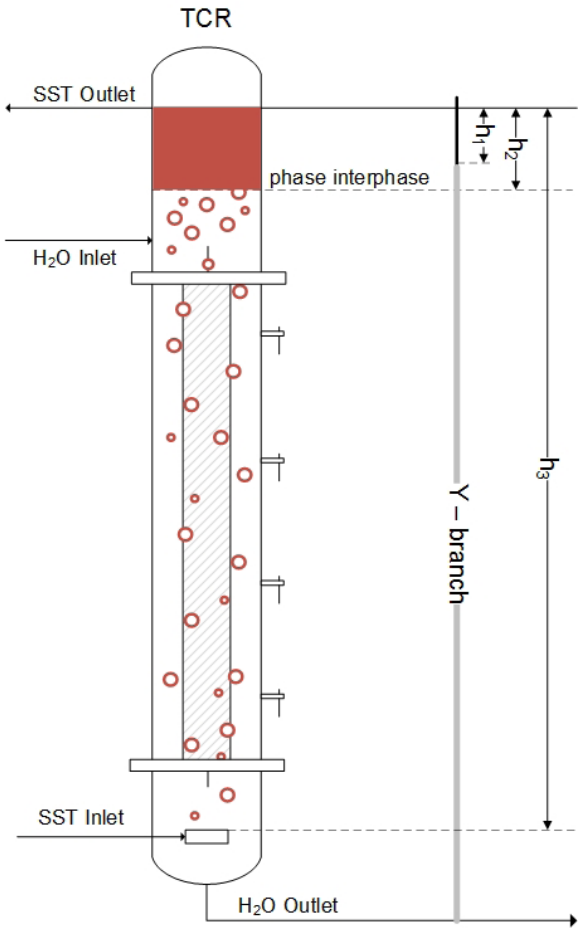

Figure 2. Schematic drawing of the TCR column with the illustrated heights $h_1 - h_3$.

and pressure equilibrium with Eq. (4)

$$(h_3 - h_1) * \rho_c = (h_3 - h_2) * \rho_{mix} + h_2 * \rho_d \quad (4)$$

a correlation between the heights $h_1 - h_3$ and the dispersed phase holdup can be defined.

$$\varphi = \frac{h_2 * \rho_d - (h_2 - h_1) * \rho_c}{(h_3 - h_2) * (\rho_d - \rho_c)} \quad (5)$$

A schematic drawing of the TCR column with the illustrated heights $h_1 - h_3$ needed for holdup measurements is shown in Fig. 2.

Residence time distribution

Via tracer experiments, the RTD was determined by spiking the aqueous feed at the top of the column with 2 ml saturated sodium chloride solution. At four positions along the active column height, the electric conductivity was recorded via non-commercial probes

with sensor tip diameters of 0.6 mm. Due to the small tip diameter, the non-commercial sensors have a minimum invasive impact on the flow pattern. The resulting RTD curves were interpreted with the dispersion model as well as the tank-in-series model. For the evaluation with the dispersion model, open–open boundary conditions were applied for large deviation from plug flow $D_{ax}/uL > 0.01$ and thus distinct backmixing according to Levenspiel:[14]

$$E_{\theta,oo} = \frac{1}{2}\sqrt{\frac{\bar{t}}{\pi\, t * \left(\frac{D_{ax}}{uL}\right)}}\ \exp\left[-\frac{\bar{t}\left(1-\frac{t}{\bar{t}}\right)^2}{4\, t * \left(\frac{D_{ax}}{uL}\right)}\right] \quad (6)$$

In Eq. (6), t represents the time, $\bar{t}$ the mean residence time, and D_{ax}/uL the vessel dispersion number with the axial dispersion coefficient D_{ax}. For comparison with the dispersion model, the corresponding number of vessels in series N was calculated from the maximum of the dimensionless exit age distribution $E_{\theta,\,\max}$ according to Levenspiel:[14]

$$E_{\theta,\max} = \frac{N*(N-1)^{N-1}}{(N-1)!} * e^{-(N-1)} \quad (7)$$

Droplet size

The droplet size was measured noninvasive with a FDR-AX700 4K HDR camcorder synchronized with a stroboscopic light source. The shutter speed of the stroboscope was adjusted to the frequency of droplet strains to freeze them for recording. Image analyzing was done via a MATLAB routine to enhance the image quality and the precision of drop size measurement. Droplet size was measured at different positions in the 10th compartment above the bottom.

Results and discussion

All experiments were performed in the turbulent flow regime with high radial Reynolds number $Re_{rad} > 2400$. High Reynolds numbers were necessary, since vorticity of the continuous phase is needed to overcome sedimentation force of the dispersed phase for appropriate holdup and residence time of the dispersed phase. Exemplarily, the two-phase flow pattern formed in the gap for radius ratios of $\eta = 0.5$, 0.6, 0.7 and 0.8 for equal total hydraulic load and centrifugation number is shown in Fig. 3. After exceeding a critical centrifugation number depending on the hydraulic load and radius ratio, the flow pattern switched from spiral two-phase flow to annular banded flow pattern with the formation of a finely dispersed holdup, called secondary holdup. The secondary holdup is a phenomenon that definitely differs from the standard holdup. At high hydraulic load and high centrifugation number, formation of the secondary holdup started at the top shaft bearing of the column to make its way down to the bottom. The column flooded when the secondary holdup reached the bottom bearing after several hours within an experiment. Thus, all experiments were performed at lower critical centrifugation numbers to avoid flooding of the column.

Dispersed phase holdup

In Fig. 4a, the effect of the radius ratio on the dispersed phase holdup for varying centrifugation number is exemplarily shown for $B = 30\ m^3\ m^{-2}h^{-1}$. Increasing centrifugation number results in exponentially increase of the holdup. With increasing radius ratio, same holdup values can be obtained at lower centrifugation numbers. As shown in Fig. 4b, the centrifugation numbers and holdup for radius ratios less than 0.8 seemingly correlate

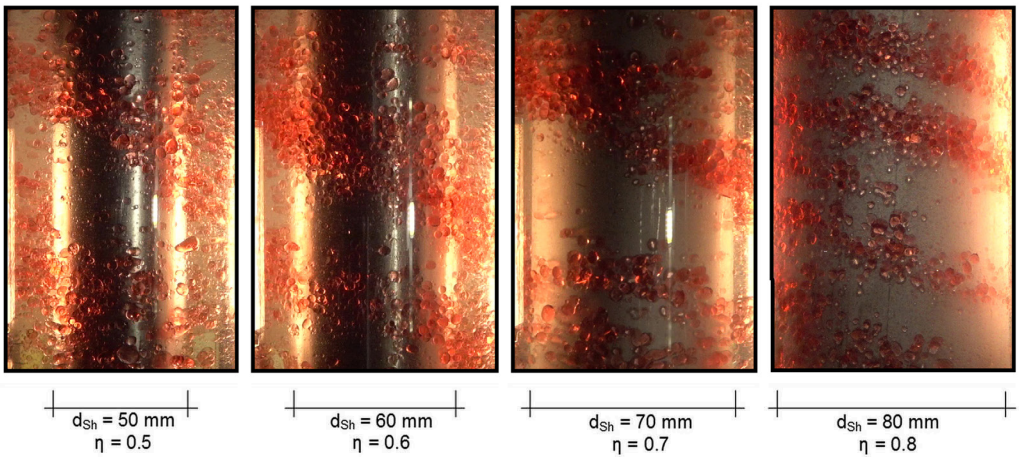

Figure 3. Spiral two-phase flow pattern at a total hydraulic load of $B = 30\ m^3\ m^{-2}h^{-1}$ and centrifugation number of $Z = 12$.

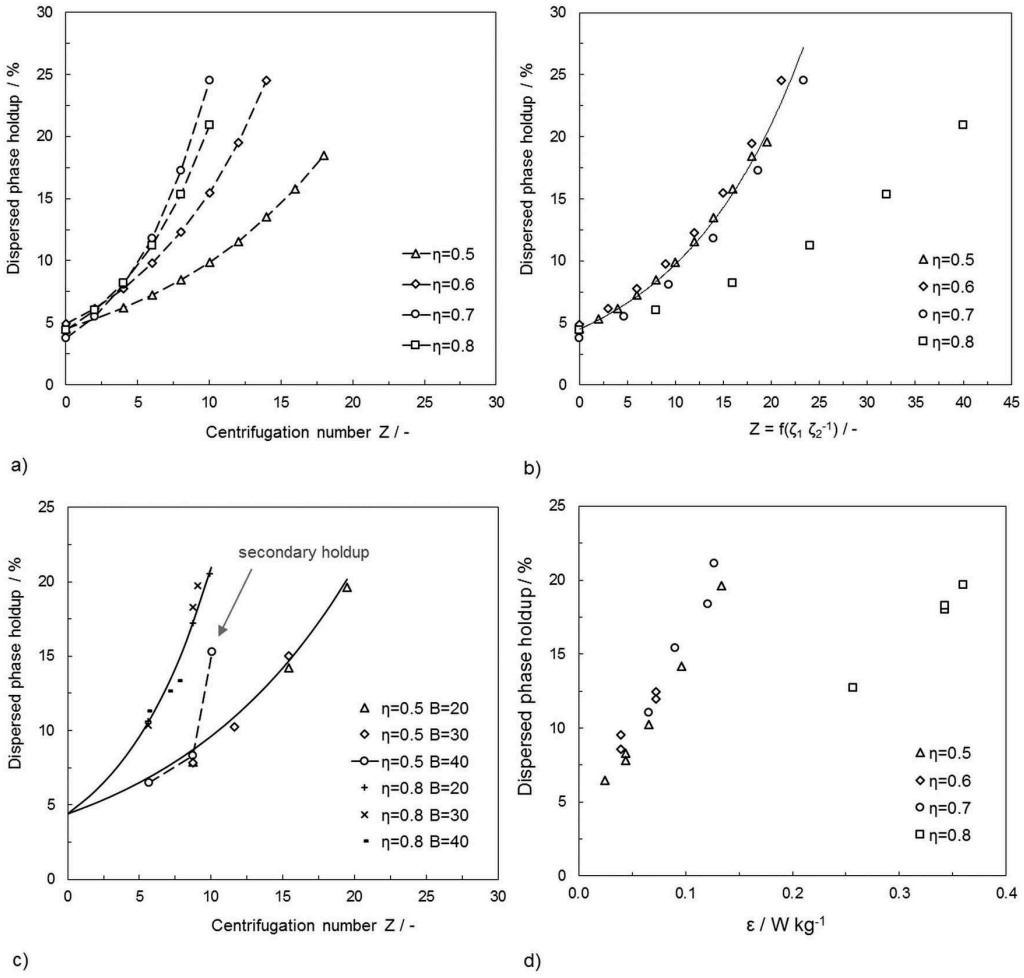

Figure 4. (a) Effect of radius ratio η = 0.5, 0.6, 0.7, and 0.8 on the dispersed phase holdup for varying centrifugation number and total hydraulic load of B = 30 m^3 m^{-2}h^{-1} (b) Dispersed phase holdup at total hydraulic load of B = 20, 30, and 40 m^3 m^{-2}h^{-1} for radius ratio η = 0.5, 0.6, 0.7, and 0.8 correlated with the centrifugation number calculated according to Eq. (8). (c) Dispersed phase holdup for varying hydraulic load B = 20, 30, and 40 m^3 m^{-2}h^{-1} and radius ratio η = 0.5 and 0.8. (d) Dispersed phase holdup for radius ratio η = 0.5, 0.6, 0.7, and 0.8 correlated with the dissipation rate ε according to Eqs. (9) and (12).

with the dimensionless gap ratio $\zeta = 2b/d_{Sh}$ according to Eq. (8), indicating similar flow pattern. Thus there is a correlation between centrifugation number and holdup at different geometries, which is shown in Eq. (8).

$$Z_2 = \frac{\zeta_1}{\zeta_2} * Z_1 = \frac{b_1}{d_{Sh,1}} * \frac{d_{Sh,2}}{b_2} * Z_1 \qquad (8)$$

Figure 4c shows the effect of the hydraulic load on the dispersed phase holdup for radius ratio η = 0.5 and 0.8. The hydraulic load has a negligible effect on holdup values. In this figure, the impact of secondary holdup, already mentioned above, on the overall holdup values is marked. Due to the fine dispersion of the secondary holdup, the overall holdup values increases rapidly, indicating flooding of the column. The effect of secondary holdup formation on the flow behavior in Taylor–Couette columns will need further investigations. Since secondary holdup formation starts on top of the rotated shaft, it is assumed that the shear in the vicinity of the top bearing is a predominant reason for droplet cleavage. Even in small-scale equipment, it will last several hours from first indication of secondary holdup formation until break down by flooding. The effect has already been reported by Takeshita.[7] Seemingly, secondary holdup formation is the outcome of a construction weakness of the top bearing that can be avoided by lower rotation rates and design improvement.

To check for comparability of flow patterns, the holdup for different radius ratios (η = 0.5, 0.6, 0.7 and

0.8) and different overall flow rates (20, 30, and 40 $m^3m^{-2}h^{-1}$) was also correlated with the dissipation rate ε. There is a linear correlation of the holdup for different flow rates and different geometries with the dissipation rate ε, which is shown in Fig. 4d. This linearity confirms same flow pattern for radius ratio of less than 0.8. The results for radius ratio $\eta = 0.8$ show a different slope. Qualitatively, the different behavior may be explained by rapid formation of banded flow for radius ratio $\eta = 0.8$, while spiral flow governs the flow pattern for radius ratio $\eta < 0.8$ over a wide operation range.

Residence time distribution

The RTD of the continuous phase was investigated for varying hydraulic load, centrifugation number, and radius ratio. Exemplarily, the dimensionless exit age distribution E_θ curves for all radius ratios at same hydraulic load and centrifugation number is shown in Fig. 5. The non-symmetrical E_θ curves indicate large deviation from plug flow, resulting in high $D_{ax,c}$ values. The axial dispersion coefficient of the continuous phase $D_{ax,c}$ is shown in Fig. 6a for varying hydraulic load and centrifugation number. At same η, higher hydraulic load results in higher $D_{ax,c}$ values. For the geometries with $\eta < 0.8$, $D_{ax,c}$ increases with increasing centrifugation number. Conversely, $\eta = 0.8$ shows a reverse behavior since the $D_{ax,c}$ values decrease with increasing centrifugation number. This effect is explained by the fact that for radius ratio $\eta \geq 0.8$ the flow regime in the gap is different due to the higher impact of friction. For $\eta \geq 0.8$, dispersed phase flow changes from spiral flow to banded two-phase flow at low centrifugation number. For $\eta < 0.8$, spiral flow governs the flow pattern. With increasing rate of rotation, the spiral pitch decreases and finally switches to banded two-phase flow as well.

As mentioned, high $D_{ax,c}$ values indicate distinct back-mixing, rather suggesting application of the tanks-in-series model. By way of comparison, the $D_{ax,c}$ values were linked with the number of corresponding vessels N, calculated with Eq. (7). In Fig. 7, the results are exemplarily shown for a radius ratio of $\eta = 0.6$. The number of corresponding vessels N correlates well with the $D_{ax,c}$. For same hydraulic load high number of vessels and less back-mixing is observed for increasing η.

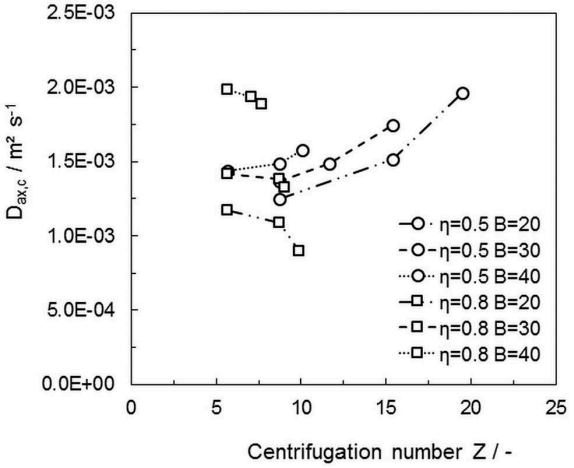

Figure 6. Effect of hydraulic load B = 20, 30, and 40 $m^3\ m^{-2}h^{-1}$, varying centrifugation number and radius ratio η = 0.5 and 0.8 on $D_{ax,c}$.

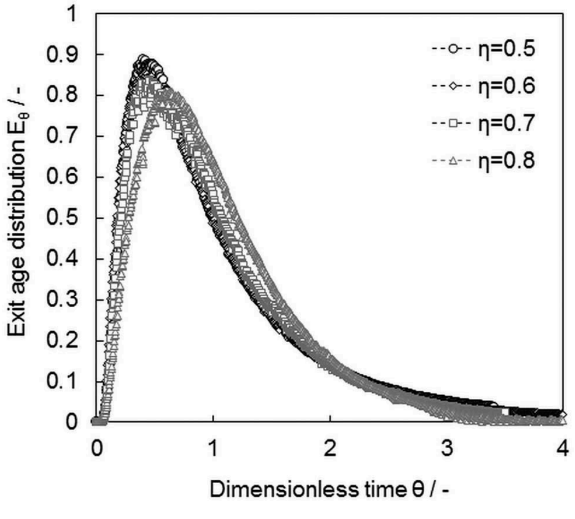

Figure 5. Dimensionless exit age distribution E_θ curves at same hydraulic load of B = 20 $m^3\ m^{-2}h^{-1}$ and centrifugation number of Z = 12 for radius ratio η = 0.5, 0.6, 0.7, and 0.8.

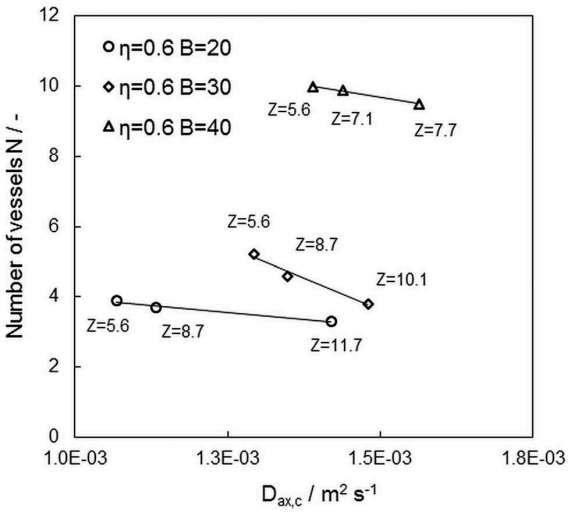

Figure 7. Comparison between $D_{ax,c}$ and the number of corresponding vessels N for η = 0.6.

Dispersed phase holdup and axial dispersion

The correlation between the dispersed phase holdup φ and the axial dispersion coefficient $D_{ax,c}$ is shown in Fig. 8 for (a) η = 0.5, 0.6, and 0.7 and for (b) η = 0.8. For radius ratio η < 0.8, $D_{ax,c}$ increases linearly with increasing holdup. The slope for all experiments is the same, the *y*-intercept decreases with lower gap ratio. Again, the device with η = 0.8 shows different behavior as the $D_{ax,c}$ decreases with increasing holdup values.

The main difference between flow patterns may definitely be deduced from visual control of experiments for both cases η < 0.8 and η > 0.8. For η < 0.8, the dispersed phase is spiraling up the column. With increasing centrifugation number the pitch of the dispersed phase spiral decreases. For η > 0.8, the flow pattern changes from spiral flow to annular banded flow even at low rate of rotation and annular banded flow stabilizes with increasing centrifugation numbers.

Dissipation rate ε and micro-mixing time

The total kinetic energy dissipated in a liquid of turbulent flow defines the energy provided for mixing. This energy, called the dissipation rate ε, can be calculated from the energy induced by the rotation of the shaft according to Eq. (9).[15] In this equation, *P* is the effective power, *T* the torque of the shaft, and *G* the dimensionless torque. Thus, the mixing performance can be determined either by measuring the torque of the inner cylinder (Eq. (10)) or by deducing the dimensionless torque G from dimensional analysis (Eqs. (11)–(13)).

$$\varepsilon = \frac{P}{\rho * V} = \frac{T * \omega}{\rho * V} = \frac{G * \nu^2 * \omega}{\pi * b * (R_a + R_i)} \quad (9)$$

$$G = \frac{T}{\rho * \nu^2 * H} \quad (10)$$

Several correlations are available for the determination of the dimensionless torque *G*, whereby all of them can be categorized into three main groups. Either the dimensionless torque *G* can be represented as a power function of the Reynolds-number,[16,17] or as two overlapping power functions of the Reynolds-number,[18,19] or by a power function in which the exponent itself is a function of the Reynolds-number.[20,21] The first approach was chosen for the evaluation of the dissipation rate. Therefore, the correlation according to Racina[15] was used for further calculations, which is given in Eq. (12).

$$G = 2.13 * \frac{\sqrt{\eta^3}}{(1-\eta)^{\frac{7}{4}}} * Re_{Sh}^{1.445} \; for \; 800 < Re_{Sh} < 10^4 \quad (11)$$

$$G = 0.113 * \frac{\sqrt{\eta^3}}{(1-\eta)^{\frac{7}{4}}} * Re_{Sh}^{1.764} \; for \; 10^4 < Re_{Sh} < 3 * 10^4 \quad (12)$$

$$Re_{Sh} = \frac{\omega * R_i * b}{\nu} \quad (13)$$

Via the ratio of the kinematic viscosity and the energy dissipation rate, the mean micro-mixing time, an important value needed *e.g.* for chemical reactions, can be calculated as well.

$$t_\mu = \sqrt{\frac{\nu}{\varepsilon}} \quad (14)$$

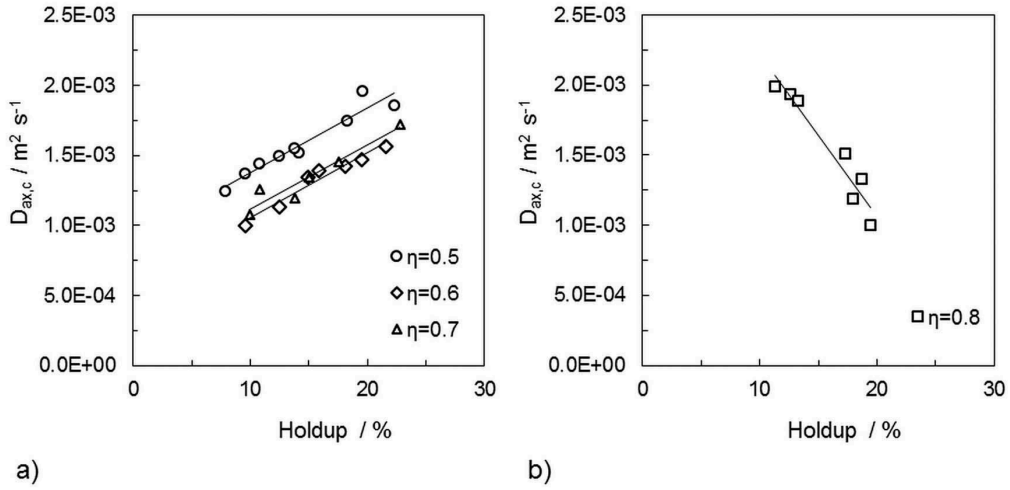

Figure 8. Correlation between $D_{ax,c}$ and η at B = 20, 30, and 40 $m^3\ m^{-2}h^{-1}$ at varying rotational speed for (a) η = 0.5, 0.6, and 0.7 and (b) η = 0.8.

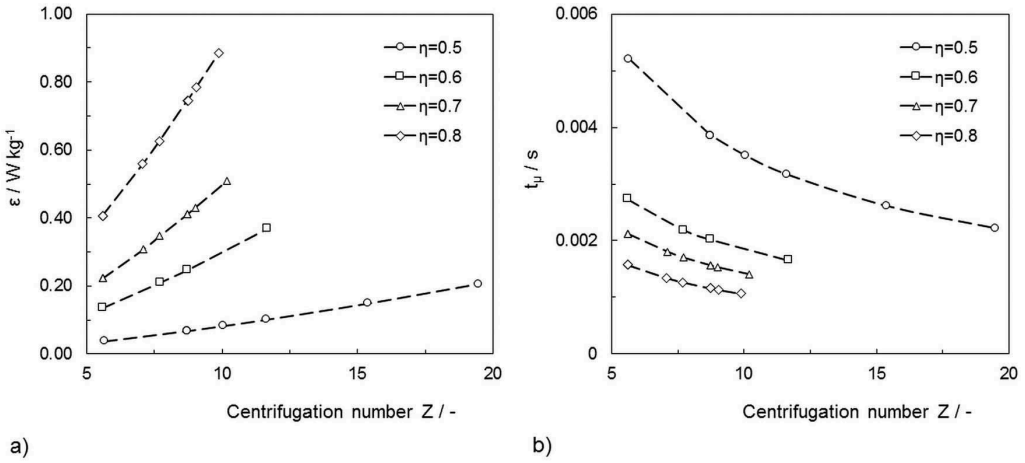

Figure 9. (a) Dissipation rate as a function of the centrifugation number for varying radius ratio and (b) micro-mixing time as a function of the centrifugation number for varying radius ratio.

The dissipation rate ε for varying radius ratio is shown in Fig. 9a and the mean micro-mixing time is shown in Fig. 9b. The dissipation rate range of the investigated setup was between 0.88 W kg^{-1} for high radius ratio η and centrifugation number and 0.04 W kg^{-1} for low radius ratio and low centrifugation number. The dissipation rate increases with increasing centrifugation number. The micro-mixing time decreases with increasing centrifugal force and increasing radius ratio and it decreases with increasing radius ratio.

Drop size

The evaluation of drop size measurements resulted in a bimodal drop size distribution for all radius ratios. For better interpretation, the mean droplet size is denoted as large mean droplet size $d_{large,m}$ for the peak of larger droplets and small mean droplet size $d_{small,m}$ for the peak of small droplets. Throughout all experiments the mean droplet size of the large droplets was within a standard deviation of ±0.2 mm and the mean droplet size of the small droplets was within a standard deviation of ±0.05 mm. The effect of varying radius ratio at a hydraulic load of $B = 20$ m^3 m^{-2}h^{-1} on the mean droplet size is depicted in Fig. 10, whereby (a) represents $d_{large,m}$ values and (b) $d_{smal,m}$ values. For both cases, the mean droplet size shifts toward smaller diameters with increasing centrifugation number. The slope of $d_{large,m}$ vs. the centrifugation number for the radius ratio of $\eta = 0.5$ is similar to the radius ratio $\eta = 0.6$. Higher radius ratios result in a steep decline of the slope. The effect of stronger decreasing slope could not be observed for small droplet

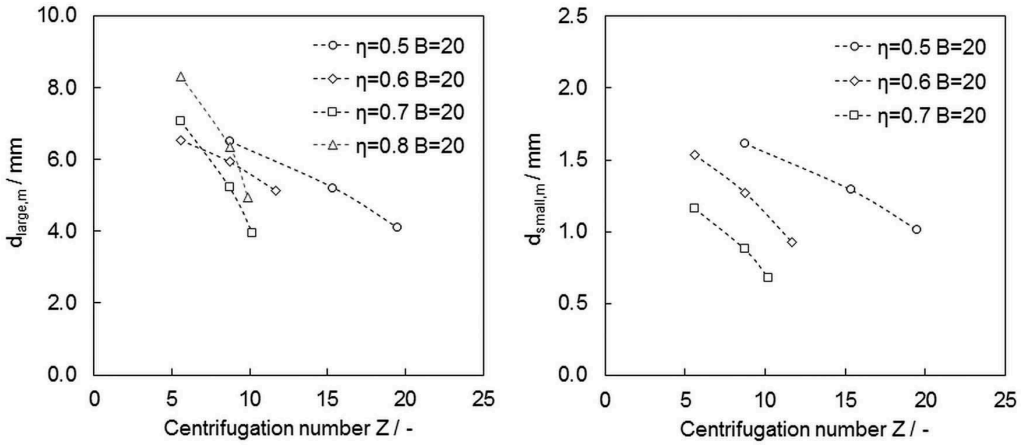

Figure 10. Effect of radius ratio η and centrifugation number on mean droplet size at $B = 20$ m^3 m^{-2}h^{-1}.

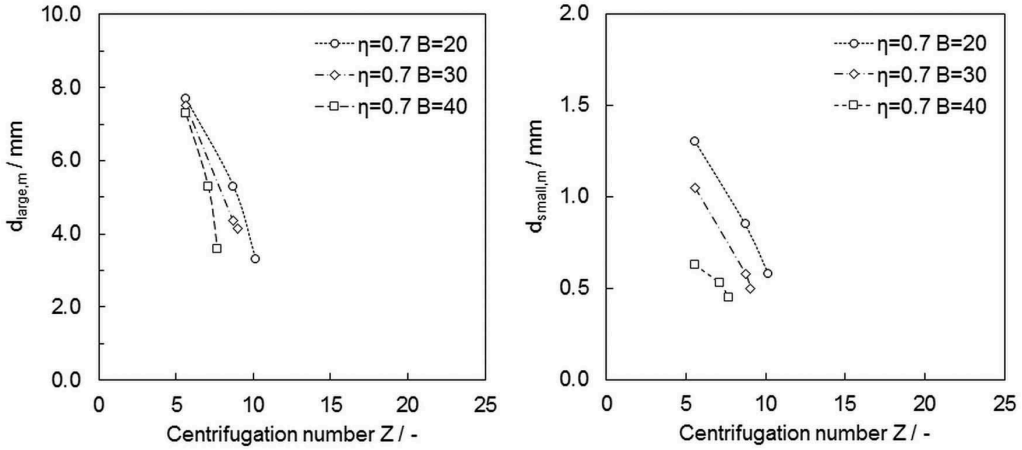

Figure 11. Effect of varying hydraulic load B = 20, 30, and 40 $m^3\ m^{-2}h^{-1}$ and centrifugation number on mean droplet size for radius ratio η = 0.7.

size $d_{small,m}$ as shown in Fig. 10b, indicating a different source of dissipation rate as already mentioned in the discussion of the secondary holdup. The evaluation of $d_{small,m}$ for the radius ratio of 0.8 was not possible, since very small droplets were not observed at low hydraulic loads and centrifugation numbers. In Fig. 11, the effect of hydraulic load on the mean droplet size is exemplarily shown for the radius ratio η = 0.7. Higher hydraulic load of the solvent phase does form smaller droplets at the single-nozzle disperser, as can be seen in Fig. 11.

Conclusion

The missing industrial application of two-phase Taylor–Couette flow contactors is assumed to be due to limitation and classification of Taylor–Couette flow as a gap phenomenon. The recommended minimum radius ratio of η = 0.75 to achieve stable toroidal vortices limits the free cross-sectional area dramatically, excluding industrial implementation due to limited economic feasibility. Nevertheless, the simple design of Taylor–Couette contactors would provide flexible operation under harsh operation conditions, as needed in two-phase flow such as liquid–liquid extraction. To overcome this bottleneck of limited hydraulic performance of Taylor–Couette contactors, the effect of small shaft diameter on two-phase operation was investigated in pilot scale. The effect of various radius ratios on the hydrodynamics of two-phase Taylor–Couette flow was investigated in detail. For hydrodynamic characterization, the dispersed phase holdup, the RTD, as well as the mean droplet size for varying hydraulic load and centrifugation number of the shaft were determined.

Dispersed phase holdup experiments show the formation of a secondary holdup after exceeding a critical centrifugation number. Several results indicate a different source of dissipation energy for secondary holdup. It is assumed that the shear of the top bearing plays an unwanted role in secondary holdup formation. Analysis of the RTD of the continuous phase indicates a very different effect of the radius ratio η = 0.8 on axial dispersion coefficient compared to small radius ratio. For η = 0.8, the axial dispersion coefficient decreases with increasing centrifugation number. The signal response of the RTD of pulse function measurements indicates distinct back-mixing and therefore suggests application of the tanks-in-series model for evaluation. The experimental data of drop size measurement depict a bimodal drop size distribution for all radius ratios.

Within this project, it was experimentally confirmed that the Taylor–Couette contactor does not need a minimum radius ratio of η > 0.75 for appropriate operation. The governing characteristics of stable operation and flexible hydraulic load as well as the positive effect of simple apparatus design on operation under harsh operation conditions have to be outlined.

Symbols used

Symbols

B[$m^3\ m^{-m}h^{-m}$]	total hydraulic load
b[m]	= R – R_i = gap width
D[m]	column diameter (outer cylinder diameter)
$D_{ax,c}$[$m^2\ s^{-1}$]	axial dispersion coefficient of continuous phase
d_m[mm]	mean droplet size
d_{Sh}[m]	shaft diameter (inner cylinder diameter)
E_θ[-]	dimensionless exit age distribution
g[$m\ s^{-2}$]	gravity (9.81)
H[m]	active column height

N[-]	number of corresponding vessels in series
n[1 s^{-1}]	rate of rotation
R[m]	column radius (outer cylinder radius)
R_i[m]	shaft radius (inner cylinder radius)
t[s]	time
$\bar{t}$[s]	mean residence time
V[m^3]	volume
w[rad s^{-1}]	angular velocity
Z[-]	$=(w^2 d_{Sh})/(2g)$ = centrifugation number

Greek symbols

ε[W kg^{-1}]	dissipation rate
η[-]	$= R_i/R$ = radius ratio
Γ[-]	= H/b = aspect ratio
ρ[kg m^{-3}]	density
ν[m^2 s^{-1}]	kinematic viscosity
φ[-]	dispersed phase holdup
θ[-]	dimensionless time ($\theta = t\ \bar{t}^{-1}$)
ζ[-]	$= b/d_{Sh}$ = gap ratio

Subscripts

c	continuous phase
d	dispersed phase

Abbreviations

CFD	computational fluid dynamics
RTD	residence time distribution
SST	ShellSol-T
TCR	Taylor–Couette reactor

References

[1] Berthelot; Pasteur; Friedel; Becquerel. (1890) *Annales de chimie et de physique*, G. Masson: Paris.

[2] Taylor, G.I. (1923) Stability of a viscous liquid contained between two rotating cylinders. *Philosophical Transactions of the Royal Society A Mathematical Physical and Engineering Sciences*, 223 (605–615): 289–343. doi:10.1098/rsta.1923.0008

[3] Baier, G.;. (1999) *Liquid-Liquid Extraction Based on a New Flow Pattern: Two-Fluid Taylor-Couette Flow*, University of Wisconsin: Madison.

[4] Aksamija, E.; Weinländer, C.; Sarzio, R.; Siebenhofer, M. (2015) The Taylor-Couette disc contactor: A novel apparatus for liquid/liquid extraction. *Separation Science and Technology*, 50 (18): 2844–2852.

[5] Nakase, M.; Rokkaku, H.; Takeshita, K. (2013) High-performance extraction operation using emulsion flow protected by surfactants in a liquid-liquid countercurrent centrifugal extractor. *Journal of Nuclear Science and Technology*, 50 (7): 723–730. doi:10.1080/00223131.2013.799399

[6] Nakase, M.; Rokkaku, H.; Takeshita, K. (2013) Relation between oil–water flow and extraction performance in liquid–liquid countercurrent centrifugal extractors with Taylor vortices. *Journal of Nuclear Science and Technology*, 50 (3): 287–295. doi:10.1080/00223131.2013.772445

[7] Takeshita, K.;. (2010) Development of liquid-liquid countercurrent centrifugal extractor with Taylor-Couette flow. *Journal of Multiphase Flow*, 24 (3): 267–274. doi:10.3811/jjmf.24.267

[8] Aksamija, E.;. (2015) *Der Taylor-Couette Disc Contactor (TCDC); ein vereinfachtes und optimiertes Design von Drehscheibenextraktoren*, Graz University of Technology.

[9] Jones, C.A.;. (1981) Non-Linear Taylor vortices and their stability. *Journal of Fluid Mechanics*, 102 (5): 249–261. doi:10.1017/S0022112081002620

[10] Jones, C.A.;. (1985) The transition to wavy Taylor vortices. *Journal of Fluid Mechanics*, 157: 135–162. doi:10.1017/S0022112085002336

[11] Nakase, M.; Matsuzawa, Y.; Takeshita, K. (2018) Continuous separation of molybdenum and zirconium from simulated high-level liquid waste with a Taylor-Couette contactor. *Journal of Nuclear Science and Technology*, 55 (11): 1317–1323. doi:10.1080/00223131.2018.1509029

[12] Nakase, M.; Matsuzawa, Y.; Takeshita, K. (2018) Modified flow geometry for higher extraction performance with a liquid-liquid centrifugal contactor with Taylor vortices. *Journal of Nuclear Science and Technology*, 55 (8): 829–837. doi:10.1080/00223131.2018.1439414

[13] Stieß, M. (2009) *Mechanische Verfahrenstechnik-Partikeltechnologie 1*, Springer-Lehrbuch.

[14] Levenspiel, O. (1999) *Chemical Reaction Engineering*, New York: Wiley.

[15] Racina, A. (2008) *Vermischung in Taylor-Couette Strömung*, Universität Karlsruhe.

[16] Wendt, F. (1933) Turbulente Strömungen zwischen zwei rotierenden koaxialen Zylindern. *Ingenieur-Archiv*, 4 (6): 577–595. doi:10.1007/BF02084936

[17] Bjorklund, W.; Kays, I.S. (1959) Heat transfer between concentric rotating cylinders. *Heat Transfer*, 81 (8): 175–186.

[18] Stuart, J.T. (1958) On the non-linear mechanics of hydrodynamic stability. *Journal of Fluid Mechanics*, 4 (1): 1. doi:10.1017/S0022112058000276

[19] Donnelly, R.J.; Simon, N.J. (1960) An empirical torque relation for supercritical flow between rotating cylinders. *Journal of Fluid Mechanics*, 7 (3): 401. doi:10.1017/S0022112060000177

[20] Lathrop, D.P.; Fineberg, J.; Swinney, H.L. (1992) Transition to shear-driven turbulence in Couette-Taylor flow. *Physical Review. A*, 46 (10): 6390–6405. doi:10.1103/PhysRevA.46.6390

[21] Lewis, G.S.; Swinney, H.L. (1999) Velocity structure functions, scaling, and transitions in high-Reynolds-number Couette-Taylor flow. *Physical Review. E*, 59 (5): 5457–5467. doi:10.1103/PhysRevE.59.5457

Chapter 3

Effect of Rotor Disc Diameter on Holdup, Axial Dispersion and Droplet Size in a Taylor-Couette Disc Contactor

3. Effect of Rotor Disc Diameter on Holdup, Axial Dispersion and Droplet Size in a Taylor-Couette Disc Contactor

Dedicated to the 65th anniversary of Prof. Hans Jörg Bart

Annika Grafschafter[1] and Matthäus Siebenhofer[1]

[1]Institute of Chemical Engineering and Environmental Technology, Graz University of Technology

Abstract

The effect of different rotor disc diameter of the Taylor-Couette Disc Contactor on the dispersed phase holdup, axial dispersion and droplet size was investigated. At constant centrifugation number the dispersed phase holdup decreases with decreasing rotor disc diameter. The initially distinct bimodal drop size distribution at small rotor disc diameter changes with increasing rotor disc diameter into monomodale distribution. It was shown that with smaller rotor disc diameter stable operation is still feasible, but higher axial backmixing has to be expected.

Keywords: Taylor-Couette Disc Contactor; dispersed phase holdup; axial dispersion, droplet size

1. Introduction

Liquid-liquid extraction is a leading mass transfer technology in separations, and it is widely applied in industry whenever feasible. Umpteen extraction devices are offered on the market, covering stagewise or continuous phase contact, nevertheless equipment design and optimization is still on the research agenda. Particularly the shift from fossil to biobased raw materials, triggered in recent years, makes adaption of existing extraction devices necessary to suffice the needs of unfavorable physical properties of

[1] This chapter was submitted to *Chemie Ingenieur Technik* on January 14th, 2019

liquors to be processed. Utilization in biotechnology demands simple design of robust equipment with stable operation under harsh operation conditions. However, the requirement of robust and simple equipment design is not limited to biotechnological applications. The nuclear industry as well as metallurgy provide harsh operation conditions, demanding robust technologies and equipment too.

In liquid-liquid extraction the Taylor-Couette Disc Contactor is highly recommended for harsh operation conditions due to the simple design of the internals. With the simple design of internals and with the feasibility of gaining a wide stable operation range, the TCDC may cover many fields of application. The TCDC design is similar to the design of the Rotating Disc Contactor (RDC), except that the TCDC is not equipped with stator rings [1]. Compared to the RDC the TCDC has an increased shaft diameter to make use of the benefits of Taylor-Couette vortexes. The hydrodynamic characteristics of the TCDC with internals constructed according to the design recommendations of Aksamija [1, 2], suggesting that the rotor disc diameter should occupy 85 - 90% of the column diameter, have been investigated in detail for 86% [3 - 5]. However, CFD analysis of different rotor to column ratio did not confirm this rigid design recommendation. In order to make the TCDC more flexible, the hydrodynamics resulting from three different rotor disc diameters where investigated in detail and compared with the rotor disc diameter recommended by Aksamija. The dispersed phase holdup, the axial dispersion of the continuous phase and the mean droplet size were thus measured and evaluated.

2. Experimental setup and measurement procedure

The effect of varying rotor disc diameter (d_R) and thus varying gap sizes (δ) on the hydrodynamic performance of Taylor-Couette Disc Contactors was investigated in terms of the dispersed phase holdup (φ), the residence time distribution (RTD) and the mean droplet size in a pilot plant with 1 m active column height and 0.1 m column diameter (D_C). A shaft diameter of $d_{Sh} = 0.5*D_C$ prevents from formation of dead zones at the shaft [2]. The rotating shaft is stabilized at both ends with friction bearings. At a distance of $H_C = d_{Sh}$ rotor discs are arranged along the shaft. The compartment height H_c ensures an optimal area utilization of the vortexes (vorticity and vortex strength) in the compartment [2]. The shaft and the rotor discs are made of stainless steel, the column

is made of glass. To determine the effect of the rotor disc diameter on hydrodynamics, three different rotor disc diameters d_R = 60 mm (dR60), d_R = 70 mm (dR70) and d_R = 80 mm (dR80) were investigated in this study and were compared with experimental data [5] of d_R = 86 mm (dR86). The schematic drawing of a single compartment of the TCDC is shown in Fig. 1, the design specifications of the rotor disc geometries and the operation conditions are listed in Tab. 1.

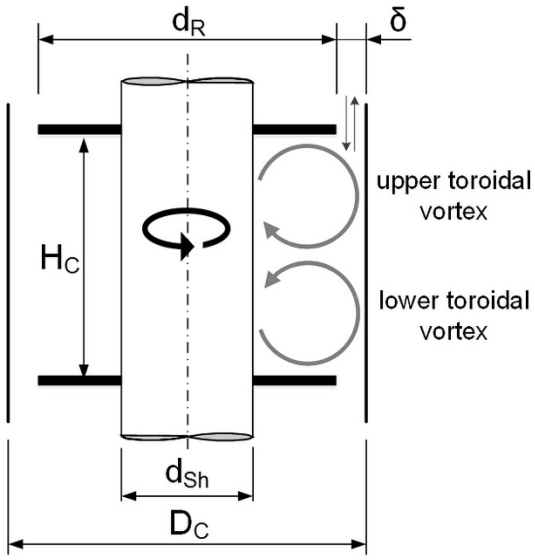

Figure 1: Schematic drawing of a single compartment of the Taylor-Couette Disc Contactor

Table 1: Design specifications of the rotor disc geometries and operation conditions

	Abbreviation	Value	Unit
Column diameter	D_C	100	mm
Shaft diameter	d_{Sh}	50	mm
Column height	H	1000	mm
Compartment height	H_c	50	mm
Rotor disc diameter	dR60, dR70, dR80 and dR86	60, 70, 80 and 86	mm
Gap width	δ	20, 15, 10 and 7	mm
Centrifugation number	Z	5.4 - 24	-
Total hydraulic load	B	20, 30, 40	$m^3\,m^{-2}h^{-1}$

For two-phase operation, ShellSol T (SST) was used as dispersed phase and deionized water was used as continuous phase. The density of ShellSol T at ambient conditions is ρ_{SST} = 756.8 kg m^{-3} and the kinematic viscosity is $\nu = 1.85*10^{-6}$ m^2 s^{-1}. At ambient operation conditions the density of deionized water is ρ_{H20} = 998.1 kg m^{-3} and the kinematic viscosity is $\nu = 1.102*10^{-6}$ m^2 s^{-1}. The setup was operated in counter current

operation mode, therefore the solvent phase was fed at the bottom of the column and water was fed at the top. For hydrodynamics investigation, the rate of rotation n (s^{-1}) of the shaft as well as the total hydraulic load B ($m^3\ m^{-2}h^{-1}$) of the column was varied. The total hydraulic load B is related to the free net cross sectional area A_{net} of the column A_C without shaft area A_{Sh} ($A_{net} = A_C - A_{Sh}$). The phase ratio of the dispersed phase and the continuous phase was kept constant at 1 throughout all experiments. The effect of different phase ratio on TCDC operation was reported in [5].

The centrifugation number Z provides comparability of energy input for the different rotor disc diameters. The rate of rotation for a given centrifugation number Z is calculated according to Eq. 1, based on the rotor disc diameter d_R, the angular velocity w and gravity g.

$$Z = \frac{w^2 * d_R}{2 * g} = \frac{(2 * \pi * n)^2 * d_R}{2 * g} \quad (1)$$

2.1 Dispersed phase holdup

The mean dispersed phase holdup was calculated with Eq. 2 according to the hydrostatic equilibrium method after reaching steady state operation. Then the height of the continuous phase h_1, the height of the interfacial area h_2 (mixed phase) and the overall height h_3 of both liquids were recorded.

$$\varphi = \frac{h_2 * \rho_d - (h_2 - h_1) * \rho_c}{(h_3 - h_2) * (\rho_d - \rho_c)} \quad (2)$$

2.2 Residence time distribution

Via tracer experiments the residence time distribution (RTD) was determined by injecting the tracer of 2 ml saturated sodium chloride solution into the aqueous feed at the top of the column. At four positions along the active column height, the electric conductivity was recorded via non-commercial probes with sensor tip diameters of 0.6 mm. Due to the small tip diameter the non-commercial sensors have a minimum invasive impact on the flow pattern. The resulting RTD curves were interpreted with the dispersion model. For the evaluation with the dispersion model, open-open boundary conditions were

applied for large deviation from plug flow $D_{ax}/uL > 0.01$ and thus distinct backmixing according to Levenspiel [6]:

$$E_{\theta,oo} = \frac{1}{2}\sqrt{\frac{\bar{t}}{\pi\, t*\left(\frac{D_{ax}}{uL}\right)}}\; exp\left[-\frac{\bar{t}\left(1-\frac{t}{\bar{t}}\right)^2}{4\, t*\left(\frac{D_{ax}}{uL}\right)}\right] \tag{3}$$

In Eq. 3, t represents the time, $\bar{t}$ the mean residence time and D_{ax}/uL the vessel dispersion number with the axial dispersion coefficient D_{ax}. For comparison with the dispersion model, the corresponding number of vessels in series N was calculated from the maximum of the dimensionless exit age distribution $E_{\theta,\,max}$ according to Levenspiel [6].

$$E_{\theta,max} = \frac{N*(N-1)^{N-1}}{(N-1)!} * e^{-(N-1)} \tag{4}$$

2.3 Droplet size

The droplet size was measured noninvasive with a FDR-AX700 4K HDR camcorder synchronized with a flashing stroboscopic light source. The shutter speed of the stroboscope was adjusted to the rate of rotation of the shaft. A schematic illustration of the experimental setup is shown in Fig. 2. For better illumination and for capturing the area covered by the shaft, a mirror was installed at an angle of 45° to the camera lens. Since a commercial camera was used for monitoring the droplet size, two high power light sources were installed at the area of the mirror to provide the light intensity needed for short exposure time. Image analyzing was done via a MATLAB routine to enhance the image quality and the precision of drop size measurement.

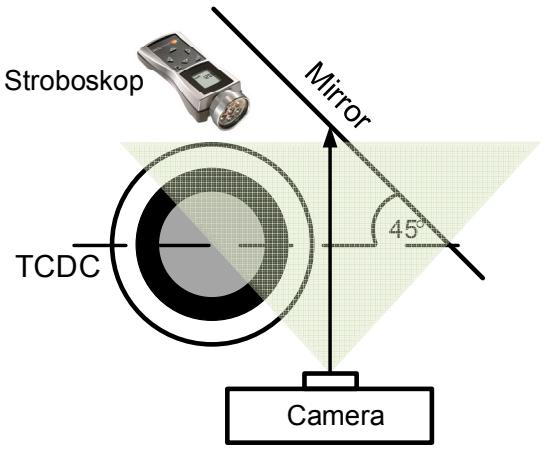

Figure 2: Schematic illustration of the experimental setup for measuring the droplet sizes

3. Results and discussion

For establishing turbulent flow conditions, all experiments were performed with high radial Reynolds number $Re_{rad} > 2400$. This was necessary, since the vorticity of the continuous phase needs to overcome sedimentation force of the dispersed phase for appropriate holdup and residence time of the dispersed phase in the active mixing zone of the single compartment. After exceeding a critical centrifugation number, which depends on the hydraulic load and the diameter of the rotor discs, the flow pattern does switch to banded two phase flow, indicating the operation on-set. For visual indication of the on-set, the formation of the lower toroidal vortex inside a single compartment is sufficient. The lower vortex becomes visible when vorticity of the continuous phase overcomes sedimentation force of the dispersed phase. The local holdup in the single compartment as well as the average holdup increase significantly. At high hydraulic load ($B = 40\ m^3\ m^{-2}h^{-1}$) and high centrifugation number ($Z > 20$), the formation of a finely dispersed secondary holdup was observed. The secondary holdup accumulates continually from the top friction bearing of the column to the bottom, whereby column flooding is obtained when the secondary holdup is fully developed between top and bottom bearing. Since secondary holdup formation starts on top of the rotating shaft, it is assumed that the shear in the vicinity of the top friction bearing is a predominant reason for droplet cleavage.

3.1 Dispersed phase holdup

The effect of the rotor disc diameter on the dispersed phase holdup for increasing centrifugation number is exemplarily shown for $B = 20\ m^3\ m^{-2}h^{-1}$ in Fig. 3a and for $B = 30\ m^3\ m^{-2}h^{-1}$ in Fig. 3b. Increasing centrifugation number results in increasing holdup. With larger rotor disc diameter, same holdup values can be obtained at lower centrifugation numbers. At low hydraulic load ($B = 20\ m^3\ m^{-2}h^{-1}$) and centrifugation number ($Z = 3$ -13), the effect of the rotor disc diameter on the holdup is negligible, as can be seen in Fig. 3a. Fig. 3b shows that higher hydraulic load leads to higher holdup values at same centrifugation number. Furthermore, the effect of the rotor disc diameter is more distinct even at lower centrifugation number. The sudden change in holdup

higher axial backmixing. The positive dynamic stabilization effect of the vortexes due to larger rotor disc diameter is also shown in Fig. 4b which depicts the impact of the rotor disc diameter on $D_{ax,c}$. An increase of the rotor disc diameter entails lower $D_{ax,c}$ values for same centrifugation number. For comparison, the $D_{ax,c}$ values obtained from measurements with the geometric design dR50 (shaft without rotor discs) is shown in Fig. 4b. In Fig. 4b the positive effect of the rotor discs on axial backmixing can impressively be demonstrated when comparing dR50 with dR86 at centrifugation number Z = 8. The results are summarized in Tab. 2.

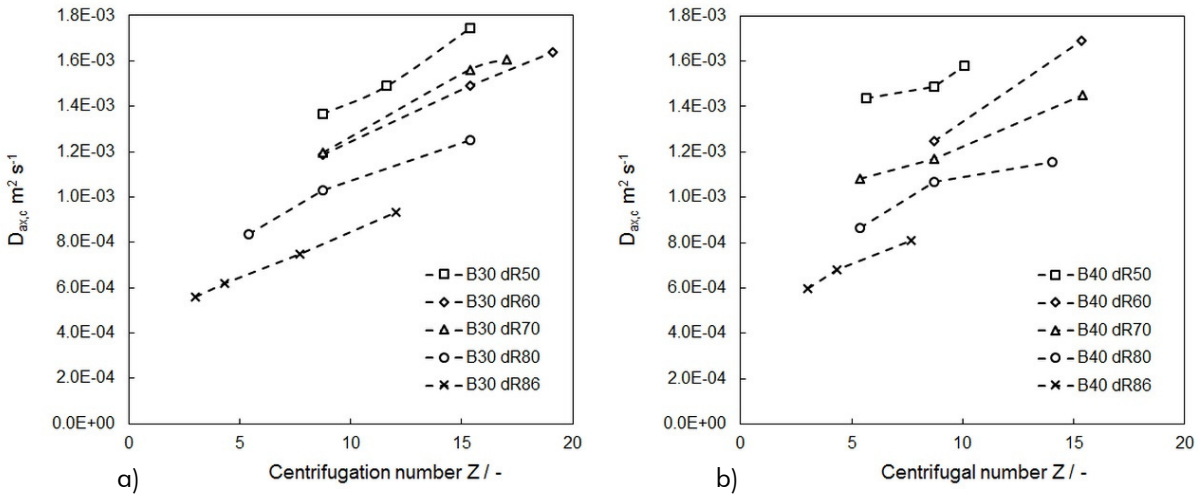

Figure 4: a) Effect of the hydraulic load on $D_{ax,c}$; b) Effect of rotor disc diameter on $D_{ax,c}$ at total hydraulic load of B = 40 $m^3 m^{-2} h^{-1}$

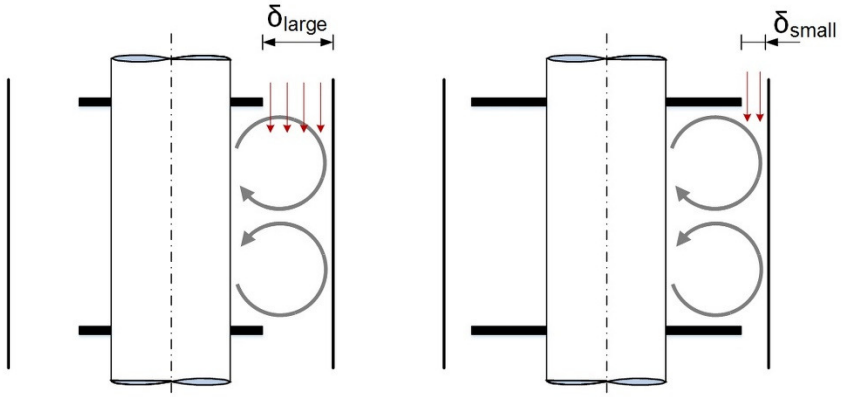

Figure 5: Schematic drawing of the effect of different rotor disc diameter and gap width on the vortexes in a single compartment of the TCDC

Table 2: Axial dispersion coefficient of the continuous phase ($D_{ax,c}$) calculated from residence time distribution measurements for varying hydraulic load and centrifugation number

	dR60		dR70		dR80	
B	Z	$D_{ax,c}$	Z	$D_{ax,c}$	Z	$D_{ax,c}$
$m^3\ m^{-2}h^{-1}$	-	$m^2\ s^{-1}$	-	$m^2\ s^{-1}$	-	$m^2\ s^{-1}$
20	5.4	9.84E-04	5.4	1.05E-03	5.4	8.55E-04
20	8.7	1.09E-03	8.7	1.13E-03	8.7	1.03E-03
20	15.4	1.46E-03	15.4	1.41E-03	15.4	1.17E-03
20	23.9	1.78E-03	23.9	flooding	23.9	flooding
30	8.7	1.19E-03	8.7	1.19E-03	5.4	8.35E-04
30	15.4	1.59E-03	15.4	1.56E-03	8.7	1.03E-03
30	19.1	1.64E-03	17.0	1.61E-03	15.4	1.25E-03
40	5.4	-	5.4	1.08E-03	5.4	8.67E-04
40	8.7	1.25E-03	8.7	1.17E-03	8.7	1.07E-03
40	15.4	1.69E-03	15.4	1.45E-03	14.0	1.15E-03

The dimensionless exit age distribution E_θ curves for all rotor disc diameters at same hydraulic load and centrifugation number is shown in Fig. 6a. The non-symmetrical shape of the E_θ curves indicates large deviation from plug flow, rather suggesting application of the tanks-in-series model. By way of comparison, the $D_{ax,c}$ values were correlated with the number of corresponding vessels N, calculated with Eq. 4. In Fig. 6b the results are exemplarily shown for the rotor disc diameter dR80. The number of corresponding vessels N correlates linearly with $D_{ax,c}$. The number of corresponding vessels N increase strongly with increasing hydraulic load. With increasing centrifugation number, the number of N decreases.

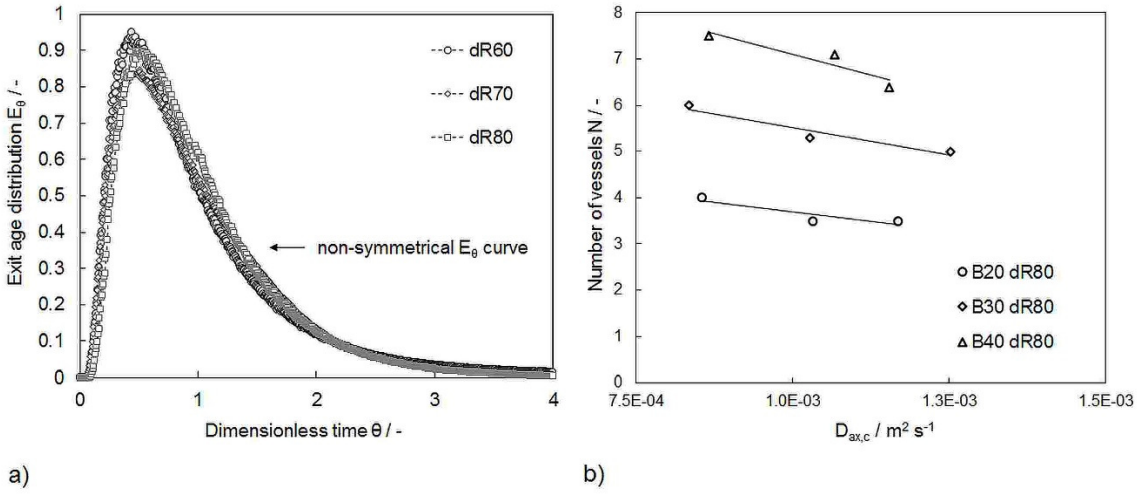

Figure 6: a) Exit age distribution E_θ curves for all rotor disc diameter; b) Comparison of $D_{ax,c}$ and the number of corresponding vessels N for dR80

3.3 Dispersed phase holdup and axial dispersion

The correlation between the axial dispersion coefficient $D_{ax,c}$ and the dispersed phase holdup for the investigated rotor disc diameters is shown in Fig. 7. With increasing disc diameter $D_{ax,c}$ decreases. The difference is more distinct for dR > 60. For dR60, dR80 and dR86 a sudden change of the curve shape at the holdup value of 12% can be observed. For dR70 the change of the curve shape occurs at 15% holdup. Again, the significant change of the slope can be interpreted as the on-set of fully developed operation, indicated by stable lower vortexes. For comparison, the results of the geometry without rotor discs, dR50, are also depicted in Fig. 7. When operating the TCDC in TCR mode (shaft without rotor rings) $D_{ax,c}$ increase linearly with increasing holdup as long as the flow pattern is located in the spiral flow range. To switch from spiral flow into banded two phase flow in TCR operation does need much higher centrifugation numbers. That simply explains why $D_{ax,c}$ linearly correlates for dR50 operation in Fig. 7. The on-set behavior of fully developed TCDC operation has been discussed in [4, 5].

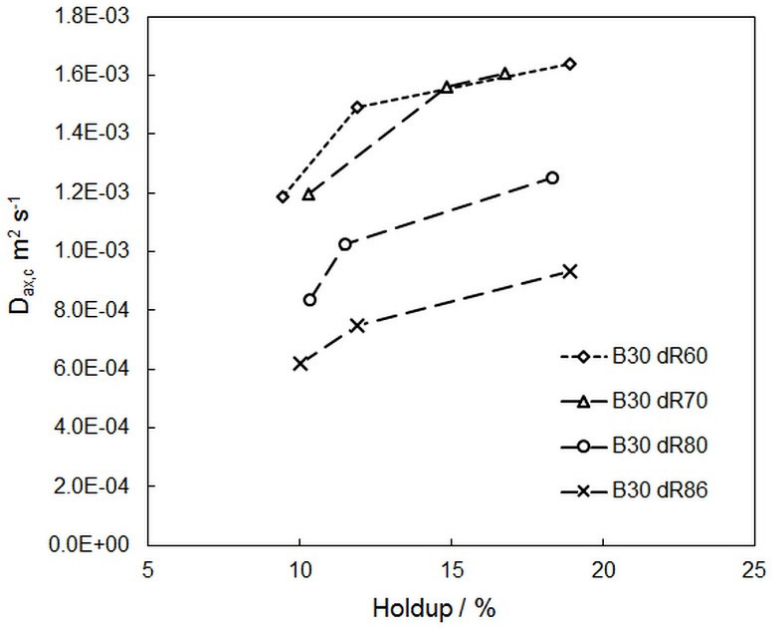

Figure 7: Correlation between $D_{ax,c}$ and φ for dR50, dR60, dR70, dR80 and dR86

3.4 Drop size

The evaluation of drop size measurements reveals a bimodal drop size distribution for the rotor disc diameter dR60, dR70 and dR80. For rotor disc diameter dR86 the bimodal distribution changes to a monomodal distribution [5]. The effect of varying rotor disc diameter at a constant hydraulic load of B = 20 $m^3\ m^{-2}h^{-1}$ on the mean droplet size for the large droplets as well as the small droplets is depicted in Fig. 8a. For both cases, the mean droplet size shifts towards smaller diameters with increasing centrifugation number whereby the decline of the larger droplets is more distinct. With increasing rotor disc diameter the droplet size decrease for same centrifugation number. This is due to higher dissipation rates offered by the larger rotor disc area. In Fig. 8b the effect of varying hydraulic load on the mean droplet size is exemplarily shown for the rotor disc diameter dR70. Higher hydraulic load leads to smaller droplet size since an increase of the phase velocities engenders more turbulent peaks in the compartment, enforcing droplet breakup. From Matlab image analyses the mean droplet size of the large droplets was within a standard deviation of +/- 0.3 mm and the mean droplet size of the small droplets was within a standard deviation of +/- 0.04 mm throughout all experiments.

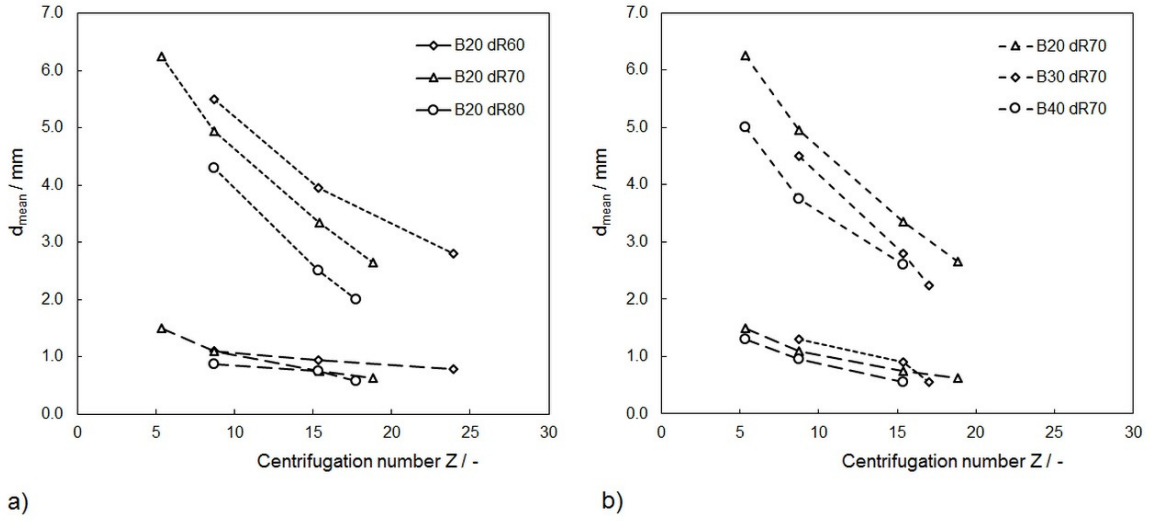

Figure 8: a) Effect of rotor disc diameter and centrifugation number on mean droplet size; b) Effect of hydraulic load and centrifugation number on mean droplet size for dR70

4. Summary and Conclusions

The Taylor-Couette Disc Contactor is a liquid-liquid extraction column with a simple design of rotating internals. The internals consist of a shaft with rotor disc arranged along the shaft. The simple design is the main benefit of the column, since it can withstand harsh operation conditions and does not provide dead zones for crud accumulation, as required in the biorefinery, nuclear industry and metallurgy. The TCDC design offers a broad range of application. In order to investigate the design flexibility of the TCDC, the effect of different rotor disc diameters on the hydrodynamics was investigated. For hydrodynamic characterization, the dispersed phase holdup, the residence time distribution as well as the mean droplet size for varying hydraulic load and centrifugation number of the rotor disc were determined. Dispersed phase holdup experiments show the formation of a secondary holdup at high hydraulic load and high centrifugation number, indicating a different source of dissipation energy for secondary holdup formation. It is assumed that the shear of the top friction bearing plays an undesirable role in secondary holdup formation. The dimensionless exit age distribution E_θ of RTD measurements indicates distinct backmixing, rather suggesting application of the tanks-in-series model for evaluation. The experimental data of drop size measurement depict a bimodal drop size distribution for the rotor disc diameter Dr < dR86. The results of these investigations show that except dR60 and less the hydraulic load does nearly not affect backmixing. With increasing rate of rotation backmixing increases too. The operation range of fully developed lower and upper vortex, classified as operation onset, does significantly change the holdup, backmixing and the droplet size. Larger rotor disc diameter expectedly shifts same holdup values to lower centrifugation number. Droplet size is smaller, and axial dispersion is less for increasing rotor diameter.

In conclusion from the results of these investigations the rotor disc diameter of the TCDC can be varied from operation without discs to a maximum rotor disc diameter of 90% of the column diameter. With increasing rotor disc diameter operation stability in terms of holdup, mean droplet size, specific mass transfer area and backmixing become better. The total hydraulic load B is not affected by the ratio of rotor disc diameter to column diameter.

Acknowledgement

The authors gratefully acknowledge the support of Maximillian Hübner doing all the experiments. Special thanks go to Georg Rudelstorfer as well as Rene Fras for their constant support in column construction.

Symbols used

Symbols

A	$[m^2]$	area
B	$[m^3\ m^{-2}h^{-1}]$	total hydraulic load
D_C	[m]	column diameter
$D_{ax,c}$	$[m^2\ s^{-1}]$	axial dispersion coefficient of continuous phase
d_m	[mm]	mean droplet size
d_R, dR	[mm]	rotor disc diameter
d_{SH}	[m]	shaft diameter (inner cylinder diameter)
E_θ	[-]	dimensionless exit age distribution
g	$[m\ s^{-2}]$	gravity (9.81)
H	[m]	active column height
H_C	[m]	compartment height
N	[-]	number of corresponding vessels in series
n	$[1\ s^{-1}]$	rate of rotation
t	[s]	time
$\bar{t}$	[s]	mean residence time
V	$[m^3]$	volume
w	$[rad\ s^{-1}]$	angular velocity
Z	[-]	$=(w^2 d_{Sh})/(2g)$ = centrifugation number

Greek symbols

δ	[mm]	gap width
ρ	$[kg\ m^{-3}]$	density

ν	[$m^2\ s^{-1}$]	kinematic viscosity
φ	[-]	dispersed phase holdup
θ	[-]	dimensionless time ($\theta = t\ \bar{t}^{-1}$)

Subscripts

C	column
c	continuous phase
d	dispersed phase
Sh	shaft

Abbreviations

CFD	computational fluid dynamics
RDC	Rotating Disc Contactor
RTD	residence time distribution
SST	ShellSol T
TCDC	Taylor-Couette Disc Contactor
TCR	Taylor-Couette reactor

References

[1] E. Aksamija, C. Weinländer, R. Sarzio, and M. Siebenhofer, Sep. Sci. Technol., 2015, 50 (18), 2844. DOI: 10.1080/01496395.2015.1085406.

[2] E. Aksamija, Ph.D. Thesis, Graz University of Technology, 2015.

[3] A. Grafschafter, E. Aksamija, and M. Siebenhofer, Chem. Eng. Technol., 2016, 39 (11), DOI: 10.1002/ceat.201600191.

[4] A. Grafschafter and M. Siebenhofer, Chemie Ing. Tech., 2017, 4, DOI: 10.1002/cite.201600142.

[5] A. Grafschafter, G. Rudelstorfer, and M. Siebenhofer, Chemie-Ingenieur-Technik, 2018, DOI: 10.1002/cite.201800031.

[6] O. Levenspiel, Chemical Reaction Engineering. Wiley, 1999.

Chapter 4

The Taylor-Couette Disc Contactor

Chemical Engineering & Technology Research Article 2087

Annika Grafschafter
Enes Aksamija
Matthäus Siebenhofer

Graz University of Technology, NAWI Graz, Institute of Chemical Engineering and Environmental Technology, Graz, Austria

The Taylor-Couette Disc Contactor

The Taylor-Couette disc contactor is a hydrodynamic hybrid of a rotating disc contactor and a Taylor-Couette contactor. For application in reactive bioseparations, this type of liquid-liquid contactor may offer advantageous operation features. This paper summarizes the design characteristics of the Taylor-Couette disc contactor. For hydrodynamic characterization, experimental data of the mean Sauter diameter and dispersed-phase hold-up were compared with results predicted by empirical correlations, which were originally developed for rotating disc contactors. Several correlations were modified for the application on Taylor-Couette disc contactors. Operation characteristics have been deduced from mass-transfer experiments on the pilot-plant scale.

Keywords: Design algorithms, Hydraulic correlations, Reactive separations, Separation efficiency, Taylor-Couette disc contactor

Received: April 04, 2016; *revised:* May 25, 2016; *accepted:* August 17, 2016

DOI: 10.1002/ceat.201600191

1 Introduction

Many attempts in the biorefinery business suffer from poor economics. Target constituents do not show up in appropriate concentration for simple isolation technologies. Rather, they have to be separated from multicomponent mixtures with low concentration from side streams and low-quality broths. Reactive separations may contribute to solving the gap between expectations and needs. Liquid-liquid extraction has been a leading technology in contributing to raise the economic feasibility of separation processes. Beyond applications in solvent extraction, liquid-liquid separation processes give access to combinations of chemical reactions in either phase in addition to separation. Therefore, detailed knowledge of the hydrodynamics of two-phase reactors is needed.

Liquid-liquid two-phase reactors are preferably stirred tank reactors. For mixing liquid systems that tend towards emulsification and for highly viscous or particle-laden liquids the most suitable energy inputs can be generated with Taylor-Couette reactors or rotating disc contactors (RDCs). A Taylor-Couette reactor forms banded two-phase flow without internals, which results in a small droplet size, thereby providing a large mass-transfer area and narrow residence-time distribution. Since banded two-phase flow in Taylor-Couette reactors is a gap phenomenon, a big disadvantage is the limited hydraulic capacity. A similar flow pattern to banded two-phase flow is obtained in RDC columns, in which the flow pattern is stabilized by stator rings. RDC design is well established on the industrial scale, nevertheless the design suffers from some uncertainties regarding the optimum ratio of the shaft to the shell [1]. The shaft diameter is sized very small because of fear of the loss of active cross-sectional area [2]. As a consequence of this design weakness the disperse phase tends to form stable coalesced layers at the shaft since limited vortex strength cannot keep the solvent phase dispersed in the toroidal vortex [3]. Furthermore, crud accumulation and fouling at stator rings are crucial problems of this type of solvent extractor. To target improved hydraulic capacity and banded two-phase flow, a hydrodynamic hybrid of a Taylor-Couette reactor and RDC, the Taylor-Couette disc contactor (TCDC) was developed [3].

For application in reactive bioseparations the Taylor-Couette disc contactor may offer advantageous operation features since this type of liquid-liquid contactor does not contain any installations that might cause dead-zone formation and crud accumulation. For practical application the hydrodynamics and the design rules based on CFD simulation and experimental validation in a pilot-plant scale TCDC100 have been developed. Empirical correlations for drop-size estimation and dispersed-phase hold-up, originally developed for RDC design were applied to predict drop size and hold-up in the TCDC. The results were compared with experimental data. Thus, it was possible to examine whether existing correlations for the hydrodynamic design of stirred extraction columns can be applied to designed TCDC contactors by adapting the parameters of selected correlations. The separation efficiency was determined experimentally and, according to the mode of operation, plug flow design was compared with continuously stirred tank reactor (CSTR) cascade design.

Correspondence: Annika Grafschafter (a.grafschafter@tugraz.at), Graz University of Technology, NAWI Graz, Institute of Chemical Engineering and Environmental Technology, Inffeldgasse 25C, 8010 Graz, Austria.

1.1 Taylor-Couette Disc Contactor

The Taylor-Couette disc contactor is a hydrodynamic hybrid of a rotating disc contactor and a Taylor-Couette reactor [3]. The design without stator rings and an increased shaft diameter (D_{SH})[1)] improve the classical RDC design and tie in a similar flow pattern to the banded two-phase flow of a Taylor-Couette reactor. Increased rotor discs form compartments during operation, stabilize the flow pattern, and inhibit high axial dispersion. Fouling and crud accumulation is avoided because of the missing stator rings. Compared with Taylor-Couette reactors, the active reactor volume is significantly increased. This results in more stable Taylor-Couette vortexes even at higher flow rates. Fig. 1 shows the dispersed-phase distribution in a TCDC100.

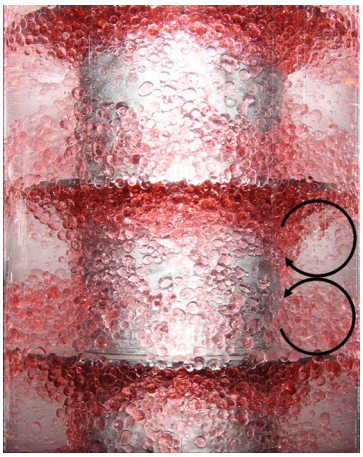

Figure 1. Dispersed-phase distribution at 450 rpm and phase ratio 1. Shaft diameter: 0.05 m, rotor diameter: 0.086 m, compartment height: 0.05 mm, column diameter 0.1 m.

Recommended design rules for the geometric ratios of the internals of a TCDC were deduced from experimentally validated CFD simulations [3] (see Eqs. (1)–(4) in which D_R is the rotor disc diameter, D is the column diameter, and B_C is the column width):

$$D_R = (0.85 \ldots 0.9)D \tag{1}$$

$$D_{SH} \approx 0.5D \tag{2}$$

Lower limit for the compartment height (H_C):

$$H_C = 1.3B_C \tag{3}$$

For the formation of highly symmetric toroidal vortexes, the compartment height shall approximate:

$$H_C = 2B_C \tag{4}$$

1) List of symbols at the end of the paper.

1.2 Reactor Modeling

For the design of continuously operating reactors, the continuously stirred tank reactor (CSTR) cascade and the ideal plug flow reactor (PFR) model were applied. With these basic design concepts, either the required column height for continuous separation processes, or the separation efficiency for a given column height can be obtained. Liquid-liquid extraction columns are generally designed as ideal PFRs, according to Eqs. (5)–(7) in which F_A is the molar flow, r is the rate of reaction, $(-r\mathrm{A})\mathrm{d}V$ is the conversion of reactant by reaction, CS is the cross-section area, h is the height, a is the specific mass-transfer area, k'' is the overall mass-transfer coefficient, c is the concentration, c^* is the equilibrium concentration, and subscripts c and d refer to the continuous and dispersed phases, respectively.

$$\text{mass balance: } F_A = F_A + \mathrm{d}F_A + (-r_A)\mathrm{d}V \text{ and } \mathrm{d}V = CS\mathrm{d}h \tag{5}$$

$$r_A = \frac{A}{V_c + V_d} r_A'' = a r_A'' \quad \text{and} \quad r_A'' = -k''(c_A - c_A^*) \tag{6}$$

$$H_{column} = \int \mathrm{d}h = \frac{F_A}{CSk''a} \int_{c_{A0}}^{c_{A1}} \frac{dc_A}{c_A - c_A^*} \tag{7}$$

Ideal plug flow assumes an axial flow pattern without axial dispersion. However, stirred liquid-liquid extraction columns may show distinct axial back-mixing, which is a big issue in column design and scale-up. In practical applications, the HTU/NTU concept is extended by using the height of the dispersion unit (HDU) value that considers axial back-mixing with the aid of the axial dispersion coefficient (D_{ax}) [4]:

$$H_{column} = \overline{\mathrm{HTU}}\ \mathrm{NTU} \tag{8}$$

$$\overline{\mathrm{HTU}} = \mathrm{HTU} + \mathrm{HDU} \tag{9}$$

$$\mathrm{HDU} = \frac{D_{ax,c}}{v_c} + \frac{D_{ax,d}}{v_d} \quad \text{if the extraction factor } (\varepsilon) = 1 \tag{10}$$

To quantify the specific mass-transfer area, the drop size and the hold-up are needed for column design. These parameters can be evaluated by time-consuming experimental methods, by validated computational fluid dynamics, or empirical correlations. In this paper, the mean Sauter diameter (d_{32}) and the dispersed-phase hold-up (φ) for a RDC100 and a TCDC100 were evaluated by several empirical correlations and compared to experimental results.

1.3 Empirical Correlations

1.3.1 Mean Sauter Diameter

As a key feature of the drop-size distribution, the average droplet diameter used in the form of the volume-surface diameter, called the mean Sauter diameter (d_{32}), can be calculated [5, 6]:

$$d_{32} = \frac{\alpha^3 3!}{\alpha^2 2!} = 3\alpha \tag{11}$$

The distribution parameter α can be calculated according to the following, in which ρ is the density, σ is the surface tension, g is the force of gravity, and η is the dynamic viscosity [5]:

$$\alpha = \alpha_0(1+B)\exp(-B) \tag{12}$$

$$\alpha_0 = 0.807\left(\frac{\sigma}{\Delta\rho g}\right)^{0.478}\left(\frac{\eta_c^2}{\sigma\rho_c}\right)^{0.0448} \tag{13}$$

$$B = 0.041\left(\frac{(nD_R - 0.0999)^2 D_R\rho_c}{\sigma}\right)^{(0.563-\sigma 3.95)} + 4.44\left(\frac{(nD_R - 0.0385)\eta_c}{\sigma}\right)^{(0.637-\sigma 7.15)} \tag{14}$$

Further correlations, which were used for evaluation of the mean Sauter diameter, are summarized in Tab. 1.

1.3.2 Dispersed-Phase Hold-Up

The dispersed-phase hold-up φ is defined as the fraction of dispersed phase relative to the total volume:

$$\varphi = \frac{V_c}{V_d + V_c} \tag{15}$$

The correlations used for the evaluation of the dispersed-phase hold-up in the TCDC are summarized in Tab. 2. For the evaluation, the stator diameter D_S was replaced by the column diameter D.

2 Experimental Setup and Procedure

To evaluate the mean Sauter diameter, the dispersed-phase hold-up, and the separation efficiency of the TCDC, experiments were performed on a pilot-plant scale TCDC100. The design data of the extractor are: H_{Active} = 1 m, D = 0.1 m, D_{SH} = 0.05 m, D_R = 0.085 m, H_C = 0.05 m. The mean Sauter diameter at different operating points, evaluated experimentally [3] was compared with empirical correlations.

Table 1. Several empirical correlations proposed for the evaluation of the mean Sauter diameter in RDC columns and information about the proposed geometry design and system properties.

Correlation	Author	System properties	Geometry [m]
$d_{32} = 16.7\left(\frac{\sigma}{\rho_c g}\right)^{0.5}\left(\frac{D_R n\rho_c}{\eta_c}\right)^{-0.3}\left(\frac{n^2 D_R}{g}\right)^{-0.3} N_c^{-0.23}$	Kagan [7]	ρ_C = 1000–1230 kg m^{-3} ρ_D = 725–1430 kg m^{-3} η_C = 1–2.5 mPa s η_D = 0.3–48 mPa s σ = 13–38.5 mN m^{-1}	D = 0.054–0.2
$d_{32} = 0.62\frac{D_R}{We^{0.52}}\left(1+\frac{35}{N_C^{1.22}We^{0.5}}\right)(1+2\varphi)$ $We = \frac{n^2 D_R^3\rho_c}{\sigma}$	Fischer [8]	$\rho_C \approx$ 1000 kg m^{-3} $\Delta\rho$ = 95–335 kg m^{-3} η_C = 1–4.8 mPa s σ = 12–44.5 mN m^{-1}	D = 0.150
$\frac{d_{32}}{D_R} = \frac{C_1}{0.07+\sqrt{Fr_R}}\left(\frac{\eta_c}{\sqrt{\sigma}\rho_c D_R}\right)^{-0.12}\left(\frac{\rho_d}{\rho_c}\right)^{0.16}$ $\left(\frac{D_R^2\rho_c g}{\sigma}\right)^{-0.59}\left(\frac{H_C}{D}\right)^{0.25}\left(\frac{D}{D_R}\right)^{0.46}$ $Fr_R = \frac{n^2 D_R}{g}$ $C_1 = 0.53$	Kumar and Hartland [9]	–	–
$n = \frac{0.374^{0.667}}{D_R^{0.778}(\rho_{cc})^{0.332} d_{32}^{0.556}}$	Marr [10]	–	–

Table 2. Several empirical correlations proposed for the evaluation of the dispersed-phase hold-up original design for RDC and information about the proposed geometry design and system properties.

Correlation	Author	System properties	Geometry [m]
$\varphi = \left[530.53 + 747.78\left(\frac{n^2 D_R}{g}\right)^{1.28}\right]\left(\frac{D_S^2 H_C^2\rho_C}{\sigma D^2}\right)^{-0.45}\left(\frac{\rho}{\rho_C}\right)^{0.58}$ $\left(\frac{\eta_C g^{0.25}}{\rho_G^{0.25^{0.75}}}\right)^{0.85}\left(\frac{v_D^4\rho_C}{g\sigma}\right)^{0.22}\left(1+\frac{v_C}{v_D}\right)^{0.35}$	Kumar and Hartland [11]	ρ_C = 786–1141 kg m^{-3} ρ_D = 686–1595 kg m^{-3} η_C = 0.85–9.1 mPa s σ = 5.4–50 mN m^{-1}	D = 0.05–0.450 D_R = 0.027–0.2 H_C = 0.014–0.225

Table 2. Continued.

Correlation	Author	System properties	Geometry [m]
$\varphi = 0.0133\left(\frac{D_R}{D}\right)\left(\frac{a_1}{d_{32}-a_2}\right)^{\frac{1}{a_3}} + a_4 - a_5$ $a_1 = 7.01\times10^{-6}\sigma^{-0.5} + 5.869\times10^{-3}\left(\frac{\rho_C}{\rho_D}\right)^{0.865} + 5.64\times10^{-3}$ $\left(\frac{0.001}{\sigma-0.0124}\right)^3 - 10^{-3}\left(\frac{0.235\eta_C^2+0.1\eta_D^2}{\eta_C\eta_D}\right) + 0.349\times10^{-3}$ $\left(\frac{0.04}{D^2}-1\right)^3$ $a_2 = 0.000225$ *for* $(v_C + v_D) > 0.0036\ [\mathrm{m\,s^{-1}}]$ and $d_{32} > 0.000225$ [m] else $a_2 = 0$ $a_3 = 8.82\sigma^{1.406} + 0.775\left(\frac{\rho_C}{\rho_D}\right)^{0.138} + 0.172\left(\frac{0.001}{\sigma-0.0124}\right)^3$ $-\frac{0.0293\eta_C^2+0.0138\eta_D^2}{\eta_C\eta_D}$ $a_4 = 0.039\left(\frac{(\dot V_C+\dot V_D)1257}{D^2\pi}-1\right)$ $a_5 = 0$ *for* $\frac{\dot V_C}{\dot V_D} \le 3.5$ and $a_5 = 0.0139\left(\frac{\dot V_C}{\dot V_D 3.5}-1\right)^{1.15}$ $+0.0037$ for $\frac{\dot V_C}{\dot V_D} > 3.5$	Möhring [12]	ρ_C = 875–1614 kg m^{-3} ρ_D = 998–1590 kg m^{-3} η_C = 1–12 mPa s η_D = 0.74–25 mPa s σ = 3.5–43 mN m^{-1}	–
$\varphi = 1.58\frac{nD_R}{v_C}\left(\frac{v_D}{v_C}\right)^{0.96}\left(\frac{v_C^2}{gD^2}\right)^{0.96}\left(\frac{\Delta\rho}{\rho_C}\right)^{-1.31}\left(\frac{D_S^2-D_R^2}{D^2}\right)^{-0.7}$ $\left(\frac{H_C}{H}\right)^{-0.426}\left(\frac{\rho_C v_C D}{\eta_C}\right)^{-0.13}\left(\frac{\rho_C v_C^2 D}{\sigma}\right)^{0.245}$	Kasatkin et al. [13]	trichloro-ethylene-water	D = 0.054 D_R = 0.027 and 0.042 H_C = 0.014–0.028 H = 0.54
$\varphi = 3.3\left(\frac{nD_R}{v_C}\right)^{0.55}\left(\frac{v_C}{v_D}\right)^{0.8}\left(\frac{v_C^2}{gD}\right)^{0.6}\left(\frac{\Delta\rho}{\rho_C}\right)^{-0.13}$ $\left(\frac{D_s^2-D_R^2}{D^2}\right)^{-0.3}\left(\frac{H_C}{D}\right)^{-0.66}\left(\frac{D_R}{D}\right)^{0.4}\left(\frac{\rho_C v_C^2 D}{\sigma}\right)^{0.18}$	Murakami et al. [14]	MIBK-water acetic acid/butyric acid, kerosene-water-acetic acid/ butyric acid	D = 0.079–0.3 D_R = 0.040–0.2 H_C = 0.04–0.225 H = 0.71–1.2

2.1 Hold-Up

The hold-up was determined in dual-phase operation without mass transfer with the test system ShellSol-T (SST)/water, in which ShellSol-T was used as the disperse phase. The averaged hold-up was determined by means of static pressures. To determine the disperse-phase hold-up at several operating points the rotational speed of the rotor was increased stepwise and the change of the axial position of the phase interface on the top of the column was monitored.

2.2 Mass-Transfer Experiments

The separation efficiency of the TCDC100 was determined by mass-transfer experiments with the SST/*n*-butanol/water system. The physical properties of the test system and the equilibrium data according to Eq. (16) as well as the operation conditions are shown in Tab. 3–5.

$$c_w = 0.6\frac{27.57c_{SST}}{1+27.57c_{SST}} \quad (16)$$

Table 3. Physical properties of the test system SST/*n*-butanol/water

	Density [kg m^{-3}]	Kinetic Viscosity [m^{2}s^{-1}]
ShellSol-T	756.8	1.85×10^{-6}
deionized water	998.1	1.102×10^{-6}
n-butanol	810	3.64×10^{-6}

The system was chosen because of the advantageous distribution of *n*-butanol in the aqueous and solvent phases. Deionized water (w) was used as the continuous phase and ShellSol-T as the dispersed phase. The *n*-butanol was mixed with ShellSol-T and the mixture was than fed into the extractor at the bottom and water was fed into the top of the column. Samples were taken at the inlet and outlet of the column as well as at four sampling positions along the column height. Analysis of *n*-butanol in both phases was conducted by using gas chromatography.

Table 4. Equilibrium data (Eq. (16)) of the test system SST/*n*-butanol/water.

c_{SST} [mol L^{-1}]	c_W [mol L^{-1}]
0.020	0.213
0.040	0.315
0.060	0.374
0.080	0.413
0.100	0.441
0.120	0.461
0.140	0.477
0.160	0.489
0.180	0.500
0.200	0.508
0.220	0.515
0.240	0.522
0.260	0.527

Table 5. Operation conditions of mass-transfer experiments.

Parameter	Value
rotational speed [rpm]	380
phase ratio [–]	1
mass fraction [wt %]	3
d_{32} [mm]	2.274
φ [%]	7.8
a [m^{2}m^{-3}]	205.8

3 Results

3.1 Mean Sauter Diameter

Fig. 2 a shows the experimentally evaluated mean Sauter diameter [3] at varying rotational speeds in a RDC100. As expected, the mean Sauter diameter decreases with increasing rotational speed. The experimental results were compared with the mean Sauter diameter determined with the distribution parameter α [5] and empirical correlations proposed by Kagan [7], Fischer [8], Kumar and Hartland [9], and Marr [10]. The best fit was given by the Kumar and Hartland [9] correlation. At higher rotational speed the correlation of Fischer [8] fit the experimental results well. The data determined with the distribution parameter α [5] and with the correlations by Kagan [7] and Marr [10] were not suitable for this application.

In Fig. 2 b the evaluation of the mean Sauter diameter is shown for the TCDC100. Compared to the RDC100, the experimentally evaluated mean Sauter diameter is smaller at higher rotational speed. For lower agitation intensity of 250 and 350 rpm the RDC100 shows a smaller drop size. The evaluation of the correlations shows that Fischer [8] gives the best fit at lower rotational speed. The Kumar and Hartland [9] correlation showed better accuracy at higher agitation intensities of 350 and 500 rpm. However, the evaluation of the TCDC100 compared to the RDC100 showed larger deviation from the experimental results. The average percentage errors between the correlations to the experimental results for the RDC100 and TCDC100 are listed in Tab. 6.

To pre-estimate the mean Sauter diameter in the TCDC the correlations have to be altered since the TCDC design does not separate compartments with stator rings. Therefore, the parameter of the correlations was fitted to experimental results. The best outcomes were obtained by using the fitting parameters of Marr [10] and Fischer [8], as shown in Fig. 3. The modi-

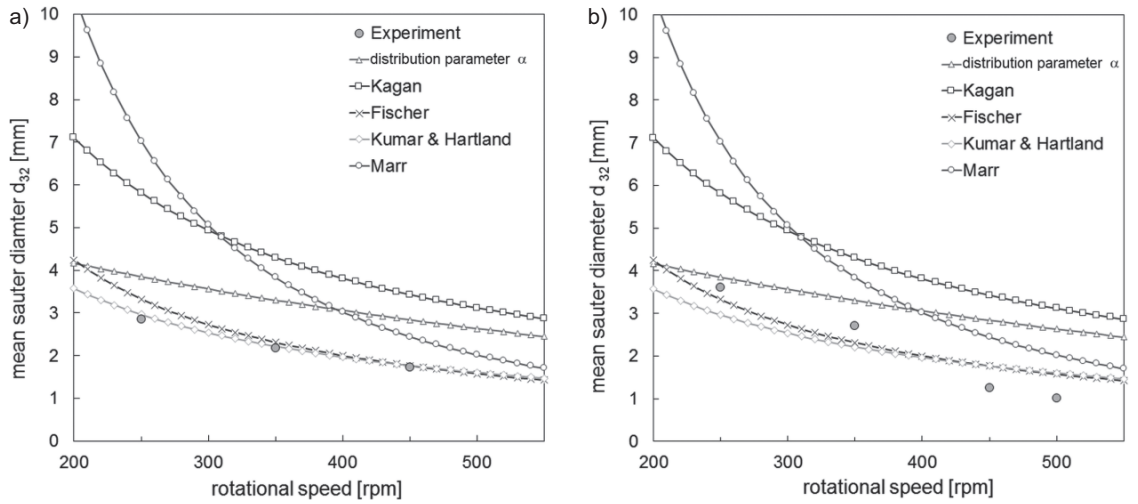

Figure 2. (a) Mean Sauter diameter in the RDC100 at a total hydraulic load of $B = 20\ m^3m^{-2}h^{-1}$ compared with empirical correlations; (b) mean Sauter diameter in the TCDC100 at a total hydraulic load of $B = 20\ m^3m^{-2}h^{-1}$ compared with empirical correlations.

Table 6. Average percentage error of the mean Sauter diameter d_{32} between experimental results and correlations by distribution parameter α [5], Kagan [7], Fischer [8], Kumar and Hartland [9], and Marr [10] evaluated for RDC and TCDC.

Rotational speed [rpm]	d_{32} [mm]	Deviation [%]				
		α [5]	Kagan [7]	Fischer [8]	Kumar and Hartland [9]	Marr [10]
		RDC				
250	2.847	45	106	27	11	213
350	2.176	68	99	16	9	124
450	1.722	88	101	12	10	80
		TCDC				
250	3.608	7	47	10	25	95
350	2.709	22	44	16	26	42
450	1.261	125	148	39	27	94
500	1.012	160	181	54	44	100

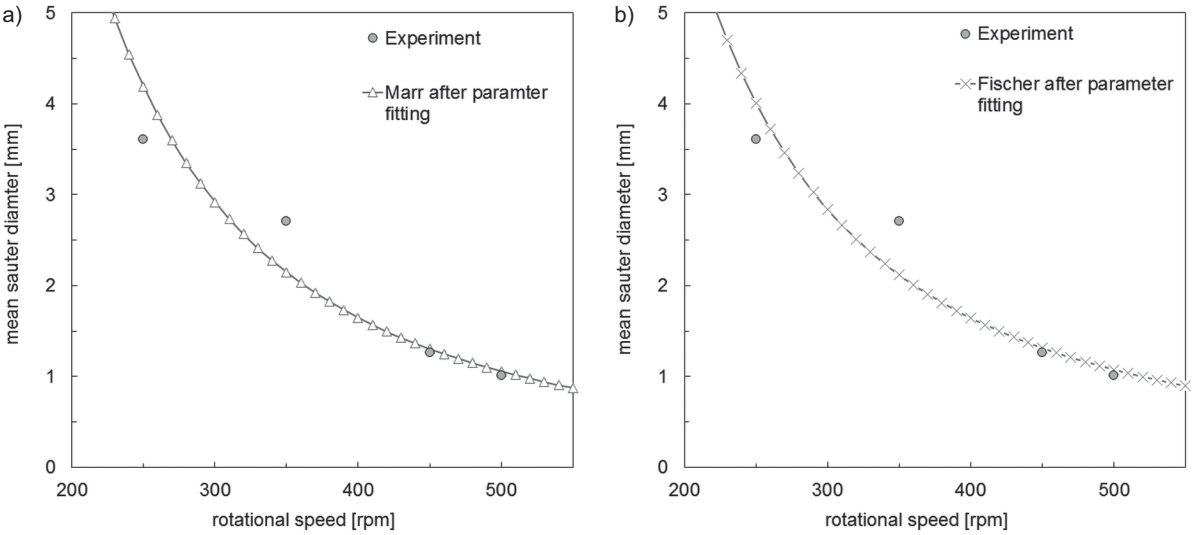

Figure 3. (a) Mean Sauter diameter in the TCDC100 at a total hydraulic load of $B = 20\ m^3m^{-2}h^{-1}$ compared with modified empirical correlation by Marr [10], (b) Mean Sauter diameter in the TCDC100 at a total hydraulic load of $B = 20\ m^3m^{-2}h^{-1}$ compared with modified empirical correlation by Fischer [8].

fied correlations reproduced the experimental results with little deviation at rotational speeds of 450 and 500 rpm. The largest deviation was obtained for 350 rpm. The average percentage errors between the original and modified correlations by Marr [10] and Fischer [8] to the experimental results are listed in Tab. 7.

3.2 Dispersed-Phase Hold-Up

Fig. 4 depicts the results of dispersed-phase hold-up measurements in the TCDC at varying rotational speed. As expected, the average hold-up increases with higher agitation intensity. Just before reaching the flooding point the hold-up increases significantly. The experimental results are compared with values predicted by correlations, originally evaluated for the RDC by Kumar and Hartland [11], Möhring [12], Kasatkin [13], and Murakami [14], as shown in Fig. 4. In the range of 100 to 450 rpm the results of Murakami [14] show the lowest deviation compared to the experiments. The correlation by Murakami [14] was based on data obtained with similar column geometries and system properties of the continuous and disperse phases. However, the significant increase of the hold-up before reaching the flooding limit of the column could not be reproduced. Kasatkin's correlation [13] derives more precise results for 400 and 500 rpm but shows large deviation at lower agitation intensity. The correlations by Kumar and Hartland [11] were unsuitable for pre-calculating the hold-up in a TCDC al-

Table 7. Average percentage error of the mean Sauter diameter d_{32} between experimental results and original and modified correlations by Marr [10] and Fischer [8].

		Original correlations				Modified correlations			
		Marr [10]		Fischer [8]		Marr [10]		Fischer [8]	
rotational speed [rpm]	d_{32} [mm]	d_{32} [mm]	deviation [%]	d_{32} [mm]	deviation [%]	d_{32} [mm]	deviation [%]	d_{32} [mm]	deviation [%]
250	3.608	7.027	94.8	3.262	9.6	4.190	16.1	3.464	4.0
350	2.709	3.836	41.6	2.279	15.8	2.148	20.7	2.467	8.9
450	1.261	2.441	93.6	1.747	38.5	1.304	3.4	1.315	4.3
500	1.012	2.0	99.6	1.563	54.5	1.058	4.516	1.077	6.4

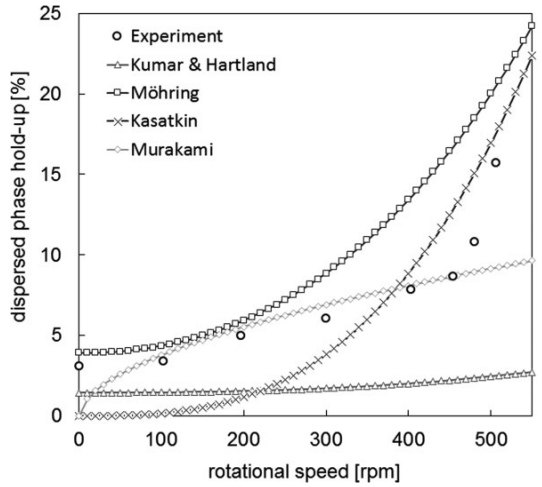

Figure 4. Dispersed-phase hold-up in a TCDC100 at total hydraulic load of $B = 20\ m^3m^{-2}h^{-1}$ compared with empirical correlation.

though the requirements for geometry and system properties were suitable. The course of the curve provided by Möhring [12] describes the dispersed-phase hold-up profile very well but the hold-up values are too high. The data proposed by the correlations differ with different rotational speed to varying degree from the experimental results. The deviation of the correlations from experimental results primarily arises from the modified internals of the TCDC.

Again, the parameters of the correlations were fitted to the experimental data. Parameters that correspond to the physical system properties were kept constant and the parameters that correspond to the column geometry were adjusted. The best result was delivered by fitting the parameters of Kumar and Hartland [11] (Fig. 5). In Tab. 8 the original and modified parameter of the correlation by Kumar and Hartland [11] are listed.

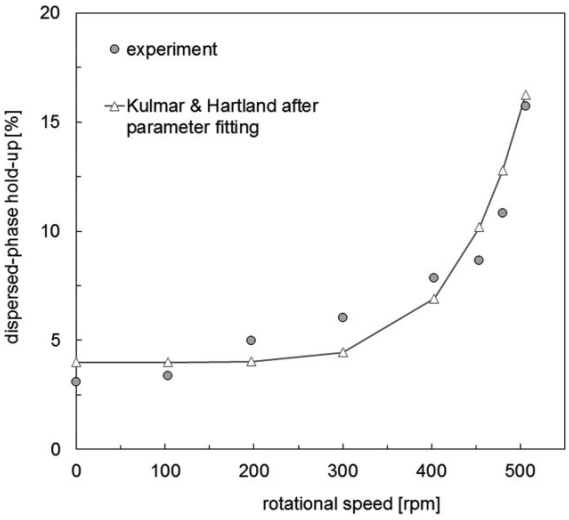

Figure 5. Dispersed-phase hold-up in a TCDC100 at total hydraulic load of $B = 20\ m^3m^{-2}h^{-1}$ compared with the modified empirical correlation by Kumar and Hartland [11].

Table 8. Original and modified parameters of the correlation by Kumar and Hartland [11] for prediction of dispersed-phase hold-up.

Parameter	Original parameter	Modified parameter
C1	570.53	10
C2	747.78	141
exponent n1	1.28	3.15
exponent n2	–0.45	0.4
exponent n3	0.58	0.58
exponent n4	0.85	0.85
exponent n5	0.22	0.22
exponent n6	0.35	0.35

3.3 Separation Efficiency

Based on PFR design according to Eq. (7), the overall mass-transfer coefficient $k''_{PFR} = ((4.3\times10^{-5})\pm(0.1\times10^{-5}))\ m\ s^{-1}$ for the system SST/*n*-butanol/water was deduced from mass-transfer experiments with the specific mass-transfer area $a = 205.8\ m^2\ m^{-3}$, as determined from the mean Sauter diameter d_{32} from the drop size distribution and the experimentally determined dispersed-phase hold-up φ (Tab. 5). Fig. 6 a shows the concentration profile of the solvent along the column height for several mass-transfer experiments. The concentration profile for the case of ideal plug flow and apparently pronounced axial back-mixing are depicted. The concentration profile evaluated with ideal plug flow does not fit the experimental results. By altering the overall mass-transfer coefficient k''_{PFR} from $((4.3\times10^{-5})\pm(0.1\times10^{-5}))$ to $((1.3\times10^{-4})\pm(0.1\times10^{-4}))\ m\ s^{-1}$ the concentration profile can be adjusted to the experimental data. However, the adaption of the concentration profile does cause concentration leaps at the bottom and the top of the column implying high uncertainty for scale-up. The mass balance calculated with the PFR design cannot reproduce the experimentally obtained data. As already mentioned, the HDU value considers the axial dispersion of the continuous and disperse phases and enables more appropriate calculations for scale-up. Nevertheless, the determination of the axial dispersion of the disperse phase can be very difficult. Seemingly, the application of the PFR model does not reflect operation conditions well, although consideration of HDU may improve results.

For comparison, the CSTR cascade model was applied. By approximating each compartment of the TCDC with two ideal stirred tank reactors, the concentration profile can be evaluated by a CSTR design algorithm according to Eqs. (17)–(19).

$$\text{mass balance:}\quad F_{A,0} = F_A - r_A''aV_r \text{ and } F_{A,0} = F_V c_{A,0} \tag{17}$$

$$r_A = \frac{A}{V_c + V_d} r_A'' = a r_A'' \text{ and } r_A'' = -k''(c_A - c_A^*) \tag{18}$$

$$c_{A,n} = \frac{c_{A,n-1} \pm k'' \frac{V_r}{F_V} a c_A^*}{1 + k'' \frac{V_r}{F_V} a} \tag{19}$$

Owing to the formation of toroidal vortexes, each compartment of the TCDC acts like continuous stirred tank reactors in series with ideal mixing. Through interpretation of mass-transfer experiments with Eq. (19) and the operation conditions from Tab. 5, the overall mass-transfer coefficient was calculated to be $k''_{CSTR} = ((1.4\times10^{-4})\pm(0.1\times10^{-4}))\ m\ s^{-1}$. This value is comparable with the result from applying the PFR design algorithm with Eq. (7). Fig. 6 b shows the comparison of the concentration profile as calculated with Eq. (19) for a CSTR cascade of 40 compartments (corresponding to twice the number of compartments in the TCDC) with the experimental results. The concentration profile as well as the mass balance calculated with the CSTR model fit well with the experimental data.

4 Conclusions

The hydrodynamic characteristics of the Taylor-Couette disc contactor have been investigated. The Taylor-Couette disc contactor is a hydraulic hybrid of a Taylor-Couette reactor and rotating disc contactor. Experimental data of the mean Sauter diameter and dispersed-phase hold-up have been compared with results predicted by empirical correlations. The modified

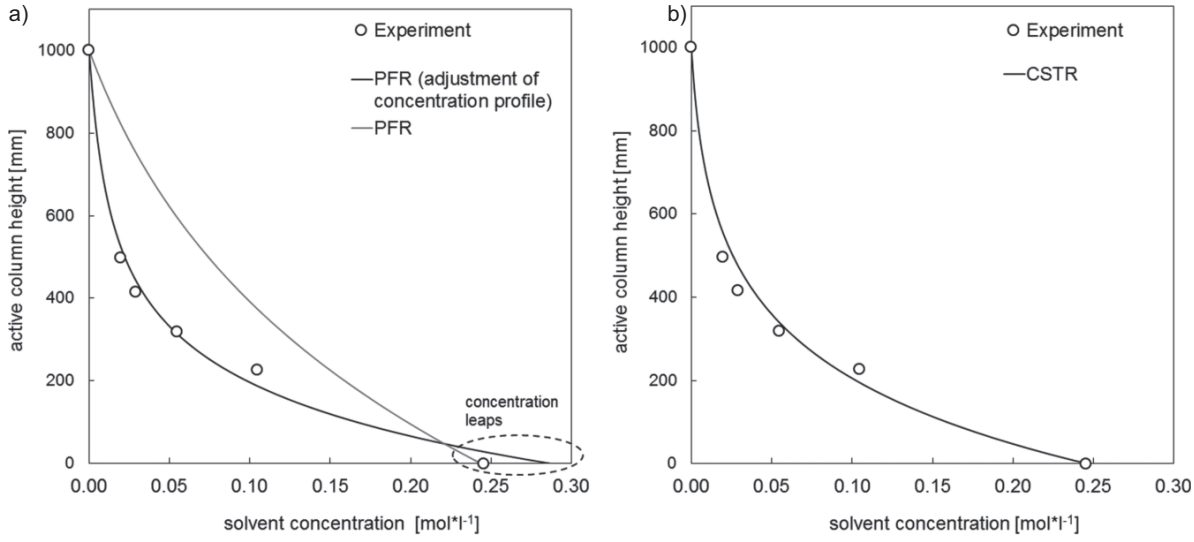

Figure 6. Experiment: $B = 20\ m^3m^{-2}h^{-1}$, $n = 380$ rpm, $w = 3$ wt %. (a) Concentration profile as calculated with the PFR design according to Eq. (7) compared with adjusted concentration profile and experiments; (b) concentration profiles as calculated with the CSTR cascade according to Eq. (19) compared with experiments.

correlations fit well to the experiments. The results of mass-transfer experiments in a pilot-plant scale TCDC100 confirm complete back-mixing in each compartment, best approached with the CSTR cascade model. The mass balance and concentration profile calculated with the CSTR design algorithm compare well with experimental data.

The authors have declared no conflict of interest.

Symbols used

A	[m^2]	mass-transfer area
a	[m^2m^{-3}]	specific mass transfer area
B	[$m^3m^{-2}h^{-1}$]	total hydraulic load
B_C	[m]	compartment width
c	[mol m^{-3}]	concentration
c^*	[mol m^{-3}]	equilibrium concentration
CS	[m^2]	cross-section area
D	[m]	column diameter
d	[m]	diameter
d_{32}	[m]	mean Sauter diameter
D_{ax}	[m^2s^{-1}]	axial dispersion coefficient
D_R	[m]	rotor disc diameter
D_S	[m]	stator disc diameter
D_{SH}	[m]	shaft diameter
F_A	[mol s^{-1}]	molar flow
F_V	[m^3s^{-1}]	volumetric flow
g	[m s^{-2}]	force of gravity, 9.81
H_{active}	[m]	active column height
H_C	[m]	compartment height
HDU	[m]	height of dispersion unit
HTU	[m]	height of one transfer unit
k''	[m s^{-1}]	overall mass transfer coefficient
n	[1 s^{-1}]	rotational speed
N_C	[–]	number of compartments
NTU	[–]	number of transfer units
r	[mol $m^{-3}s^{-1}$]	rate of reaction
r''	[mol $m^{-2}s^{-1}$]	rate of reaction
v	[m s^{-1}]	phase velocity
V_R	[m^3]	reactor volume

Greek symbols

α	[–]	distribution parameter
ε	[–]	extraction factor
φ	[–]	dispersed-phase hold-up
η	[Pa s]	dynamic viscosity
ρ	[kg m^{-3}]	density
σ	[kg s^{-2}]	surface tension

Subscripts

A	component A
c	continuous phase
d	dispersed phase
w	water
SST	ShellSol-T

Abbreviations

CSTR	continuously stirred tank reactor
PFR	plug flow reactor
RDC	rotating disc contactor
TCDC	Taylor-Couette disc contactor

References

[1] W. C. G. Kosters, *Handbook of Solvent Extraction*, Wiley, New York **1983**, 391–406.

[2] E. Müller, R. Berger, E. Blass, D. Sluyts, A. Pfennig, *Ullmann's Encyclopedia of Industrial Chemistry*, Vol. 21, Wiley-VCH, Weinheim **2008**, 250–300.

[3] E. Aksamija, *Ph.D. Thesis*, Graz University of Technology **2015**.

[4] K. Sattler, H. J. Feindt, *Thermal Separation Processes*, Wiley-VCH, Weinheim **1995**.

[5] S. Weiß, Berghoff, E. Grahn, G. Gruhn, M. Güsewell, W. Plötner, H. Robel, M. Schubert, *Verfahrenstechnische Berechnungsmethoden 2. Thermisches Trennen – Ausrüstungen und ihre Berechnung*, Wiley-VCH, Weinheim **1986**.

[6] S. Weiß, E. Militzer, K. Gramlich, *Thermische Verfahrenstechnik*. Brundstoffindustrie Leipzig, Leipzig **1993**.

[7] S. Z. Kagan, M. E. Aerov, T. S. Volkova, V. G. Trukhanov, *J. Appl. Chem. USSR* **1964**, *37*, 67–73.

[8] E. A. Fischer, *Verfahrenstechnik* **1971**, 360–365.

[9] A. Kumar, S. Hartland, *Can. J. Chem. Eng.* **1986**, *64*, 915–924. DOI: 10.1002/cjce.5450640605

[10] R. Marr, G. Husung, F. Moser, *Verfahrenstechnik* **1978**, *12*, 139–144.

[11] A. Kumar, S. Hartland, *Chem. Eng. Commun.* **1987**, *56*, 87–106. DOI: 10.1080/00986448708911939

[12] W. Späthe, D. Möhring, S. Weiss, *Verfahrenstechnik* **1976**, *10*, 567–571.

[13] A. G. Kasatkin, S. Z. Kagan, V. G. Trukhanov, *J. Appl. Chem.* **1962**, *35*, 1903–1910.

[14] A. Murakami, A. Misonou, K. Inoue, *Int. Chem. Eng.* **1978**, *18*, 16–22.

Chapter 5

Design Rules for the Taylor-Couette Disc Contactor

Chemie Ingenieur Technik Research Article 409

Design Rules for the Taylor-Couette Disc Contactor

Annika Grafschafter* and Matthäus Siebenhofer

DOI: 10.1002/cite.201600142

The Taylor-Couette disc contactor (TCDC) is a stirred liquid-liquid phase contactor which is suitable for applications in bioseparations. For liquid-liquid reactor design, information about the specific mass transfer area is inevitable. Therefore, the drop size distribution and holdup in the TCDC were investigated under various operating conditions and appropriate correlations for the prediction of these parameters have been determined. Experimental data of drop size distributions were correlated with lognormal, Gaussian, and Weibull drop size distribution functions.

Keywords: Correlation, Drop size distribution, Holdup, Sauter mean diameter, Taylor-Couette disc contactor

Received: September 30, 2016; *revised:* January 03, 2017; *accepted:* January 26, 2017

1 Introduction

Increasing scarcity of fossil resources and massive environmental degradation, e.g., global warming, are roughly summarized the main issues that have to be dealt with nowadays. To cope with these issues, a global change of raw materials from fossil to biogenic raw materials is inevitable. Evidently, biogenic raw materials do not show the same properties as fossil raw materials. During product isolation, downstream processing may suffer from poor economics due to highly diluted feed and low quality broths. Target constituents may suffer from deficiency in chemical and thermal stability, may be sensible to mechanical stress, and bio-based feedstock may contain a high amount of solids. Therefore, new separation technologies have to be developed or existing technologies need to be optimized and adapted to suffice the needs of biorefinery. Among existing technologies, solvent extraction and reactive extraction have been leading technologies to raise the economic feasibility of separation processes. They provide considerable potential for efficient and cost effective treatment and isolation of products [1, 2].

The pulp industry, for instance, has successfully applied solvent extraction for the separation of carboxylic acid from aqueous pulping residues. Nevertheless, nearly 50 % of the processed wood is finally used for steam production, with a significant loss of additional bulk products [1]. Process optimization may be obtained by combining isolation of carboxylic acids from pulp effluents by solvent extraction with reactive separation by esterification, addressing economics of isolation and the added value potential. Esterification can be accelerated by heterogeneous catalysis in the aqueous phase with the product being continuously transferred into the solvent phase.

However, integration of heterogeneously catalyzed esterification with extraction in a continuous process poses new requirements to the apparatus design. The Taylor-Couette disc contactor (TCDC), a stirred liquid-liquid phase contactor, has proven appropriate to meet the hydrodynamic requirements for the application in heterogeneously catalyzed reactions with liquid-liquid extraction [3]. The TCDC is particularly suitable for applications in reactive bioseparations since this type of contactor does not contain any installations which may provide dead zones for crud accumulation. In TCDC design, the continuous stirred-tank reactor (CSTR) cascade model has proven suitable [4]. Regardless whether the rate of reaction r_A'' of a simple solvent extraction (Eq. (1)) or of extraction with chemical reaction has to be applied for process and apparatus design, information about the specific mass transfer area a_s (Eq. (2)) is indispensable [5]. The specific mass transfer area provides information about the area available for mass transfer and affects the overall mass transfer coefficient k'' and thus the rate of reaction r_A''. The specific mass transfer area can be determined via the dispersed-phase holdup φ and Sauter mean diameter d_{32} (Eq. (3)) or by the drop size distribution.

$$-r_A'' = k''(c_A - c_A^*) \tag{1}$$

$$\text{mass balance (CSTR):}\quad F_{A,0} = F_A - r_A'' a_s V_R \text{ and } F_{A,0} = F_V c_{A,0} \tag{2}$$

Annika Grafschafter, Prof. Dr. Matthäus Siebenhofer
a.grafschafter@tugraz.at
Graz University of Technology, Institute of Chemical Engineering, Environmental Technology, Inffeldgasse 25C, 8010 Graz, Austria.

$$a_s = 6\frac{\varphi}{d_{32}} \quad (3)$$

However, the Sauter mean diameter is an approximate average value of the drop size distribution. Information about the drop size distribution may therefore be more useful, since it is possible to consider several drop size classes. Several distribution functions are available for prediction of the drop size distribution in liquid-liquid stirred systems. For instance, Hematti et al. [6] have shown that drop size distribution in a perforated rotating disc contactor (PRDC) can be reproduced satisfactorily by normal and logarithmic normal (lognormal) probability distribution function.

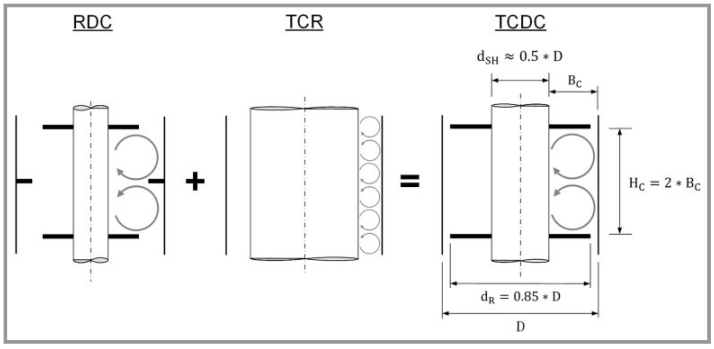

Figure 1. Comparison of RDC, TCR, and TCDC with design recommendations for the TCDC according to [7].

Since design rules for the prediction of hydrodynamics of TCDC contactors are still not available, this paper focuses on the forecast of drop size distribution, Sauter mean diameter, and dispersed-phase holdup. For sure, it is possible to gain these design data from computational fluid dynamics (CFD) with sufficient accuracy, but simulation is time consuming and therefore rather recommended for validation of process design. Correlations for drop size distribution, Sauter mean diameter, and holdup from dimensional analysis may offer quick access to reliable figures. For that purpose, the experimental data of drop size distribution for several operation modes were compared with the lognormal, Gaussian, and Weibull probability distribution functions. Parameters for the prediction of the mean and the variance of the probability distribution functions as well as the Sauter mean diameter were then determined via dimensional analysis. The dispersed-phase holdup under various operation conditions was experimentally investigated and data were calculated via dimensional analysis.

1.1 Taylor-Couette Disc Contactor

The TCDC is a stirred liquid-liquid extraction column with a simple design of internals. From the hydrodynamic point of view, it is a combination of the rotating disc contactor (RDC) and the Taylor-Couette reactor (TCR). The column internals of the TCDC are similar to that of the RDC but without stator rings and with increased shaft and disc diameter. A recommendation for the design of internals [7] is shown in Fig. 1. The increased shaft diameter, together with the increased disc diameter, induces a similar flow pattern to banded two-phase flow of the Taylor-Couette reactor. Compared with state of the art liquid-liquid phase contactors such as the RDC, the TCDC design prevents from formation of hydrodynamic dead zones, crud accumulation, and fouling at the shaft as well as the shell. The increased rotor discs form compartments in the column with dynamic stabilization of the flow pattern. Due to the simple design, smooth energy input, and operating flexibility by rotating discs, the TCDC offers promising operation features for successful application in biorefinery [7, 8].

2 Experimental Setup and Procedure

Data of the drop size distribution, Sauter mean diameter [7, 8], and dispersed-phase holdup were determined in a 100 mm diameter pilot plant scale TCDC100. The design data of the TCDC100 are: active column height $H_{Active} = 1$ m, column diameter $D = 0.1$ m, shaft diameter $d_{SH} = 0.05$ m, rotor diameter $d_R = 0.085$ m, and compartment height $H_C = 0.05$ m. The experiments were performed in dual-phase operation without mass transfer with the system ShellSol T (SST)-water. SST was used as dispersed phase with a phase ratio to water of 1. The physical properties of the binary system are shown in Tab. 1.

Table 1. Physical properties of the binary system.

	Density [kg m^{-3}]	Kinematic viscosity [m^{2}s^{-1}]
ShellSol T (dispersed)	756.8	$1.85 \cdot 10^{-6}$
Deionized water (continuous)	998.1	$1.102 \cdot 10^{-6}$

The drop size distribution was monitored at varying rotational speed (250, 350, 450, and 500 rpm) and constant total hydraulic load $B = 20$ m^{3}m^{-2}h^{-1}, and at varying total hydraulic load (10, 15, 20, and 25 m^{3}m^{-2}h^{-1}) and constant rotational speed of 450 rpm with an optical probe (SOPAT GmbH). The graphic record evaluated 2500 droplets per experiment [8]. The averaged phase holdup was determined at varying the rotational speed (0 to 600 rpm) and the total hydraulic load (20 to 35 m^{3}m^{-2}h^{-1}) by monitoring the static pressure.

Chemie Ingenieur Technik Research Article 411

3 Results and Modeling

The main target was to develop correlations for the drop size distribution (DSD), Sauter mean diameter, and dispersed-phase holdup in the TCDC. The DSD and holdup are inevitably needed for the design of liquid-liquid contactors. The main challenge in generating these correlations is the variety of influence factors. DSD and holdup depend on the apparatus geometry, rotational speed of impellers, physical properties of the liquids, and volume flow rate. Several correlations [9 – 11], originally developed for the prediction of the Sauter mean diameter and dispersed-phase holdup in RDC columns, have successfully been modified to the needs of TCDC columns [4]. For instance, the Sauter mean diameter was predicted with an average absolute relative error (AARE) of 10.1 % for the correlation of Fischer [9] and 11.2 % for the correlation of Marr [10]. However, the modified correlations do not consider the influence of the increased shaft diameter of the TCDC, but the effect of the shaft on DSD and holdup cannot be neglected. Therefore, the DSD and holdup in the TCDC were investigated in detail and appropriate correlations for the prediction of DSD, Sauter mean diameter, and dispersed-phase holdup have been determined.

3.1 Correlations for Drop Size Distribution and Sauter Mean Diameter

Fig. 2a shows the cumulative drop size distribution Q_3 for constant hydraulic load and varying rotational speed. As expected, DSD shifts towards smaller diameters with increasing rotational speed. Fig. 2b depicts the cumulative distribution Q_3 at varying hydraulic load and constant rotational speed of 450 rpm. In column type liquid-liquid contactors, the influence of varying hydraulic load on drop size distribution is very low [6] and can therefore be neglected.

The measurement data of the DSD at varying rotational speed and constant hydraulic load were compared with three probability distribution functions as listed in Tab. 2.

In these functions, x is the drop diameter and a and b are parameters representing the variance and the mean of the DSD. For each DSD function, the parameters were calculated by fitting to the experimental data with the software TableCurve. The values of the parameters at varying rotational speed are summarized in Tab. 3.

The parameters a and b in each distribution function correlate linearly with the rotational speed. Representatively, the parameter plot for the lognormal distribution function is shown in Fig. 3.

For the analytical correlation of parameters on a physical background, the design data, the physical properties of the system, and the operation parameters, which may affect the DSD function, have been considered according to Eqs. (4) and (5). In these equations, ρ is the density, η the dynamic viscosity of the two liquids (index c means continuous, d means dispersed), σ the surface tension, n the rotational speed and $g\Delta\rho$ the specific gravity. As already mentioned, the influence of the hydraulic load on drop size distribution can be neglected.

$$a = f(d_R, D, d_{SH}, H_C; n; \rho_c, \rho_d, \eta_c, \eta_d, \sigma; g\Delta\rho) \quad (4)$$

$$b = f(d_R, D, d_{SH}, H_C; n; \rho_c, \rho_d, \eta_c, \eta_d, \sigma; g\Delta\rho) \quad (5)$$

By applying dimensionless analysis [12], the fit parameters a and b correlate with the design data, operation data, and physical properties according to Eqs. (6) and (7), whereby D, d_R, d_{SH}, and H_C and the physical properties ρ_d, ρ_c, η_d, and η_c were held constant.

$$a = A\left[G\left(\frac{d_R^2 g\Delta\rho}{\sigma}\right)^{c_1}\right]n + d \quad (6)$$

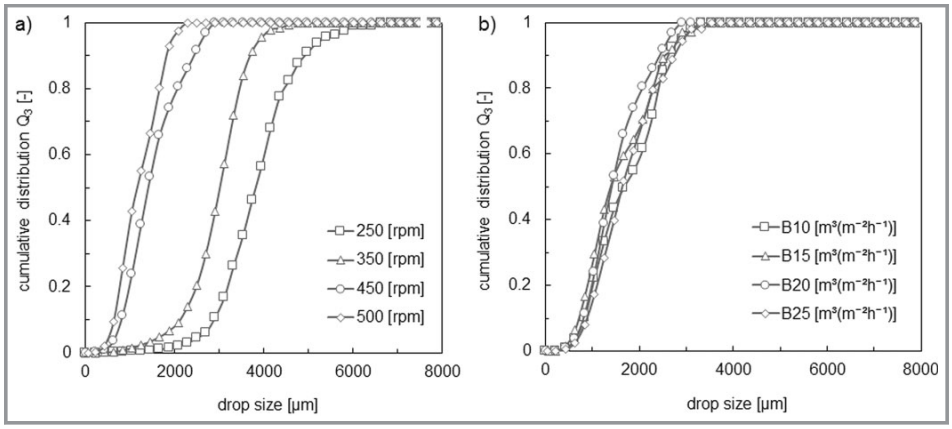

Figure 2. a) Cumulative drop size distribution Q_3 for constant hydraulic load $B = 20\ m^3m^{-2}h^{-1}$ and varying rotational speed, (b) cumulative drop size distribution Q_3 for constant rotational speed $n = 450$ rpm and varying hydraulic load [7].

Table 2. Probability distribution functions.

Name	Function	Parameter
Lognormal	$q_3(x) = \frac{1}{xa\sqrt{2\pi}} \exp\left[-\frac{\ln\left(\frac{x}{b}\right)^2}{2a^2}\right]$	$a > 0$ $b \in R$ $x \in (0, \infty)$
Gaussian (normal)	$q_3(x) = \frac{1}{xa\sqrt{2\pi}} \exp\left[-\frac{(x-b)^2}{2a^2}\right]$	$a > 0$ $b > 0$ $x \in (0, \infty)$
Weibull	$q_3(x) = \frac{a}{b}\left(\frac{x}{b}\right)^{a-1} \exp\left[-\left(\frac{x}{b}\right)^a\right]$	$a > 0$ $b > 0$ $x \in (0, \infty)$ and $x \geq 0$

Table 3. Fit parameters for variance and mean of the DSD at different rotational speed in the TCDC100.

n [rpm]	Lognormal		Gaussian		Weibull	
	a	b	a	b	a	b
250	0.20	3829.18	746.45	3783.45	5.72	3996.35
350	0.31	3122.49	645.39	2951.53	4.83	3201.94
450	0.38	1579.94	544.33	1620.05	3.29	1611.86
500	0.47	1195.31	493.80	1140.00	2.54	1367.03

$$b = A\left[G\left(\frac{d_R^2 g \Delta\rho}{\sigma}\right)^{c_1}\right] n + d \tag{7}$$

The values of the parameters A and d and the exponent c_1 for the investigated distribution functions at varying rotational speed are summarized in Tab. 4. The constant $G = 0.41$ comprises the dimensionless geometric data D/d_R, d_{SH}/d_R, and H_C/d_R of the TCDC column and the physical data ρ_d/ρ_c and η_d/η_c of the system SST-water.

The experimentally determined drop size histogram was compared with the analytical DSD functions evaluated with the calculated fit parameters a and b. A representative operating point at 250 rpm in Fig. 4 depicts the results.

To validate the accuracy of the predicted DSD functions, the Sauter mean diameter d_{32} was calculated according to Eqs. (8) and (9) in which ψ is the sphericity of the droplets and a_v is the volume-based area of the droplets. The droplets where assumed to be spheres and thus $\psi = 1$ [13].

$$a_v = 6\psi \int_{x_{min}}^{x_{max}} \frac{1}{x} q_3(x) \mathrm{d}x \tag{8}$$

$$d_{32} = \frac{6}{a_v}\psi \tag{9}$$

The results were compared with the experimentally obtained data of the Sauter mean diameter and the AARE was calculated. The results are summarized in Tab. 5. With an AARE of 7.7 %, the Weibull distribution function has proven most appropriate for representing the Sauter mean diameter in the TCDC. The lognormal distribution function shows an AARE of 11 % followed by the Gaussian distribution function with 14.1 %.

For direct prediction of the Sauter mean diameter, the column geometry, rotational speed, and physical properties of the system were also correlated. The relevance list for the prediction of the Sauter mean diameter is given in Eq. (10).

$$d_{32} = f(d_R, D, d_{SH}, H_C; \rho_c, \rho_d, \eta_c, \eta_d, \sigma; n; g\Delta\rho) \tag{10}$$

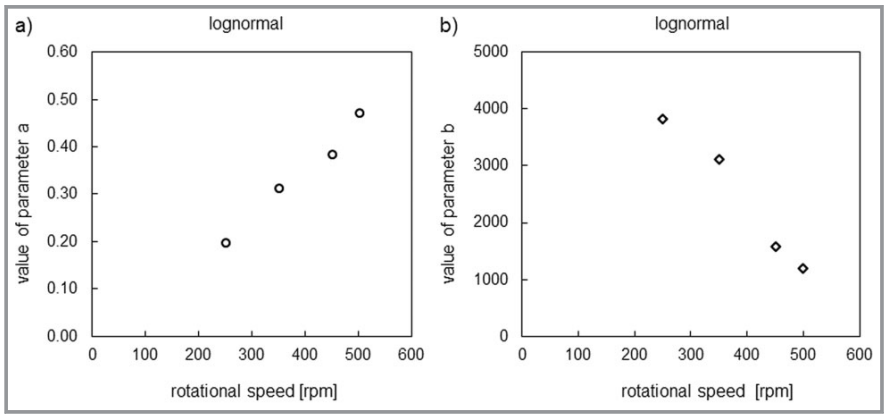

Figure 3. Parameter plot of the lognormal distribution function for different rotational speeds: a) parameter *a*, b) parameter *b*.

Table 4. Values of the constant parameters *A* and *d* and the exponent c_1 for the characteristic parameters *a* and *b* of the lognormal, Gaussian, and Weibull probability distribution functions.

	Lognormal		Gaussian		Weibull	
	a	*b*	*a*	*b*	*a*	*b*
A	0.06	−30.51	−7.40	−24.61	−0.30	−30.75
c_1	0.16	0.64	0.48	0.67	0.29	0.64
d	−0.06	6744.28	999.10	6591.90	9.10	6905.73

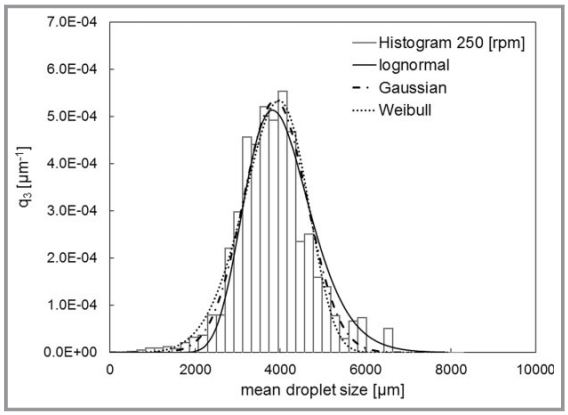

Figure 4. Experimental DSD at 250 rpm compared with lognormal, Gaussian, and Weibull distribution function, *a* and *b* calculated with the correlations Eqs. (6) and (7).

By applying dimensionless analysis, constant physical properties, and given geometry, the following correlation was determined:

$$\frac{d_{32}}{d_R} = AG\left(\frac{\sigma}{d_R^3\rho_c n^2}\right)^{c_1}\left(\frac{g\Delta\rho}{d_R\rho_c n^2}\right)^{c_2} = 2.28\cdot 0.41\left(\frac{1}{We}\right)^{0.56}\left(\frac{1}{Fr}\frac{\Delta\rho}{\rho_c}\right)^{0.35} \quad (11)$$

The constant *G* comprises again the dimensionless geometric data D/d_R, d_{SH}/d_R, and H_C/d_R of the TCDC column and the physical data ρ_d/ρ_c and η_d/η_c of the system SST-water. For varying rotational speed, the Sauter mean diameter was predicted with the proposed correlation with an AARE of 7.7 %. The results, summarized in Tab. 6, confirm that direct prediction of the Sauter mean diameter with the proposed correlation Eq. (11) is applicable.

Table 6. AARE of the Sauter mean diameter calculated with Eq. (11).

n [rpm]	Experiment	Proposed correlation	*AARE* [%]
	d_{32} [mm]	d_{32} [mm]	
250	3.6	3.7	1.4
350	2.7	2.0	26.6
450	1.3	1.3	0.1
500	1.0	1.0	2.8
Average			7.7

3.2 Correlation for Dispersed-Phase Holdup

Fig. 5 depicts the experimental data of the dispersed-phase holdup in the TCDC for different operation conditions. The holdup depends on the rotational speed and the hydraulic load of the dispersed phase and the continuous phase. The dispersed-phase holdup increases gradually up to 200 rpm with increasing rotational speed and constant hydraulic load. Between 200 rpm and at the flooding limit (marked as crosses in Fig. 5), the holdup increases significantly. With higher dispersed-phase flow rate, the holdup shows higher values at the same rotational speed and the flooding point is reached at the same holdup values but lower rotational speed. The same effect can be observed with increased flow rate of the continuous phase. At the same total hydraulic load ($B = 30\ m^3m^{-2}h^{-1}$), the holdup values remain the same.

The dispersed-phase holdup is affected by the column geometry, rotational speed, the physical properties of the system, and the flow rate (velocity) of both phases. For the analytical correlation of the holdup, the design data of the column, the physical properties of the system, and the oper-

Table 5. AARE of the Sauter mean diameter calculated for lognormal, Gaussian, and Weibull probability distribution functions.

n [rpm]	Experiment	Lognormal		Gaussian		Weibull	
	d_{32} [mm]	d_{32} [mm]	*AARE* [%]	d_{32} [mm]	*AARE* [%]	d_{32} [mm]	*AARE* [%]
250	3.6	3.9	7.9	3.7	3.2	3.6	0.2
350	2.7	2.7	1.0	2.6	3.7	2.5	7.5
450	1.3	1.6	28.1	1.3	4.3	1.4	12.2
500	1.0	1.1	6.8	0.6	45.2	0.9	10.9
Average			11.0		14.1		7.7

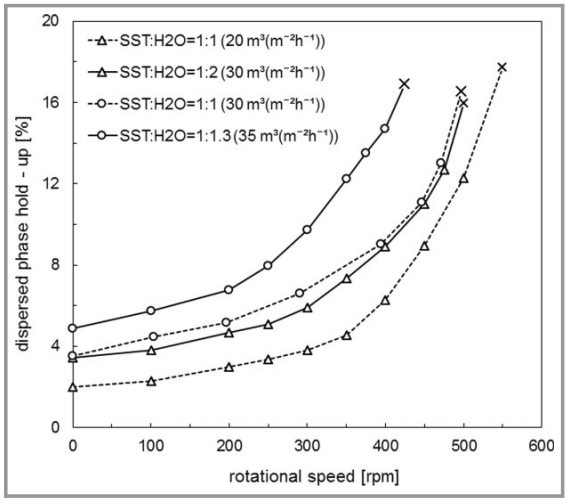

Figure 5. Dispersed-phase holdup for different hydraulic loads of the dispersed phase (B_d = 10–15 $m^3m^{-2}h^{-1}$) and the continuous phase (B_c = 10–20 $m^3m^{-2}h^{-1}$); total hydraulic load B = 20–35 $m^3m^{-2}h^{-1}$.

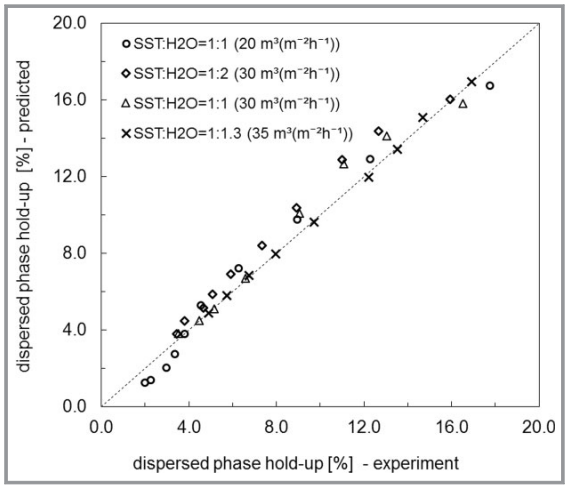

Figure 6. Predicted dispersed-phase holdup, using the proposed correlation Eq. (13), compared with experimental results.

ation parameters, which may affect the holdup, have been considered according to Eq. (12).

$$\varphi = f(d_R, D, d_{SH}, H_C; \rho_c, \rho_d, \eta_c, \eta_d, \sigma; n; g\Delta\rho; v_c, v_d) \tag{12}$$

By applying dimensionless analysis, the factors were made dimensionless, resulting in Eq. (13):

$$\varphi = G\left[C_1 + C_2\left(\frac{(v_c + v_d)}{d_R n}\right)^3\right]\left(\frac{1}{We}\right)^{0.673}\left(\frac{1}{Fr}\frac{\Delta\rho}{\rho_c}\right)^{-2.177} \tag{13}$$

The constant G (G = 0.41) comprises again the dimensionless geometric data D/d_R, d_{SH}/d_R, and H_C/d_R of the TCDC column and the physical data ρ_d/ρ_c and η_d/η_c of the system SST-water.

For low hydraulic load ($5.5 \cdot 10^{-3} < (v_c + v_d) < 9.7 \cdot 10^{-3}$ m s^{-1}), C_1 = 4.529 and $C_2 = 1.110 \cdot 10^6$ and for high hydraulic load ($(v_c + v_d) \geq 9.7 \cdot 10^{-3}$ m s^{-1}), C_1 = 7.162 and $C_2 = 8.990 \cdot 10^5$. The results depicted in Fig. 6 confirm that the predicted data, using the proposed correlation Eq. (13), agrees well with the experimental results.

4 Conclusions

The TCDC is intended to suffice the needs of harsh operation conditions in liquid-liquid phase contact, such as high particle load in the feed and three phase (liquid-liquid-solid) contact in liquid-liquid extraction with chemical reaction. For apparatus design, in mass transfer with chemical reaction, the specific mass transfer area a_s and the dispersed-phase holdup φ are needed. Experimental data of the drop size distribution and the Sauter mean diameter were therefore compared with lognormal, Gaussian, and Weibull drop size distribution functions. The characterizing parameters of these functions, representing mean and variance of the probability distribution functions, were determined, and via dimensional analysis correlations for the prediction of the parameters were derived. The Sauter mean diameter of the predicted drop size distribution correlates well with the experimentally obtained data. An empirical correlation for direct prediction of the Sauter mean diameter was also developed. The dispersed-phase holdup was investigated in detail for different operation conditions, and an empirical correlation for the prediction of the holdup was developed. The outcome of this investigation provides a simple tool for the basic design of the TCDC.

Symbols used

a	[–]	parameter representing the variance of the drop size distribution
a_s	[m^2m^{-3}]	specific mass transfer area
A	[–]	parameter
a_v	[m^2m^{-3}]	volume-based area of droplets
b	[–]	parameter representing the mean of the drop size distribution
B	[$m^3m^{-2}h^{-1}$]	total hydraulic load
B_C	[m]	compartment width
B_c	[$m^3m^{-2}h^{-1}$]	hydraulic load of the continuous phase
B_d	[$m^3m^{-2}h^{-1}$]	hydraulic load of the dispersed phase
c	[mol m^{-3}]	concentration
c^*	[mol m^{-3}]	equilibrium concentration
c_1, c_2	[–]	parameter
C_1, C_2	[–]	parameter
d	[–]	parameter
D	[m]	column diameter

d_{32}	[m]	Sauter mean diameter
d_R	[m]	rotor disc diameter
d_{SH}	[m]	shaft diameter
F	[mol s^{-1}]	molar flow
F_V	[$m^3 s^{-1}$]	volumetric flow
Fr	[–]	Froude number, $d_R n^2/g$
g	[m s^{-2}]	force of gravity, 9.81
G	[–]	constant
H_{Active}	[m]	active column height
H_C	[m]	compartment height
k''	[m s^{-1}]	overall mass transfer coefficient
n	[s^{-1}]	rotational speed
q_3	[μm^{-1}]	probability distribution
Q_3	[–]	cumulative distribution
r''	[mol $m^{-2} s^{-1}$]	rate of reaction
v	[m s^{-1}]	superficial-phase velocity
V_R	[m^3]	reactor volume
We	[–]	Weber number, $d_R^3 \rho_c n^2/\sigma$
x	[m]	drop diameter

Greek symbols

η	[Pa s]	dynamic viscosity
ρ	[kg m^{-3}]	density
$\Delta\rho$	[kg m^{-3}]	density difference between liquid phases
σ	[kg s^{-2}]	surface tension
φ	[–]	dispersed-phase holdup
ψ	[–]	sphericity

Subscripts

0	initial
A	component A
c	continuous phase
d	dispersed phase

Abbreviations

AARE	average absolute relative error
CFD	computational fluid dynamics
CSTR	continuous stirred-tank reactor
DSD	drop size distribution
PRDC	perforated rotating disc contactor
RDC	rotating disc contactor
SST	ShellSol T
TCDC	Taylor-Couette disc contactor
TCR	Taylor-Couette reactor

References

[1] M. Hundt, *Ph.D. Thesis*, Brandenburg University of Technology Cottbus-Senftenberg **2015**.

[2] D. Cascaval, A.-I. Galaction, *Hem. Ind.* **2004**, *58 (9)*, 375 – 386. DOI: 10.2298/HEMIND0409375C

[3] D. Painer, S. Lux, A. Grafschafter, A. Toth, M. Siebenhofer, *Chem. Ing. Tech.* **2017**, *89 (1 – 2)*, 161 – 171. DOI: 10.1002/cite.201600090

[4] A. Grafschafter, E. Aksamija, M. Siebenhofer, *Chem. Eng. Technol.* **2016**, *39 (11)*, 2087 – 2095. DOI: 10.1002/ceat.201600191

[5] O. Levenspiel, *Chemical Reaction Engineering*, John Wiley & Sons, Hoboken, NJ **1999**.

[6] A. Hemmati, M. Torab-Mostaedi, M. Shirvani, A. Ghaemi, *Chem. Eng. Res. Des.* **2015**, *96*, 54 – 62. DOI: 10.1016/j.cherd.2015.02.005

[7] E. Aksamija, *Ph.D. Thesis*, Graz University of Technology **2015**.

[8] E. Aksamija, C. Weinländer, R. Sarzio, M. Siebenhofer, *Sep. Sci. Technol.* **2015**, *50 (18)*, 2844 – 2852. DOI: 10.1080/01496395.2015.1085406

[9] E. A. Fischer, *Verfahrenstechnik* **1971**, *5 (9)*, 360 – 365.

[10] R. Marr, G. Husung, F. Moser, *Verfahrenstechnik* **1978**, *12 (3)*, 139 – 144.

[11] A. Kumar, S. Hartland, *Chem. Eng. Commun.* **1987**, *56 (1 – 6)*, 87 – 106. DOI: 10.1080/00986448708911939

[12] M. Zlokarnik, *Rührtechnik*, Springer, Heidelberg **1999**.

[13] J. Draxler, M. Siebenhofer, *Verfahrenstechnik in Beispielen*, Springer Vieweg, Wiesbaden **2014**.

Chapter 6

Hydraulics and Operation Performance of TCDC-Extractors

864 Research Article Chemie Ingenieur Technik

Hydraulics and Operation Performance of TCDC-Extractors

Annika Grafschafter*, Georg Rudelstorfer, and Matthäus Siebenhofer

DOI: 10.1002/cite.201800031

The Taylor-Couette disc contactor (TCDC) uses the hydrodynamic advantages of the rotating disc contactor (RDC) and Taylor-Couette reactor. Drop size distribution, dispersed phase holdup and residence time distribution (RTD) of the TCDC in 0.1 m and 0.3 m diameter scale were determined. A correlation for the prediction of the Sauer mean diameter was validated experimentally for 0.3-m scale. Analysis of RTD suggests application of the tank-in-series model. The number of vessels in series rises with increasing hydraulic load and decrease with increasing rate of rotation. The axial dispersion coefficient was determined in order to evaluate backmixing.

Keywords: Dispersed phase holdup, Drop size distribution, Residence time distribution, Taylor-Couette disc contactor

Received: April 06, 2018; *accepted:* April 26, 2018

1 Introduction

The Taylor-Couette disc contactor (TCDC) is an agitated liquid-liquid extractor with simple construction of internals. Design specifications result from CFD simulations (Ansys Fluent) with the initial aim of optimizing and simplifying the design of internals of the rotating disc contactor (RDC). Experimentally validated CFD simulations predicted a geometric optimum for hydraulics (formation of stable toroidal vortexes) when stator rings were removed and the shaft diameter as well as rotor disc diameter were increased [1]. Increased rotor discs stabilize the toroidal vortexes in the single compartment. Without stator rings, crud accumulation and fouling along the active mixing zone of the column is avoided, and thus, harsh operation conditions are feasible. The increase of the shaft diameter up to an optimum ratio of $D/D_{Sh} = 0.5$ prevents formation of hydrodynamic dead zones along the shaft. For design and scale-up of RDC columns, the shaft diameter has not been taken into consideration in detail so far. Dead zones can be formed along the shaft for too small shaft diameters. The dispersed phase may prone to form a stable coalesced layer encircling the shaft, limiting phase contact and, thus, separation efficiency. In contrast, the increased shaft diameter of the TCDC prevents formation of hydrodynamic dead zones and induces banded two-phase flow, providing appropriate operation performance in liquid-liquid extraction. Banded two-phase flow is also observed in Taylor-Couette reactors, but the TCDC offers a much higher hydraulic capacity above $30\,m^3m^{-2}h^{-1}$. Thus, the TCDC becomes a combination of a rotating disc contactor and a Taylor-Couette reactor. [1 – 4]

For successful design and operation performance of agitated extraction columns, comprehensive knowledge of hydraulics is needed. Evaluation of hydrodynamics for different operation conditions is necessary since the design of agitated columns is not a straightforward process, particularly in scale-up.

The present work summarizes the results of experimental analysis of hydrodynamics, including drop size distribution, dispersed phase holdup and residence time distribution of TCDC extractors in 0.1 m and 0.3 m diameter scale. Hydraulics and operation performance were analyzed and compared for both scales and design recommendations for the prediction of Sauter mean diameter d_{32} were deduced.

2 Experimental Setup and Procedure

Hydraulics and operation performance of the TCDC were investigated in terms of drop size distribution (DSD), dispersed phase holdup (φ) and residence time distribution (RTD) in a pilot plant scale with a tower diameter of 0.1 m (TCDC100) and 0.3 m (TCDC300). The geometrical design specifications are listed in Tab. 1. Drop size distribution and dispersed phase holdup were determined for two-phase operation without mass transfer; RTD was measured in single-phase operation as well as two-phase operation. ShellSol T (SST)/water was used as test system for all experiments with SST as dispersed phase and water as continuous phase

Annika Grafschafter, Georg Rudelsdorfer,
Univ.-Prof. Dipl.-Ing. Dr. techn. Matthäus Siebenhofer
a.grafschafter@tugraz.at
Graz University of Technology, Institute of Chemical Engineering and Environmental Technology, Inffeldgasse 25C, 8010 Graz, Austria.

Chemie Ingenieur Technik Research Article 865

in countercurrent operation. The physical key properties of the test system are summarized in Tab 2.

Table 1. Geometric design specifications of the TCDC100 and the TCDC300 column.

	TCDC100	TCDC300
H_{Active} [m]	1	1
D [m]	0.1	0.3
d_{SH} [m]	0.05	0.15
d_R [m]	0.085	0.255
H_C [m]	0.05	0.15
H_{Active}/D [–]	10	3.33
$N_{Compartment}$ [–]	20	6

Table 2. Physical properties of the test system.

	Kinematic viscosity [m^2s^{-1}]	Density [$kg\,m^{-3}$]
ShellSol T (dispersed)	$1.85 \cdot 10^{-6}$	756.8
Deionized water (continuous)	$1.102 \cdot 10^{-6}$	998.1

Equal power per volume (P/V) in both columns provides comparability of operation conditions and energy input. The rate of rotation for the TCDC300 was calculated according to Eq. (1), based on the rate of rotation of the TCDC100 ($n_{TCDC100}$) and the rotor disc diameters ($D_{R,TCDC100}$, $D_{R,TCDC300}$).

$$n_{TCDC300} = n_{TCDC100}\left(\frac{D_{R_{TCDC100}}}{D_{R_{TCDC300}}}\right)^{\frac{2}{3}} \quad (1)$$

The influence of the hydraulic load on DSD, RTD and φ was determined for both columns. For this purpose, the volumetric flow rate of the dispersed and the continuous phase were adjusted to ensure same total hydraulic load B ($m^3m^{-2}h^{-1}$) related to the free net cross-sectional area of the column (column cross section minus shaft cross section).

2.1 Drop Size Distribution

The drop size distribution was monitored with an optical probe (SOPAT GmbH). The probe consists of an endoscope with an integrated camera and a triggered flash light system. For evaluating DSD along the active column height, measurements were performed at three levels along the column height, as shown in Fig. 1. Measurement level 1 was located in a lower toroidal vortex (lower area) of one compartment, measurement level 2 at the shear interface of the two toroidal vortexes and measurement level 3 in an upper toroidal vortex (upper area) of one compartment. DSD and d_{32} were evaluated with an automated pattern matching algorithm provided by SOPAT GmbH.

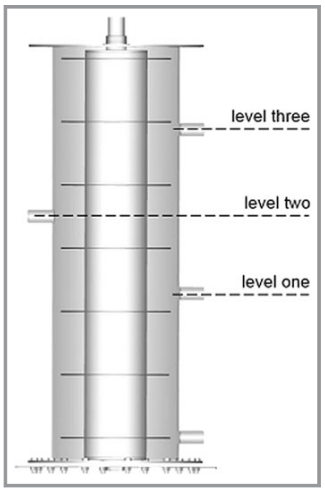

Figure 1. Measurement points along the active column height of the TCDC300.

DSD investigation in the TCDC300 was performed for varying total hydraulic load (10, 15, 20, and 25 $m^3m^{-2}h^{-1}$) with constant phase ratio of aqueous phase to solvent phase w/o = 1 and varying rate of rotation (121, 170, 218, 242 and 280 rpm). The results were compared with DSD data in the TCDC100 [2, 4]. The column start-up was investigated for the TCDC300 by recording d_{32} from $t_{start} = 0$ min to $t_{end} = 115$ min.

2.2 Holdup

The static pressure method was utilized for determining the mean dispersed phase holdup (φ). Therefore, the height of the continuous phase, the height of the interfacial area (mixed phase) and the overall height in steady state operation were measured.

Holdup results of TCDC100 experiments [4] were extended, with a specific focus on the influence of the phase ratio on the holdup. The holdup in the TCDC100 was measured at two different total hydraulic loads B (20 and 35 $m^3m^{-2}h^{-1}$), varying phase ratios w/o (0.5, 0.67, 1, 1.5, 2) and varying rate of rotation (0, 100, 200, 300, 400, 450, 500, 550 rpm, up to flooding limits).

Holdup in the TCDC300 was determined at varying rate of rotation (121, 170, 218, 242 and 280 rpm), varying total hydraulic load (10, 15, 20 and 25 $m^3m^{-2}h^{-1}$) as well as varying phase ratio w/o (0.5, 0.67, 1, 1.5, 2).

2.3 Residence Time Distribution

The residence time distribution was determined with a pulse signal by injecting 2 mL of saturated sodium chloride solution into the feed of the continuous phase (deionized water) at the top of the column. The electric conductivity was measured on four positions along the active column height via non-commercial probes [5, 6] with minimum

invasive impact to avoid disturbance of the flow pattern. Electrodes with tip sensors made of stainless steel wire (d_{Tip} = 0.6 mm) were used for this purpose. The operation conditions for the investigation of RTD in the TCDC100 and TCDC300 are listed in Tab. 3.

Results of the RTD were interpreted with the tank-in-series model and the dispersion model. The number of corresponding vessels in series N was calculated from the maximum of the dimensionless exit age distribution $E_{\theta,\max}$ according to Levenspiel [7]:

$$E_{\theta,\max} = \frac{N(N-1)^{N-1}}{(N-1)!} e^{-(N-1)} \quad (2)$$

A simplification of the basic version is proposed in [8]. The number of vessels N can be approached with Eq. (3) with sufficient accuracy:

$$N = -1.762 + 0.569\, E_{\theta,\max} + 6.206\, E_{\theta,\max}^2 \quad (3)$$

For comparison with the tank-in-series model the dispersion model with open-open boundary conditions (large deviation from plug flow $D_{ax}/uL > 0.01$) [7] was applied:

$$E_{\theta,oo} = \frac{1}{2}\sqrt{\frac{\bar{t}}{\pi\, t\left(\frac{D_{ax}}{uL}\right)}} \exp\left[-\frac{\bar{t}\left(1-\frac{t}{\bar{t}}\right)^2}{4\, t\left(\frac{D_{ax}}{uL}\right)}\right] \quad (4)$$

In Eq. (4), t represents the time, $\bar{t}$ the mean residence time and D_{ax}/uL the vessel dispersion number with D_{ax} as axial dispersion coefficient. The axial dispersion coefficient of the continuous phase $D_{ax,c}$ was calculated using Eq. (4).

3 Results

3.1 Drop Size Distribution

The effect of the operation parameters hydraulic load and rate of rotation on DSD and d_{32} in the TCDC300 was determined and compared with the data of TCDC100.

3.1.1 Effect of Measurement Level

Fig. 2 depicts the influence of the measurement level and positions on d_{32} in the TCDC300. Measurement level 2 yields lower d_{32} values than level 1 and 3. This is caused by higher shear and impact forces occurring at the contact area of the two toroidal vortexes. The results of measurement level 1 and 3 indicate decreasing d_{32} values with increasing column height, which corresponds well with real operation conditions.

3.1.2 Effect of Hydraulic Load

The influence of hydraulic load on DSD in the TCDC100 is nearly negligible [1, 4]. The minor effect of the hydraulic load on DSD was confirmed for the TCDC300. As shown in Fig. 3 d_{32} is independent of varying total hydraulic load at fixed rate of rotation. Fig. 3 also indicates a transition of

Table 3. Operation conditions for RTD experiments in the TCDC100 and TCDC300.

Operation mode	TCDC100			TCDC300		
	B [$m^3m^{-2}h^{-1}$]	n [rpm]	w/o [–]	B [$m^3m^{-2}h^{-1}$]	n [rpm]	w/o [–]
single-phase	10	250		5	121	
	15	300		10	170	
	20	400		15	218	
		500			242	
		600				
two-phase	20	250			121	
	25	300		15	170	
	30	400		20	218	
	35	500		25	242	
		600				
two-phase	20	400	0.5			
	25		0.67			
			1			
			1.5			
			2			

Chemie Ingenieur Technik

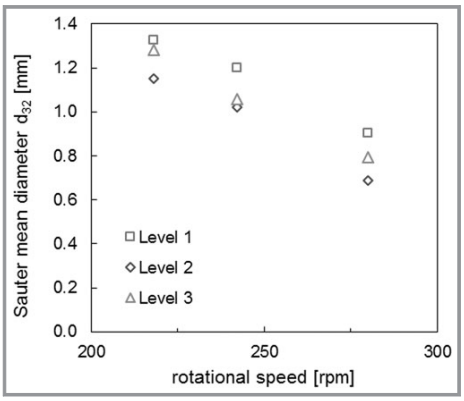

Figure 2. Effect of measurement levels on d_{32} in the TCDC300.

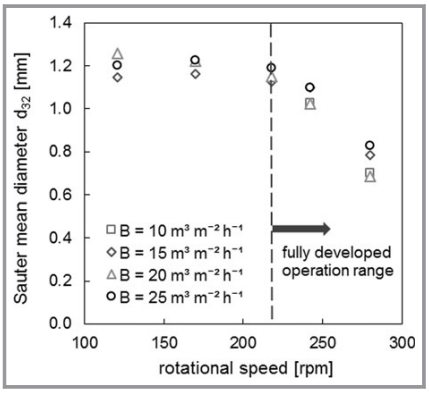

Figure 3. Effect of varying hydraulic load and rate of rotation on d_{32} in the TCDC100.

the flow regime with increasing rate of rotation. After exceeding a critical rate of rotation $n_{crit.} = 242$ rpm, significant droplet breakup is observed. Droplet breakup occurs because the force exerted by motion in the continuous phase overcomes the cohesive forces due to interfacial tension and dispersed phase viscosity. These operation conditions can be assumed as fully developed operation range. The operation range below 242 rpm is subcritical and may be classified as onset operation range.

3.1.3 DSD Comparison of the TCDC100 and the TCDC300

Fig. 4 shows the cumulative drop size distribution Q_3 for constant hydraulic load and varying rate of rotation in a) the TCDC100 [2] and b) the TCDC300. With increasing rate of rotation, DSD in the TCDC100 shift towards smaller droplet diameters. Compared to the TCDC300, the DSD in the TCDC100 shows a wider drop size range and higher d_{32} values at lower rate of rotation. Drop size range and d_{32} at low rate of rotation is smaller in the TCDC300, which is due to lower wall effects for larger column diameters. This was also reported for RDC operation by Marr et al. [9] who stated that in small-scale columns a significant amount of power is consumed in overcoming wall friction, resulting in larger droplet size range. At 450 and 500 rpm the TCDC100 shows same d_{32} values as observed in the TCDC300 at 121 to 242 rpm.

The experimentally obtained d_{32} data of the TCDC300 were compared with the correlation proposed in [4] (Eq. (5)) and the parameters for 0.3-m scale were adjusted (Tab. 4).

$$\frac{d_{32}}{d_R} = AG\left(\frac{\sigma}{d_R^3\rho_c n^2}\right)^{c_1}\left(\frac{g\Delta\rho}{d_R\rho_c n^2}\right)^{c_2} = AG\left(\frac{1}{We}\right)^{c_1}\left(\frac{1}{Fr}\frac{\Delta\rho}{\rho_c}\right)^{c_2} \quad (5)$$

The constant G includes the dimensionless geometric data D/d_R, d_{SH}/d_R and H_C/d_R of both columns and the physical property data ρ_d/ρ_c η_d/η_c of the system ShellSol T/water.

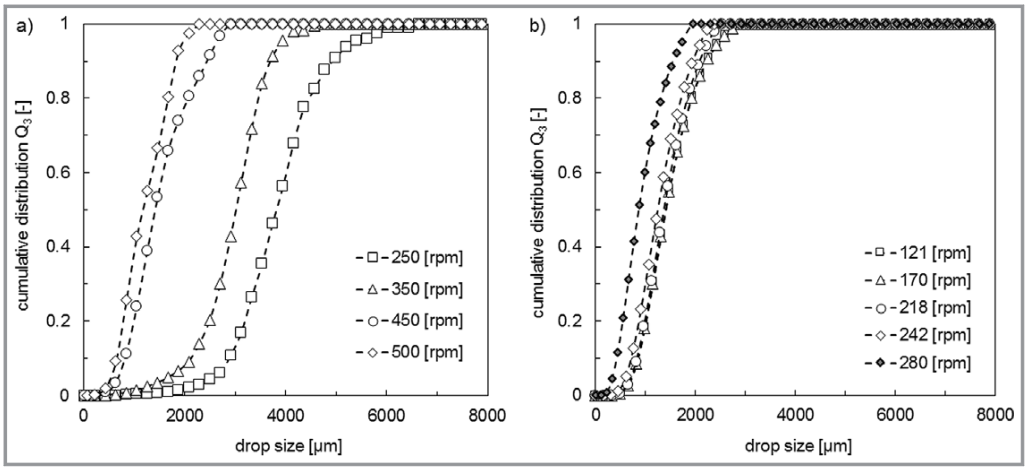

Figure 4. Comparison of the effect of varying hydraulic load and varying rate of rotation on DSD in the TCDC100 and TCDC300.

Table 4. Parameter values for prediction of d_{32} with Eq. (5) in the TCDC100 and TCDC300.

Parameter	TCDC100	TCDC300	
		onset	fully developed operation
A	2.28.	3.45	2.56
$c1$	0.56	0.67	0.59
$c2$	0.35	–0.57	0.39
G	0.41	0.39	0.39

At low rate of rotation, droplet breakup is controlled by the ratio of buoyancy to interfacial tension [10]. This ratio explains the deviating parameter values for the onset operation range of the TCDC300 compared to fully developed operation range and the parameter values of the TCDC100. Fig. 5 compares the predicted d_{32} data of the TCDC300 at varying rate of rotation with the experimental data. It is shown that the proposed correlation in Eq. (5) agrees well with the experimental results.

3.1.4 Start-up of the TCDC300

DSD during start-up of the TCDC300 was investigated at 242 rpm and a total hydraulic load of $B = 20\,m^3m^{-2}h^{-1}$. Sauter mean diameter d_{32} was evaluated from start-up time at $t = 0$ min until $t = 115$ min. After 5 min a constant d_{32} value was obtained. A leap of d_{32} from 1.3 mm to approximately 1 mm within the first measurement interval was observed.

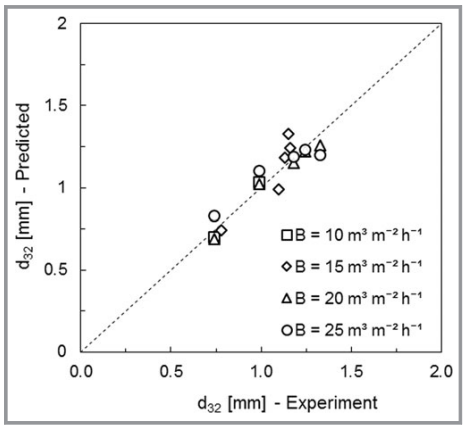

Figure 5. Predicted d_{32}, using the proposed correlation of Grafschafter et al. (Eq. (5)), compared with experimental results.

3.2 Dispersed Phase Holdup

The dispersed phase holdup was investigated for varying hydraulic load and varying phase ratio w/o in the TCDC100 and the TCDC300 extractor.

3.2.1 Effect of the Phase Ratio w/o on Dispersed Phase Holdup

Fig. 6 depicts the effect of varying phase ratio w/o on φ for low hydraulic load ($B = 20\,m^3m^{-2}h^{-1}$) and high hydraulic load ($B = 35\,m^3m^{-2}h^{-1}$) in the TCDC100. The influence of the w/o ratio on φ at low hydraulic load is negligible but at high hydraulic load the w/o ratio has a strong impact on φ. The holdup increases strongly with decreasing phase ratio, especially for w/o < 1 (the dispersed phase dominates). At low hydraulic load φ increases progressively up to about

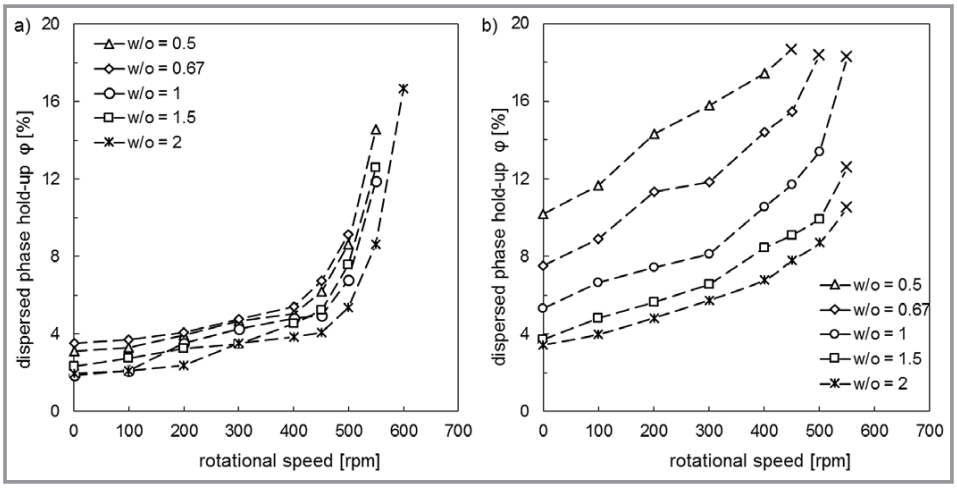

Figure 6. Effect of w/o ratio on φ for a) low hydraulic load ($B = 20\,m^3m^{-2}h^{-1}$) and b) high hydraulic load ($B = 35\,m^3m^{-2}h^{-1}$) in the TCDC100 at varying rate of rotation.

Chemie Ingenieur Technik Research Article

400 rpm with rising rate of rotation. When exceeding 400 rpm, a significant increase of holdup values was observed close to the flooding limits (marked as crosses). At high hydraulic load, the holdup approximately follows an exponential trend with increasing rate of rotation. No significant transition point was observed.

3.2.2 Comparison of Dispersed Phase Holdup of the TCDC100 and the TCDC300

A comparison of the dispersed phase holdup φ for the TCDC100 and the TCDC300 at a total hydraulic load of $B = 20\,m^3m^{-2}h^{-1}$ is shown in Fig. 7. For comparability, the holdup is plotted over power per volume (P/V values), for providing same specific power input for both columns. Compared to the TCDC100 the TCDC300 shows higher holdup values at same P/V.

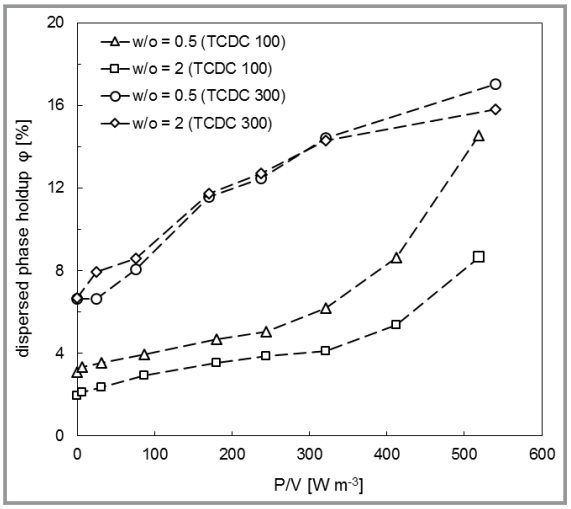

Figure 7. Comparison of φ in the TCDC100 and TCDC300 at $B = 20\,m^3m^{-2}h^{-1}$.

3.3 Residence Time Distribution

The residence time distribution was investigated for different total hydraulic load, different phase ratio w/o and varying rate of rotation in the TCDC100 and the TCDC300 extractor (see Tab. 3). Exemplarily, the E_θ curves for both column scales are shown in Fig. 8. Tailing of the RTD in the TCDC300 is more distinct compared to the TCDC100. The nonsymmetrical E_θ curves indicate large deviation from plug flow ($D/uL > 0.01$ or $Bo < 100$) in both columns, suggesting application of the tank-in-series model for RTD analysis.

The number of corresponding vessels N for the tank-in-series model can easily be evaluated via the maximum shape of the experimental RTD curves. The tank-in-series model can be used with any kind of kinetics and it can be applied to any arrangement of compartments (with or without recycle) [7]. For comparison $D_{ax,c}$ was as well deduced from the exit age distribution.

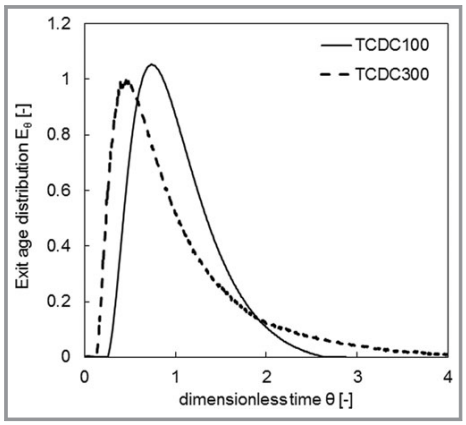

Figure 8. Exit age distribution E_θ for TCDC100 and TCDC300 at $B = 20\,m^3m^{-2}h^{-1}$ and $P/V = 240\,W\,m^{-3}$.

3.3.1 Effect of Hydraulic Load and Rate of Rotation (TCDC100)

The number of vessels N in series for single-phase and two-phase operation mode is displayed in Fig. 9a. Comparability between both operation modes is achieved by plotting N over the rate of rotation and the hydraulic load of the continuous phase B_c. With increasing hydraulic load, the number of vessels N in series increases. Higher rate of rotation leads to decreasing N due to higher axial dispersion. Compared to single-phase operation, two-phase operation engenders higher N and the effect of increasing hydraulic load is intensified. A maximum number of vessels N for single-phase and two-phase operation is obtained at $B = 40\,m^3m^{-2}h^{-1}$ ($B_c = 20\,m^3m^{-2}h^{-1}$ in single-phase operation) and $n = 250$ rpm.

The axial dispersion coefficient of the continuous phase $D_{ax,c}$ is shown in Fig 9b. $D_{ax,c}$ increases with rising rate of rotation. In single phase operation the effect of increasing hydraulic load on dispersion is negligible. Two-phase operation shows 2.5 times higher $D_{ax,c}$ values compared to single-phase operation. Furthermore, in two phase operation $D_{ax,c}$ increases more distinct with increasing rate of rotation.

The effect of varying phase ratio w/o on RTD was investigated for a total hydraulic load of $B = 20\,m^3m^{-2}h^{-1}$ and varying rate of rotation. The results are summarized in Fig. 10. High w/o values (w/o = 2) yield higher number of corresponding vessels and lower $D_{ax,c}$ values. With decreasing w/o ratio the number of vessels N in series is reduced and $D_{ax,c}$ values increase.

3.3.2 Comparison of TCDC100 and TCDC300

The number of corresponding vessels N in series for the TCDC100 and TCDC300 is displayed in Fig 11. RTD in the

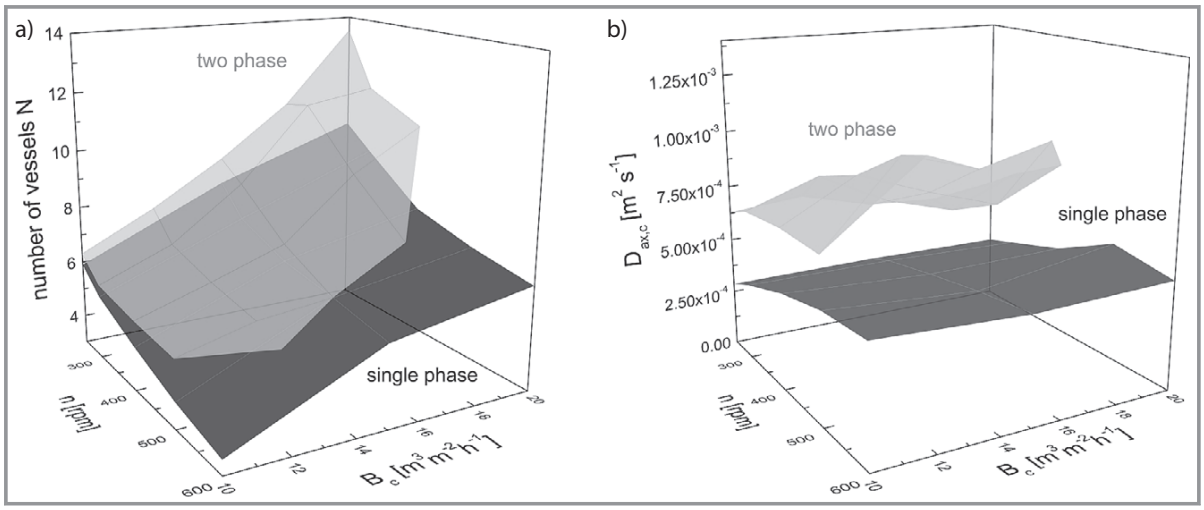

Figure 9. Results of single-phase and two-phase operation for varying hydraulic load and varying rate of rotation: a) number of corresponding vessels N in series, b) axial dispersion coefficient of continuous phase $D_{ax,c}$.

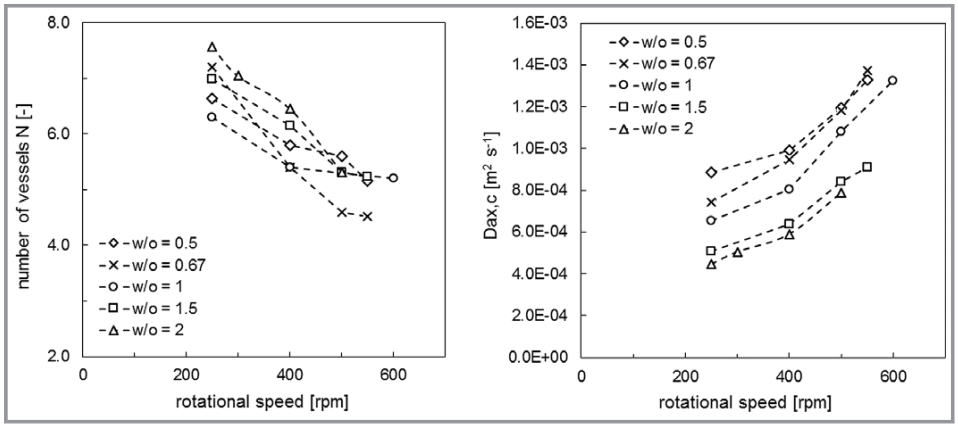

Figure 10. Effect of varying phase ratio w/o on RTD for total hydraulic load of $B = 20\,m^3m^{-2}h^{-1}$ and varying rate of rotation.

TCDC300 shows a less distinct dependency on varying hydraulic load and rate of rotation than in the TCDC100.

4 Conclusions

The Taylor-Couette disc contactor (TCDC), as evolved from CFD optimization of the RDC, has proven applicable for liquid-liquid extraction. Since TCDC design does not need stator rings, it is expected to be much less endangered of crud accumulation and fouling than conventional agitated extraction columns. The design of the TCDC follows simple rules, originating in Taylor-Couette reactors. Different to the Taylor-Couette reactor the energy transfer is intensified in the TCDC by rotor discs. Moreover, the TCDC design provides high hydraulic load.

Hydraulics and operation performance of the TCDC have been evaluated for 0.1 m and 0.3 m diameter scales. For hydrodynamic characterization the effect of the hydraulic load, rate of rotation and w/o ratio on drop size distribution, dispersed phase holdup and residence time distribution was investigated. The minimum rate of rotation necessary for formation of fully developed toroidal vortexes in a single compartment (fully developed operation range) can be predicted for specified operation conditions. Applicability of algorithms derived from 0.1-m scale has been validated experimentally for 0.3-m scale. Analysis of the residence time distribution of the continuous phase suggests application of the tank-in-series model. For given rate of rotation, the number of corresponding vessels in series increases with increasing hydraulic load. A reversed trend was observed for fixed hydraulic load and varying rate of

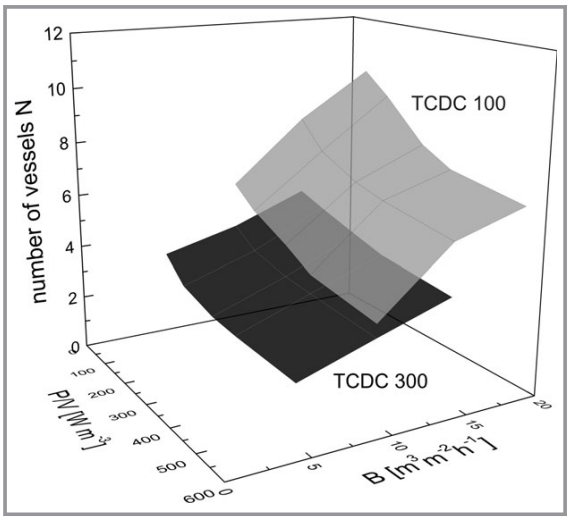

Figure 11. Comparison of the number of corresponding vessels *N* in series for the TCDC100 and the TCDC300.

rotation. Increasing rate of rotation will cause a drop of the number of corresponding vessels *N* in series.

The authors gratefully acknowledge the cooperation with SOPAT GmbH. Special thanks go to Georg Rudelsdorfer and Andreas Kottlan for column construction, Bettina Rauchdobler and Sebastian Pickl for test execution as well as Rene Fras for his excellent support in column construction.

Symbols used

A	[–]	parameter
B	[$m^3m^{-2}h^{-1}$]	total hydraulic load
B_c	[$m^3m^{-2}h^{-1}$]	hydraulic load of continuous phase
D	[m]	column diameter
D_{ax}	[m^2s^{-1}]	axial dispersion coefficient for flowing fluid
E_θ	[–]	dimensionless exit age distribution
d_{32}	[m]	Sauter mean diameter
d_R	[m]	rotor disc diameter
d_{SH}	[m]	shaft diameter
Fr	[–]	Froude number, $(d_R n^2)/g$
G	[–]	constant
g	[$m\,s^{-2}$]	gravity (9.81)
H_{Active}	[m]	active column height
H_c	[m]	compartment height
N	[–]	number of corresponding vessels in series
n	[s^{-1}]	rate of rotation (rotational speed)
Q_3	[–]	cumulative distribution
t	[s]	time
$\bar{t}$	[s]	mean residence time
V	[m^3]	volume
We	[–]	Weber number, $(d_R^3\rho_c n^2)/\sigma$

Greek symbols

η	[Pa s]	dynamic viscosity
ρ	[$kg\,m^{-3}$]	density
$\Delta\rho$	[$kg\,m^{-3}$]	density difference between liquid phases
σ	[$kg\,s^{-2}$]	surface tension
φ	[–]	dispersed phase holdup
θ	[–]	dimensionless time, $t/\bar{t}$

Subscripts

c	continuous phase
d	dispersed phase

Abbreviations

CFD	computational fluid dynamics
DSD	drop size distribution
RDC	rotating disc contactor
SST	ShellSol T
TCDC	Taylor-Couette disc contactor
TCR	Taylor-Couette reactor

References

[1] E. Aksamija, C. Weinländer, R. Sarzio, M. Siebenhofer, *Sep. Sci. Technol.* **2015**, *50 (18)*, 2844 – 2852. DOI: 10.1080/01496395.2015.1085406

[2] E. Aksamija, *Der Taylor-Couette Disc Contactor (TCDC); ein vereinfachtes und optimiertes Design von Drehscheibenextraktoren*, Ph.D. Thesis, Graz University of Technology **2015**.

[3] A. Grafschafter, E. Aksamija, M. Siebenhofer, *Chem. Eng. Technol.* **2016**, *39 (11)*, 2078 – 2095. DOI: 10.1002/ceat.201600191

[4] A. Grafschafter, M. Siebenhofer, *Chem. Ing. Tech.* **2017**, *4*, 409 – 415. DOI: 10.1002/cite.201600142

[5] T. Gurker, *Experimentelle Charakterisierung einer gerührten Extraktionskolonne und Vergleich mittels Computational Fluid Dynamics*, Ph.D. Thesis, Graz University of Technology **2010**.

[6] B. Preisack, *Aufbau und Inbetriebnahme einer 150 mm RDC Kolonne und Entwicklung eines Mess- und Auswertungssystems zur Ermittlung der Verweilzeitverteilung*, Master Thesis, Graz University of Technology, in preparation.

[7] O. Levenspiel, *Chemical Reaction Engineering*, Wiley, New York **1999**.

[8] G. Wendt, *Chem. Ing. Tech.* **1995**, *67 (10)*, 1356. DOI: 10.1002/cite.330671024

[9] R. Marr, G. Husung, F. Moser, *Verfahrenstech.* **1978**, *12 (3)*, 139 – 144.

[10] A. Kumar, S. Hartland, *Ind. Eng. Chem. Res.* **1996**, *35 (8)*, 2682 – 2695. DOI: 10.1021/ie950674w

Chapter 7

Continuous Multiphase Flow in the Taylor-Couette Disc Contactor

(Liquid-phase reaction with liquid-liquid extraction)

7. Continuous Multiphase Flow in the Taylor-Couette Disc Contactor[1]

(liquid-phase reaction with liquid-liquid extraction)

Abstract

Economic isolation of carboxylic acids from dilute aqueous effluents can be achieved by the combination of liquid-phase catalysed reaction with liquid-liquid extraction. Exemplarily the esterification of acetic acid with methanol, accelerated with a cation exchange resin, with simultaneous transfer of the product methyl acetate into the solvent biodiesel, was successfully performed in batch experiments. The experiments may serve as a first example for the demonstration of industrially relevant multiphase flow applications. Continuous multiphase flow was thus implemented in the Taylor-Couette Disc Contactor (TCDC). Applicability of multiphase flow was confirmed in lab scale, and detailed hydraulic investigations were performed.

1. Introduction

Global and sustainable implementation of biobased raw materials has become a high priority task. Unfortunately, downstream processing in the biobased industry often faces highly dilute multicomponent mixtures, making product isolation a challenge. For instance, black liquor condensate from pulping contains carboxylic acids at low concentration. Isolation of these low value constituents from aqueous effluents fails because state of the art downstream processes like distillation cannot achieve economic feasibility. Hence, nearly 50 % of the processed wood is finally used for steam production, with a significant loss of carboxylic acids as for example listed in Tab. 1 [1, 2].

[1] This chapter is intended for publication

Table 1: Total amount and composition of ingredients of black liquor beside lignin, as well as specific quantities of wood, pulp and black liquor [1]

Black liquor ingredients beside lignin	[m*m_{Wood}^{-1} %]:
Overall (Pine, Kraft - Process)	17
• Formic acid	16
• Acetic acid	11
• Glycolic acid	3
• Lactic acid	11
• 2-hydroxybutanoic acid	4
• 2.5-dihydroxyvaleric acid	3
• Glucoiso saccharini acid	39
• Xyloiso saccharin acid	4
• other	9
Specific quantities:	t
Pulp:	1
Wood:	2
Black liquor:	4

When talking about highly dilute carboxylic acids, process optimization can be obtained by properly chosen chemical conversion of acids by esterification combined with solvent extraction. Esters are important fine chemicals and have wide applicability in the industry and consumer applications [3-7]. *Berthelot and St. Gilles* [8] already studied esterification reactions in the year 1862 and found in general that esterification is an equilibrium reaction [6]. The interest in esterification reactions increases due to the fact that reaction yields of 100 % can theoretically be achieved when the products ester and water are removed as fast as they are formed [6].

Following this fundamental characteristic of equilibrium reactions suffices to indicate the potential for integrating such reactions into solvent extraction processes. Via continuous phase transfer of the product by solvent extraction, the limitation of single phase equilibrium conversion is shifted to the product side. The consecutive isolation of extracted esters by distillation will contribute to economically feasible whole-plant usage of renewable resources.

To proof the concept of chemical conversion with product separation by liquid-liquid extraction, several esterification experiments with simultaneous liquid-liquid extraction were performed in a batch reactor setup. Since esterification reactions are slow reactions, catalytic acceleration is essential. Homogeneous acid catalysts were

excluded, since they have several disadvantages as for instance corrosion problems, waste of catalyst and contamination of the product. However, the crucial drawback for using homogeneous catalysts is the huge energy consumption needed for separating the catalyst from the reaction broth [9]. Acceleration of esterification reactions with heterogeneous catalysts has found increasing interest especially for continuous operation, since they are easy to separate from the reaction broth via sedimentation [7, 9-10]. For this reason, the cation exchange resin Amberlyst15 was used for heterogeneous catalysis of esterification. Exemplarily the esterification of acetic acid (AA) with methanol (MeOH) with simultaneous transfer of the product methyl acetate into the solvent was investigated at 65 °C and 80 °C. In order to maintain process sustainability, biodiesel (FAME), provided by BDI – BioEnergy International GmbH, was used as solvent. For comparison of conversion esterification was performed without extraction at 65 °C too. The initial AA concentration was $c_{AA,0}$ = 120 g*L^{-1} and the mass fraction of the catalyst was 14 wt%. Fig. 1 presents the overall AA transfer at temperatures of 65 °C and at 80 °C and different phase ratio of w/o = 0.5 and w/o = 1 for esterification with MeOH and simultaneous product extraction. By simultaneous extraction of the product, the overall yield of AA transfer (acid extraction plus ester extraction) increased from 15 % to 32 % at same reaction temperature of 65 °C. The highest overall transfer yield of 37 % was obtained for the double amount of solvent to aqueous phase (w/o = 0.5). Several results of esterification experiments with methanol published in literature [3, 9, 14-15] show that higher temperature is favorable fo acceleration of the forward reaction. The positive effect of elevated temperature on conversion was not confirmed when extracting the product. 32 % of AA was converted at 65 °C while 29 % was converted at 80 °C. The reason for less conversion can be explained by the fact that with increasing temperature the water solubility of MeAc rises, and extraction efficiency drops, resulting in less conversion at 80 °C compared to conversion at 65 °C. Esterification with ethanol (EtOH) was investigated too and shows lower conversion of AA compared to esterification with MeOH. A comparison of AA esterification with and without liquid-liquid extraction is exemplarily shown in Fig. 2. The extracted amount of the respective product is listed in Tab. 2. Although esterification with EtOH shows lower conversion of AA, the extracted amount of EtAc is greater compared to MeAc due to the lower water solubility of EtAc. Kinetics of AA esterification with MeOH and EtOH can be

found in literature [7, 9, 11-12], and kinetics with ion-exchange resin catalysts is reported in [3, 12-15].

Table 2 – extracted amount of the respective esterification product

	Methyl Acetate (MeAc)	Methyl Acetate (MeAc)	Methyl Acetate (MeAc)	Ethyl Acetate (EtAc)
phase ratio / -	w/o = 1	w/o = 1	w/o = 0.5	w/o = 1
temperature / °C	65	80	65	65
time / h	6	6	6	6
extracted amount / g	11.7	11.0	15.5	17.8

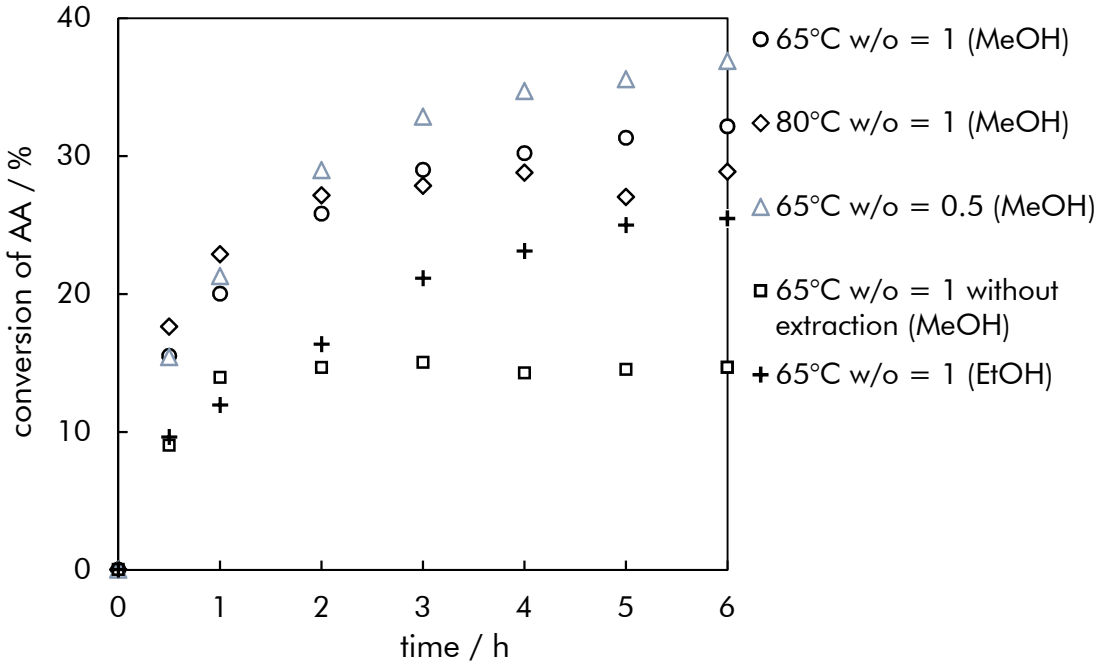

Figure 1 - Comparison of acetic acid (AA) conversion at: 65 °C and 80 °C, w/o = 0.5 and 1; methanol (MeOH) and ethanol (EtOH) were used as reactants

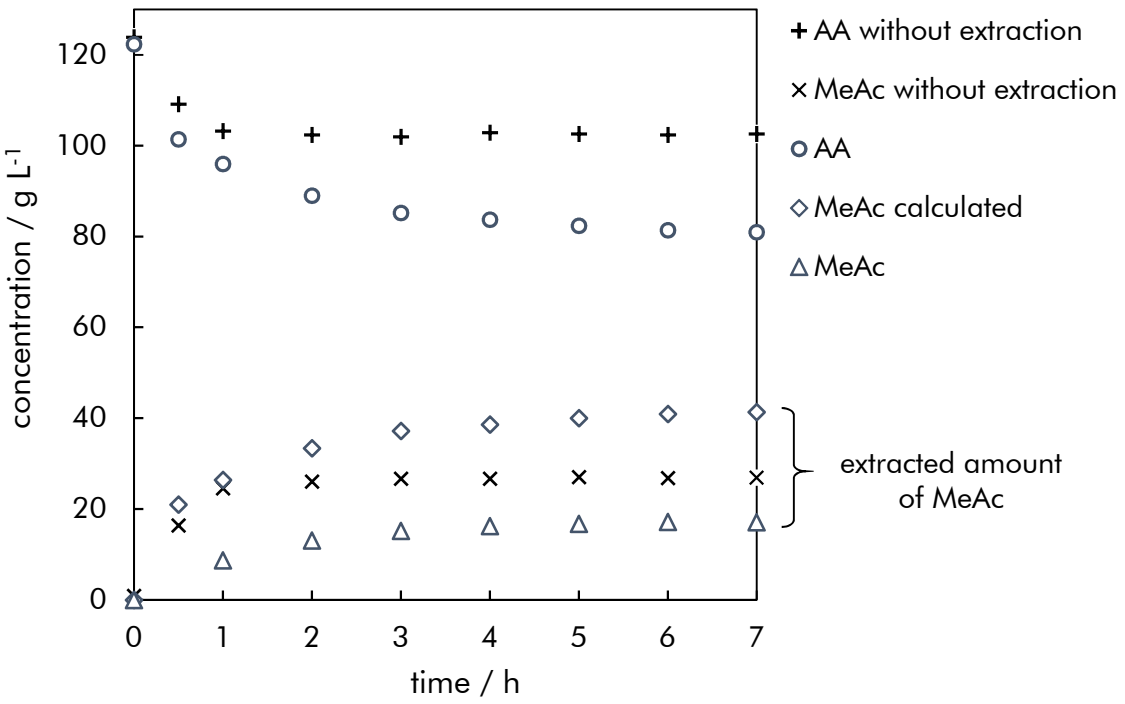

Figure 2 - Comparison of acetic acid (AA) and methyl acetate (MeAc) concentration with and without simultaneous methyl acetate (MeAc) extraction at 65 °C, m_{Cat} = 14 wt%, w/o = 1.

After the proof of concept of heterogeneously catalysed liquid-phase esterification in dilute aqueous carrier with liquid-liquid extraction, the technical needs for industrial implementation had to be solved, since industry does prefer continuous operation. The implementation of continuous multiphase flow (liquid-liquid-solid) requires adequate process and apparatus design. When focusing on column type extraction devices, the Taylor-Couette Disc Contactor (TCDC) [16, 17] satisfies the requirements of appropriate multiphase contact and simple phase separation. The TCDC is a stirred liquid-liquid extraction column with a simple design of internals. The design of internals does avoid formation of hydrodynamic dead zones for accumulation of solids and crud. The TCDC provides excellent mixing properties for liquid-liquid-solid (LLS) phase contact. The TCDC design is similar to the design of the Rotating Disc contactor (RDC), but with increased shaft and rotor disc diameter and without stator rings. The rotor discs separate the column into compartments, offering sufficient space for formation of two counter rotating toroidal vortexes in the single compartment. The vorticity of the toroidal vortexes depends on the rate of rotation of the shaft and the rotor discs. At convenient operation conditions, the shaft and rotor discs of the TCDC induce stable banded two phase flow

with appropriate mixing of the liquid phases and the solid catalyst phase, and sufficient residence time for the solid catalyst and the dispersed solvent in the single compartment.

This topic focuses on the implementation of continuous multiphase flow in the TCDC for combining heterogeneously catalysed esterification and solvent extraction. The hydraulic performance was investigated to collect data for modelling multiphase flow in the TCDC. In order to ensure comparability with hydraulic data gained from experiments in TCDC columns with 100 mm and 300 mm diameter [18-20], hydraulic investigation was also performed with ShellSol-T and deionized water. The operation range of the TCDC for liquid-liquid (LL) phase contact, including dispersed phase holdup measurements and droplet size measurements, was determined in a first series of experiments. Dispersed phase holdup measurements were then repeated with the solvent FAME and water. After detailed investigation of LL hydraulics, solid phase holdup measurements in the aqueous phase (SL) were performed. Finally, the dispersed phase holdup and solid phase holdup, as well as the on-set of appropriate liquid-liquid-solid (LLS) operation were investigated for different rate of rotation, hydraulic load and mass flow rate of the solid phase.

2. Chemicals and Experiments

2.1 Chemicals

2.1.1 Esterification

Acetic acid (AA) (Carl Roth GmbH, CAS: 64-19-7), methanol (Car Roth GmbH, CAS: 67-56-1) and ethanol (EtOH) (AustrAlco GmbH, CAS: 64-17-5) with a purity of >98% were used as reactants for esterification experiments. AA was diluted in deionized water. Biodiesel (FAME), provided by BDI – BioEnergy International GmbH, was used as solvent. Amberlyst15 (Aldrich Chemistry, CAS: 39389-20-3) was selected as heterogeneous catalyst. Amberlyst15 is a strong acidic macroreticular cation-exchange resin. The physical and chemical properties of the catalyst are shown in Tab. 3. For titrimetric analysis, 0.1 molar potassium hydroxide solution was used.

Table 3 - Chemical and physical properties of Amberlyst15

Properties	Amberlyst15
Type	macroporous
Acid site (eq/kg)	≤ 4.7
Moisture holding capacity	52 – 57 % (H^+ form)
Density	1100-1400 (kg m^{-3})
Harmonic mean size	0.6 - 0.85 mm

2.1.2 Hydraulics

For the first series of hydrodynamic investigation of multiphase flow, ShellSol-T (SST, Donau Chemie) was used as dispersed phase, deionized water as continuous phase and Amberlyst15 as solid phase. The hydraulic investigation was then repeated at same operation conditions with FAME. The properties of the test systems are listed in Tab. 4.

Table 4 - Physical properties of the solvents and the carrier

	Density [kg m^{-3}]	Kinematic Viscosity [m^2 s^{-1}]	Interfacial tension (water) [mN m^{-1}]
ShellSol-T (dispersed)	756.8	$1.85*10^{-6}$ (20°C)	34.0 (20°C)
		$6.71*10^{-6}$ (20°C)	
Biodiesel (dispersed)	844.3	$2.76*10^{-6}$ (65°C)	16.57 (65°C)
		$2.21*10^{-6}$ (80°C)	
Deionized water (continuous)	998.1	$1.102*10^{-6}$	-

2.2 Experimental set up and experimental procedure

2.2.1 Esterification

The esterification experiments mentioned in the introduction were performed in a batch reactor setup with thermostatic jacket. The temperature of the heating jacket was kept constant within ± 0.5 °C. The temperature of the reaction mixture was set to 65°C and 80 °C by using a Lauda RE206 thermostat and was measured with a digital thermometer (MGW Lauda R40/2; ±0.1 °C). A reflux condenser, cooled with water, was installed at the lid of the reactor to avoid loss of volatiles. Water with 120 g L^{-1} ($c_{AA,0}$ = 120 g L^{-1}) of AA, the solvent FAME and Amberlyst15 ($m_{Cat.}$ = 14 wt%) were heated to the desired reaction temperatures. An equimolar amount of MeOH was added to the aqueous phase after the set point reaction temperature in the tank reactor was reached. For sampling 2 x 0.3 ml of the aqueous phase was taken for titration analytics and 0.7 ml was taken for analytics with gas chromatography.

The overall transfer of acetic acid into the solvent was determined by mass balance. Esterification experiments were stopped after 6 hours. For comparison, the esterification experiments were repeated without extraction.

2.2.2 Hydraulics

For continuous multiphase operation, LLS flow was implemented in a TCDC with 50 mm column diameter and 700 mm active column height. The geometric data of the design of internals are listed in Tab. 5. The setup was operated in counter current mode. For a first series of hydraulic investigations, SST was used as dispersed phase. The solvent was fed at the bottom of the column. Deionized water with the solid catalyst was fed at the top. The continuous aqueous phase was used as carrier phase of the catalyst. At the bottom, the solid catalyst was separated from the aqueous phase via sedimentation and was collected in a downstream collector pin. From the pin, the solid catalyst was dosed continuously to the water tank where it was mixed with the water feed and pumped to the top of the column. A peristaltic pump (Ismatec Ecoline) was used for dosing the solid catalyst to the water phase as well as for pumping the suspension to the top of the column. The flow chart of the setup is depicted in Fig. 3. To gain data about the multiphase flow performance of the TCDC, the effect of total hydraulic load (B), rate of rotation (n) and mass fraction of the solid catalyst on holdup and residence time

distribution were investigated. Investigations were started with LL flow, followed by SL flow, and were then performed with continuous LLS flow. The mean droplet size was determined for different rate of rotation and hydraulic load. Holdup measurements were also performed with the solvent FAME.

Table 5 - Design specifications of the TCDC

	Abbreviation	Value	Unit
Column diameter	D_C	50	mm
Shaft diameter	d_{Sh}	25	mm
Column height	H	700	mm
Compartment height	H_c	25	mm
Rotor disc diameter	d_R	43	mm

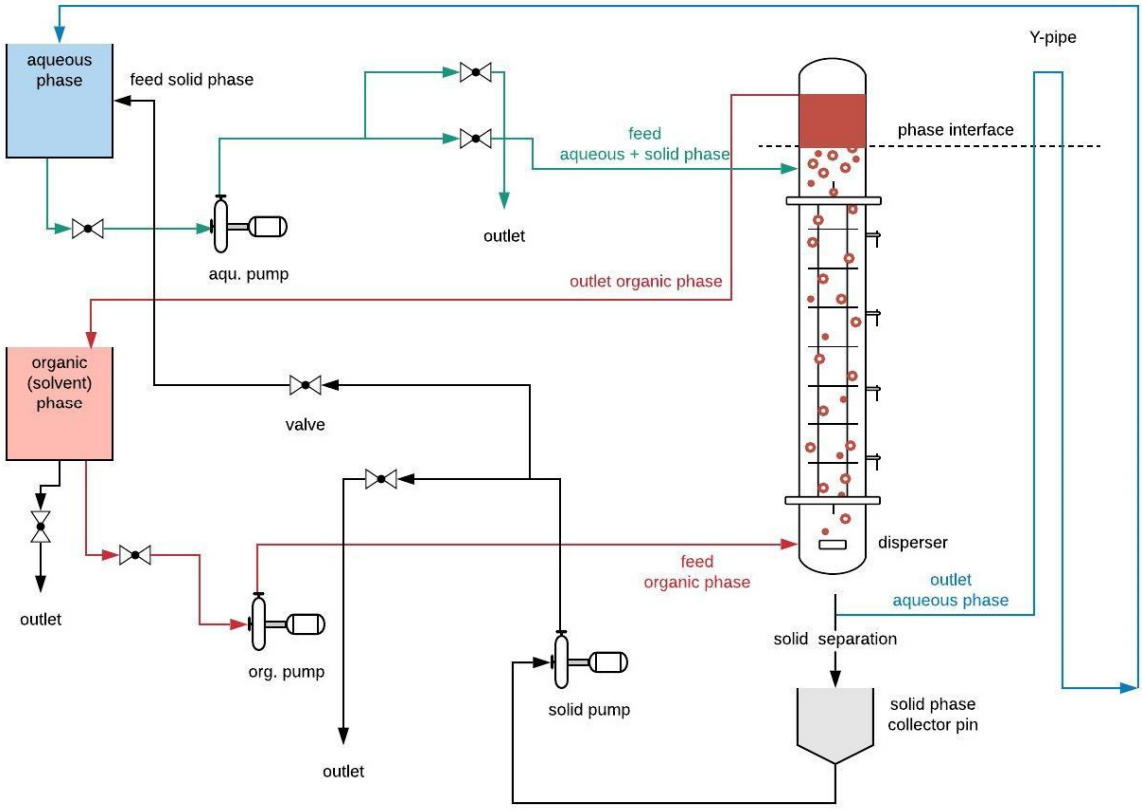

Figure 3 - Flow chart

2.2.2.1 Dispersed phase Holdup

According to equation (1) the mean dispersed phase holdup is deduced from the ratio of the volume of dispersed phase (V_d) and the total volume of the dispersed phase V_d and the continuous phase (V_c):

$$\varphi = \frac{V_d}{V_d + V_c} \tag{1}$$

The dispersed phase holdup was determined volumetrically by monitoring the level change of the phase interface at different rate of rotation.

2.2.2.2 Solid phase Holdup

The solid phase holdup was determined volumetrically by recording the level change of Amberlyst15 in the collector pin. For dense packed spheres, the volume of the catalyst amounts 74 % of the total volume of the solid phase. The solid phase holdup results were calculated according to equation (1).

2.2.2.3 Residence time distribution

The residence time distribution (RTD) of the aqueous carrier phase was determined via tracer experiments by spiking the aqueous feed at the top of the column with 1 ml saturated sodium chloride solution. The electric conductivity was recorded via a non-commercial probe with a sensor tip diameter of 0.6 mm. The RTD curves were interpreted with the dispersion model with open-open boundary conditions, according to Levenspiel [21]:

$$E_{\theta,oo} = \frac{1}{2}\sqrt{\frac{\bar{t}}{\pi\, t*\left(\frac{D_{ax}}{uL}\right)}}\,\exp\left[-\frac{\bar{t}\left(1-\frac{t}{\bar{t}}\right)^2}{4\, t*\left(\frac{D_{ax}}{uL}\right)}\right] \tag{2}$$

In equation (2), t represents the time, $\bar{t}$ the mean residence time and D_{ax}/uL the vessel dispersion number with the axial dispersion coefficient (D_{ax}).

2.2.2.4 Mean droplet size

The droplet size distribution was recorded with a FDR-AX700 4K HDR camcorder synchronized with a flashing stroboscopic light source. For better illumination and for

capturing the area covered by the shaft, a mirror was installed at an angle of 45° to the camera lens. Two high power light sources were installed at the area of the mirror to ensure the light intensity needed for short exposure time. Image analyzing was done via a Matlab routine to enhance the image quality and the precision of drop size measurement.

3. Results

The hydraulic performance of the TCDC for LLS operation was investigated for different hydraulic load of the liquid phases, rate of rotation, phase ratio and mass fraction of the solid catalyst. The hydraulic investigations started with the investigation of the LL flow pattern. Operation limits of the TCDC were determined in a first series of experiments. Dispersed phase holdup and droplet size distribution were determined with the same test system. Holdup measurements for LL flow were repeated with the test system FAME/water. Additionally, the axial dispersion coefficient of the continuous phase ($D_{ax,c}$) for single phase operation was measured for different hydraulic load and rate of rotation. The solid phase holdup was measured for SL flow and finally, holdup measurements were repeated for LLS flow. In Fig. 4 the flow pattern in a single compartment of the TCDC for LL, SL and LLS operation at 800 rpm and a total hydraulic load of B = 6 $m^3\ m^{-2}h^{-1}$ is shown.

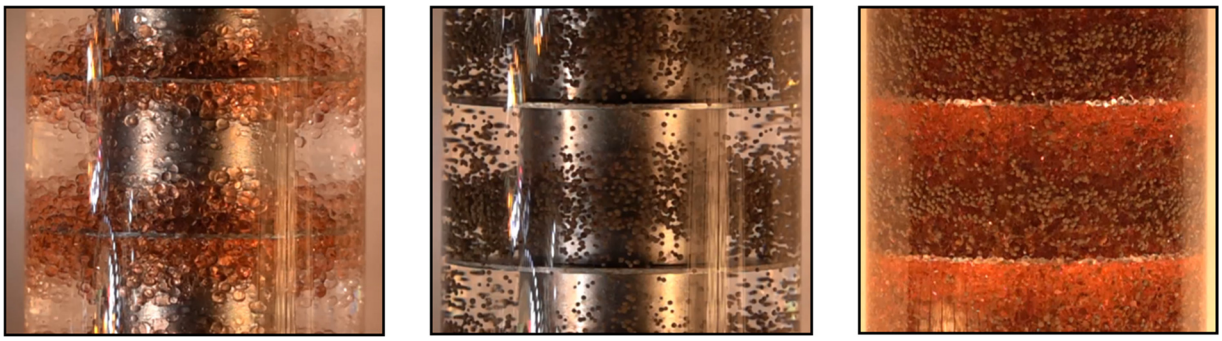

Figure 4 - Flow pattern in a single compartment of the TCDC for a) liquid-liquid; b) solid-liquid; c) liquid-liquid-solid flow at 800 rpm and a hydraulic load of B = 6 $m^3\ m^{-2}h^{-1}$.

3.1 Liquid-liquid operation

3.1.1 Operation limits

The operation limits of the TCDC for liquid-liquid (LL) flow at varying hydraulic load and w/o ratio without rotating the shaft are shown in Fig. 5. High w/o ratio will end up in flooding at the bottom of the column, while high hydraulic load starts with flooding at the top. The main reason for flooding at the bottom is a construction weakness caused by limited free cross-sectional area at the bottom bearing. Therefore, it is necessary to construct bearings with large free cross-sectional area for high hydraulic load. Flooding at the top of the column is observed when the phase interface raises constantly and the continuous phase finally reaches the outlet socket of the dispersed phase. For proper operation (w/o = 0.5 - 3) the maximum total hydraulic load should achieve B = 20 - 30 $m^3\,m^{-2}h^{-1}$. By increasing the rate of rotation, the operation limits shift towards lower hydraulic load, as indicated in Fig. 5 for n = 700 rpm and n = 800 rpm.

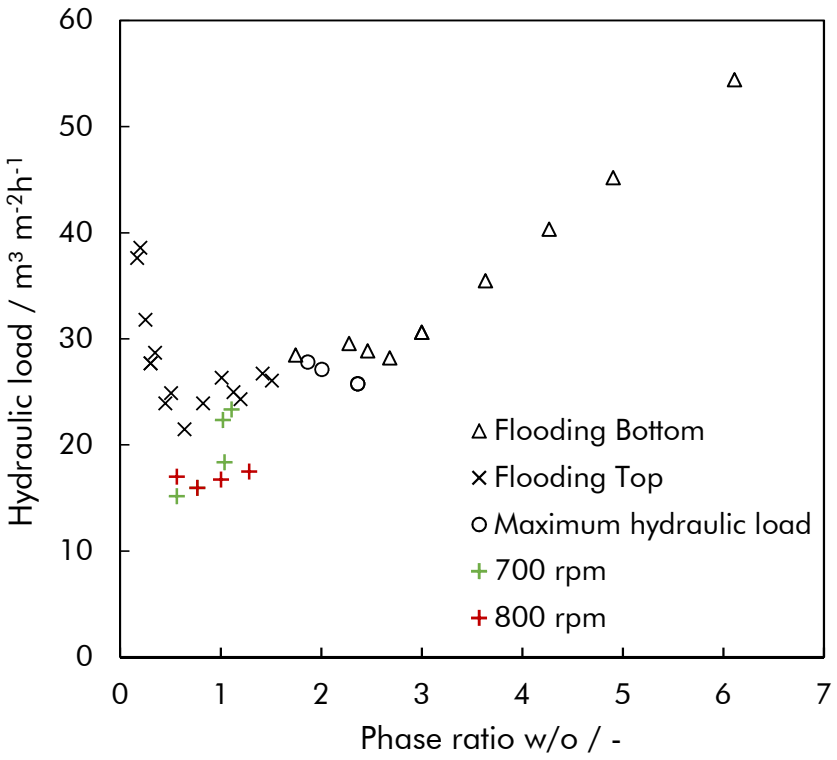

Figure 5 - Operation limits of the TCDC for different hydraulic load and phase ratio at 0 rpm (without rotating the shaft); for comparison the operation limits for n = 700 and n = 800 rpm are shown.

3.1.2 Dispersed phase holdup

Fig. 6a depicts the experimental data of the dispersed phase holdup for varying hydraulic load and rate of rotation at w/o = 1. The holdup increases steadily with increasing rate of rotation. Compared to operation of TCDC columns with larger diameter [20] the holdup curves do not show a distinct on-set. At low hydraulic load (B = 6 m^3 $m^{-2}h^{-1}$) and high rate of rotation, holdup values of even 35 % could be realized. With increasing hydraulic load, higher holdup values at same rate of rotation were measured and flooding was observed at same holdup values but lower rate of rotation. Fig. 6b shows the effect of varying w/o ratio on the holdup for the hydraulic load of B = 6 m^3 $m^{-2}h^{-1}$. Flow rate of the continuous phase and phase ratio w/o = 2.3 does not differ from higher flow rate at w/o = 1. With increasing phase ratio of the dispersed phase (w/o = 0.6), the holdup increases by ~ 50 % at same rate of rotation.

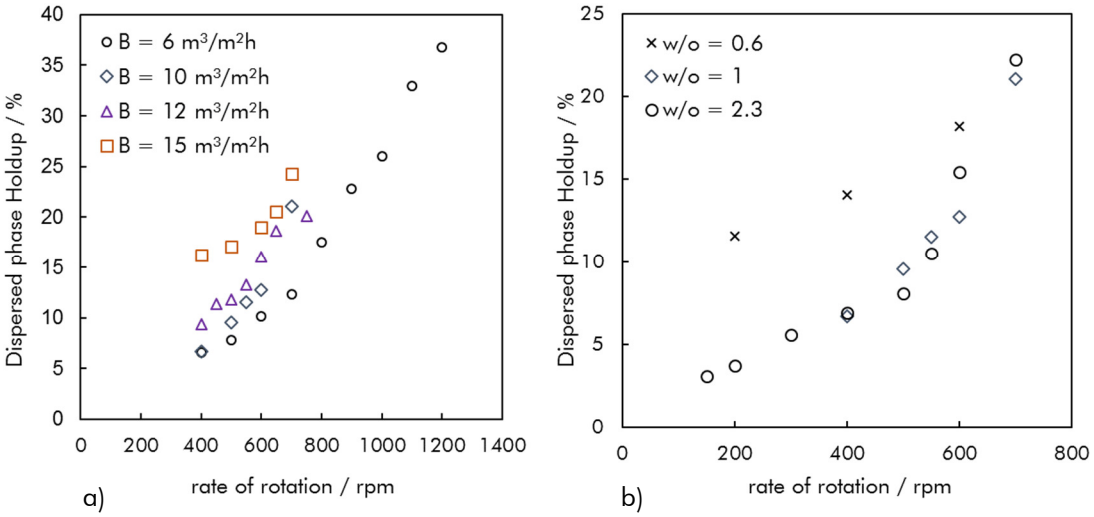

Figure 6 - a) Dispersed phase holdup for varying hydraulic load B = 6 - 15 m^3 $m^{-2}h^{-1}$ and rate of rotation at w/o = 1; b) Dispersed phase holdup at B = 10 m^3 $m^{-2}h^{-1}$for phase ratio w/o = 0.6, 1 and 2.3.

Fig. 7 shows the comparison of the dispersed phase holdup for the test system FAME/water and the test system SST/water. Due to the lower density difference of FAME/water ($\Delta\rho_{FAME/Water}$ = 153.8 kg m^{-3}) compared to SST/water ($\Delta\rho_{FAME/Water}$= 241.3), as well as lower interfacial tension, much higher holdup values were be obtained, but with tremendous limitation of the maximum total hydraulic load. Stable operation of the column for a wide range of rate of rotation was obtained for a hydraulic load of just B = 2 m^3 $m^{-2}h^{-1}$ at w/o = 2.1. Higher total hydraulic load (B > 6 m^3 $m^{-2}h^{-1}$) and phase

ratio of w/o < 1 led to very high holdup values (~ 40 %) but unstable operation of the column. At this operation point, spontaneous flooding of the column was observed.

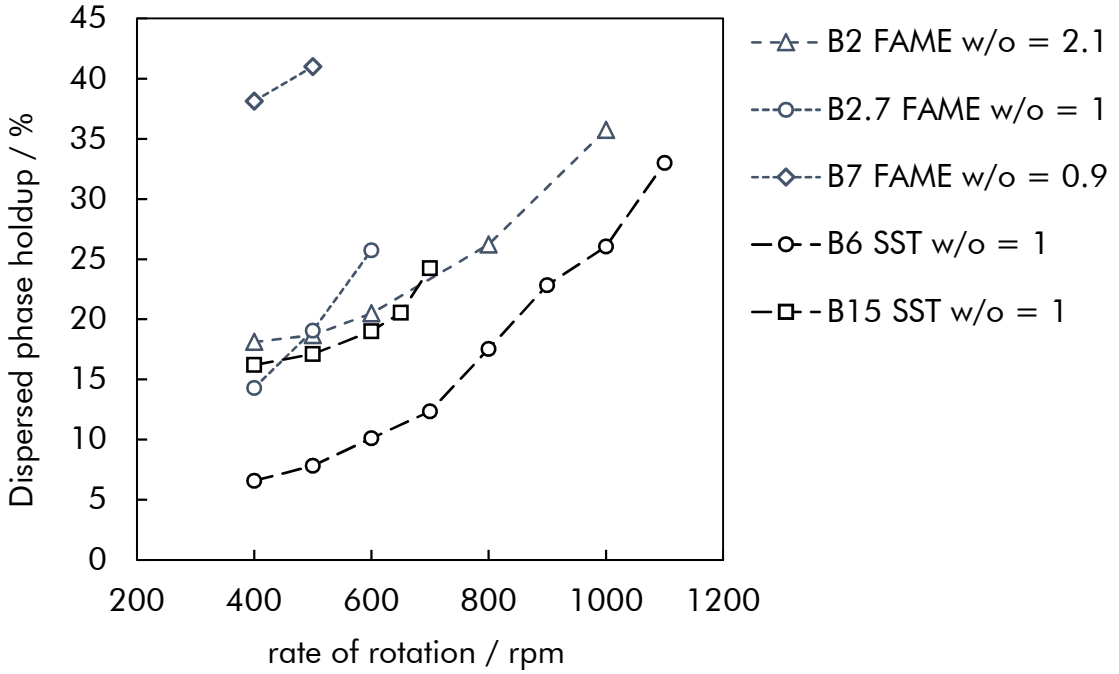

Figure 7 - Dispersed phase holdup of the test system FAME/water compared with the dispersed phase holdup of the test system SST/water.

3.1.3 Droplet size

Fig. 8a shows the mean droplet size for constant hydraulic load (B = 6 $m^3\ m^{-2}h^{-1}$) and varying rate of rotation. The red dots indicate the average value of the measurement data. As expected, the mean droplet size shifts towards smaller droplet diameter with increasing centrifugation number. From Matlab image analyses the mean droplet size of the large droplets was within a standard deviation of +/- 0.8 mm and the mean droplet size of the small droplets was within a standard deviation of +/- 0.2 mm throughout all experiments. The effect of hydraulic load on droplet size was not investigated since previous experiments in a TCDC column with 100 mm and 300 mm column diameter showed that the hydraulic load has a negligible effect on droplet size [19, 20]. The experimentally obtained Sauter mean diameter (d_{32}) data was compared with the correlation proposed in equation (3) [22] and it is shown in Fig. 8b.

$$\frac{d_{32}}{d_R} = A * G \left(\frac{\sigma}{d_R^3 \rho_c n^2}\right)^{c_1} \left(\frac{g\Delta\rho}{d_R \rho_c n^2}\right)^{c_2} = 2.28 * G \left(\frac{1}{We}\right)^{0.56} \left(\frac{1}{Fr}\frac{\Delta\rho}{\rho_c}\right)^{0.35} \quad (3)$$

In this correlation the constant G = 0.39 comprises the dimensionless geometric data of the column and the physical properties of the test system SST/Water. The green diamonds in Fig. 8b indicate the experimentally obtained d_{32} data compared with the values predicted with the correlation shown in equation (3). The proposed d_{32} values do not comply with the experimentally obtained values, indicating that the correlation is not applicable for columns of 50 mm diameter.

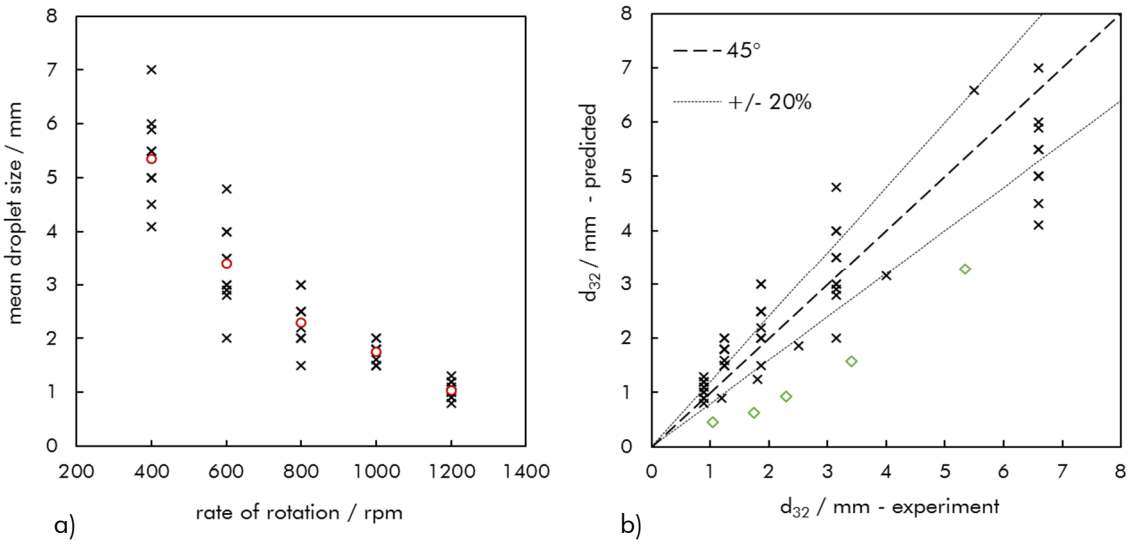

Figure 8 - a) Mean droplet size at B = 6 $m^3\ m^{-2}h^{-1}$ for varying rate of rotation (the dots indicate the average value); b) Comparison of measured and predicted d_{32} values calculated with equation (3).

3.1.4 Axial dispersion coefficient

The axial dispersion coefficient of the continuous phase ($D_{ax,c}$) was investigated for varying hydraulic load and rate of rotation. To provide comparability of energy input for different column scales, the dimensionless centrifugation number Z was calculated according to equation (4), based on the rotor disc diameter d_R, the angular velocity w and gravity g.

$$Z = \frac{w^2 * d_R}{2 * g} = \frac{(2 * \pi * n)^2 * d_R}{2 * g} \qquad (4)$$

The $D_{ax,c}$ results are shown in Fig. 10. Higher hydraulic load results in higher $D_{ax,c}$ values at same centrifugation number. For single phase operation, increasing hydraulic load causing higher $D_{ax,c}$ values could not be observed in TCDC columns with 100 mm and

300 mm column diameter [20]. This can be explained by the higher impact of wall effects on operation of columns with small diameter. With rising centrifugation number, axial dispersion increases too. For comparison, $D_{ax,c}$ at B = 15 $m^3m^{-2}h^{-1}$ in a TCDC with 100 mm column diameter is also shown in Fig. 10. $D_{ax,c}$ decreases with decreasing column diameter.

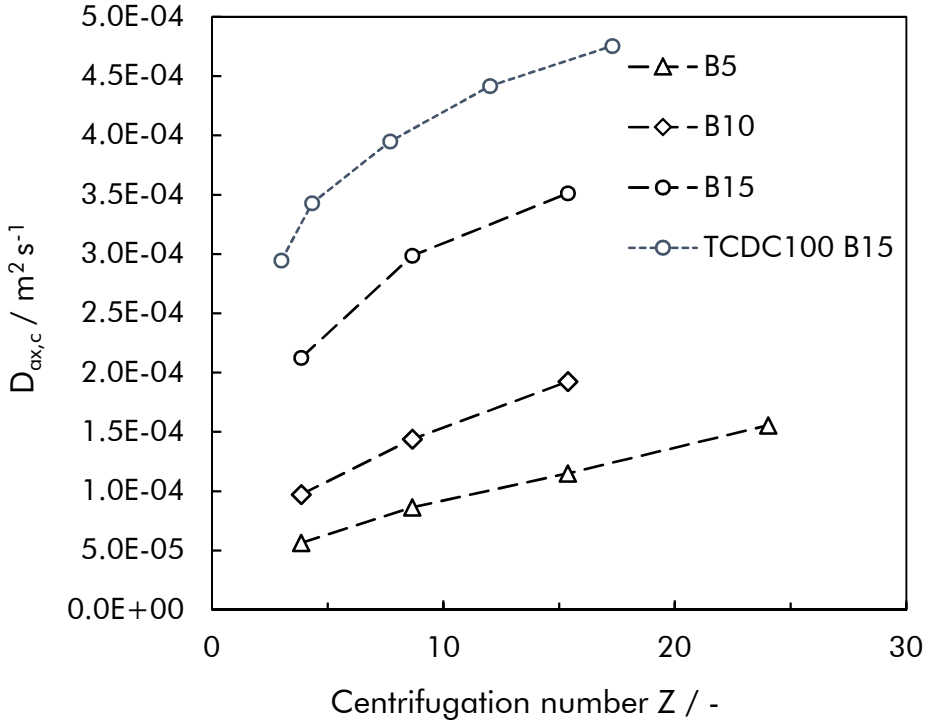

Figure 9 - Axial dispersion coefficient of the continuous phase for single phase flow at the hydraulic load of B = 5, 10 and 15 $m^3\ m^{-2}h^{-1}$ and varying rate of rotation.

3.2. Solid-liquid operation

3.2.1 Solid phase holdup

Fig. 10 shows the solid phase holdup of the catalyst for varying hydraulic load, mass fraction of the catalyst in the aqueous carrier phase and rate of rotation. With increasing rate of rotation, the solid phase holdup increases too. Higher mass fraction of the solid phase in the carrier phase and lower hydraulic load leads to increased holdup values in the active mixing height. Maximum holdup values of 8 % were achieved, resulting in a specific mass transfer area for the acceleration of the esterification reaction of a = 496 $m^2\ m^{-3}$ when assuming a mean particle diameter of 0.725 mm. The hydraulic

mean residence time of the catalyst in a single compartment for the solid phase holdup of φ_S = 7 % and B = 5 $m^3\ m^{-2}h^{-1}$ is τ_{Solid} = 25 seconds.

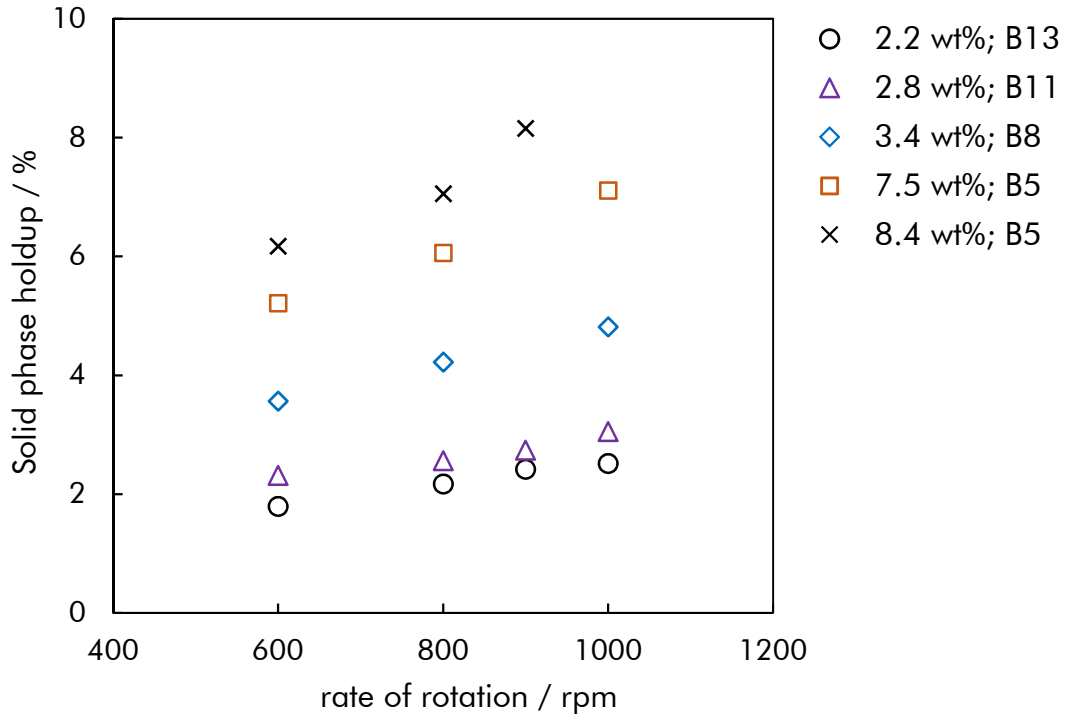

Figure 10 - Solid phase holdup at varying hydraulic load (B = 5, 8, 11 and 13 $m^3\ m^{-2}h^{-1}$), rate of rotation mass fraction of the solid phase

3.3 Liquid-liquid-solid operation

After evaluating the hydraulic parameter of LL and SL flow, LLS flow behavior was investigated. Fig. 11 depicts the flow pattern in a single compartment of the TCDC at 5 $m^3m^{-2}h^{-1}$ and 10 $m^3\ m^{-2}h^{-1}$ for varying rate of rotation. Beyond the critical rate of rotation of 150 rpm, the vorticity of the continuous phase overcomes sedimentation force of the solid phase and the solid catalyst is dragged by the toroidal vortexes. The solid phase is mainly accumulating in the lower area of the compartment (lower vortex) due to the flow direction of the continuous carrier phase from top to the bottom. The vortex of the continuous phase in the lower area of the compartment becomes visible due to the accumulated solid phase, indicating the on-set point for operation. Buoyancy of the dispersed phase dominates the flow pattern up to ~ 350 rpm. The dispersed phase accumulates below the rotor discs with low holdup values and large droplet size. Beyond 350 rpm the vorticity of the continuous phase also overcomes buoyancy of the

dispersed phase and drags the dispersed phase in the compartment for a reasonable residence time. The vortex in the upper area of the compartment becomes visible and indicates the on-set point for the dispersed phase. Beyond 800 rpm, a fully developed flow pattern is achieved, ensuring intensive phase contact of the three phases. Fully developed flow pattern shows high mixing performance in the single compartment with high holdup values and small droplet size and thus high specific mass transfer area. The solid phase remains dispersed in the continuous phase due to its hydrophilic properties, despite the high mixing performance and high holdup values in the compartments of the TCDC.

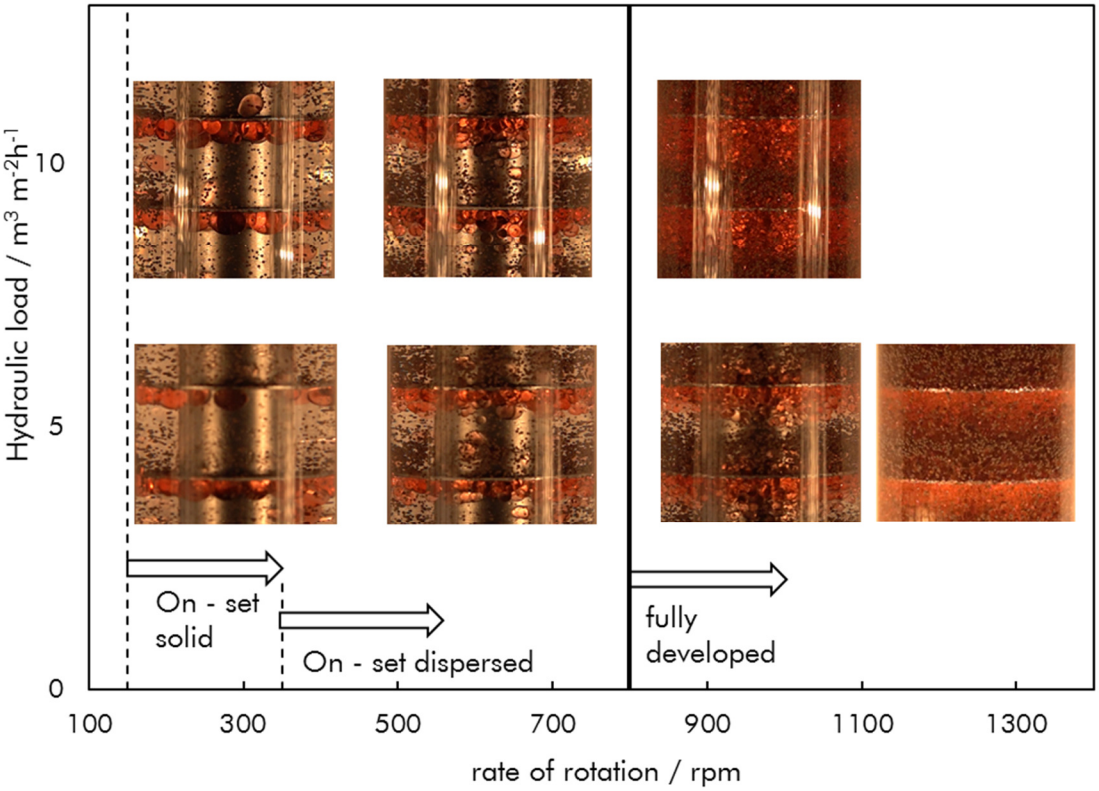

Figure 11 - Flow pattern of continuous LLS flow for 5 $m^3\ m^{-2}h^{-1}$ and 10 $m^3\ m^{-2}h^{-1}$

3.3.1 Holdup

In Fig. 12, a comparison of the dispersed phase holdup for LL and LLS flow is shown. At lower rate of rotation (~ 600 rpm) same holdup values for LL and LLS flow were measured. With increasing rate of rotation, holdup values up to 45 % were achieved for LLS flow without flooding of the column. Compared to LLS flow flooding of the column occurs at lower rate of rotation for LL flow. Since the flooding point is shifted towards

higher rotational speed, much higher holdup values for LLS flow can be realized. The solid phase holdup remains the same for SL and LLS flow, as shown in Fig. 13.

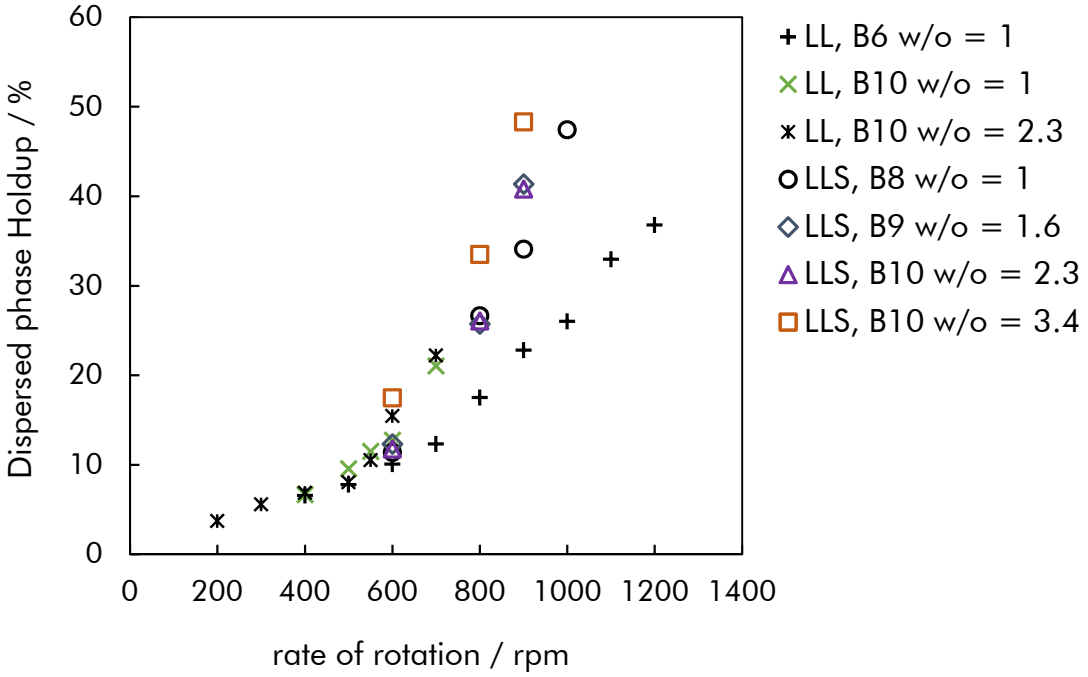

Figure 12 - Comparison of dispersed phase holdup for LL and LLS flow at varying hydraulic load (B = 6, 8, 9 and 10 $m^3\ m^{-2}h^{-1}$), phase ratio (w/o=1, 1.6, 2.3 and 3.4) and rate of rotation

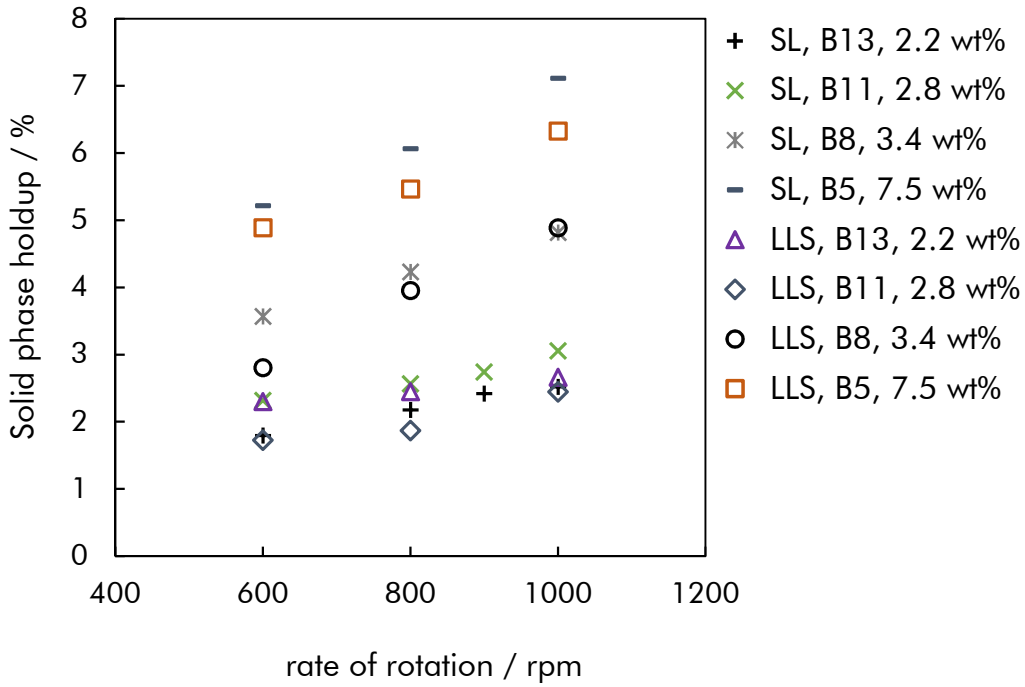

Figure 13 - Comparison of solid phase holdup for LS and LLS flow at varying hydraulic load (B = 5, 8, 11 and 13 $m^3\ m^{-2}h^{-1}$), solid mass fraction (2.2, 2.8, 3.4 and 7.5 wt%) and rate of rotation

4. Conclusion

This topic reports results of experience with implementation of continuous multiphase flow in the Taylor-Couette Disc Contactor (TCDC). Continuous multiphase flow can be used for combining chemical conversion with liquid-liquid extraction, such as isolating highly dilute carboxylic acids from aqueous effluents. Exemplarily the esterification of acetic acid (AA) with methanol, accelerated by heterogeneous catalysis with a cation exchange resin, with simultaneous transfer of the product methyl acetate into the solvent biodiesel, as successfully performed in batch experiments at 65 °C and 80 °C, may serve as a first example for demonstration of industrially relevant multiphase flow applications. In the batch experiments conversion of AA was increased from 15 % without product extraction up to 32 % with simultaneous product extraction at same reaction temperatures of 65 °C. Therefore, continuous multiphase flow in the TCDC was investigated. Hydrodynamic investigations of liquid-liquid (LL), solid-liquid (SL) and liquid-liquid-solid (LLS) flow behavior confirm applicability of this column design for intensifying heterogeneously catalysed reactions combined with liquid-liquid extraction. Dispersed phase holdup values up to 45 % and solid phase holdup values up to 8 % were measured, confirming great hydraulic performance of the column for LLS flow. The on-set behavior of appropriate LLS operation was investigated for varying rate of rotation, hydraulic load and mass fraction of the solid phase.

The outcome of this basic project confirms applicability of the Taylor-Couette Disc contactor for continuous multiphase flow applications. Stable operation of two phase flow in the TCDC despite the presence of a third (solid) phase, as well as the positive effect of simple apparatus design on operation under harsh operation conditions have to be highlighted.

Symbols and Abbreviations

Symbols

B	[$m^3\ m^{-2}h^{-1}$]	total hydraulic load
D_C	[m]	column diameter
$D_{ax,c}$	[$m^2\ s^{-1}$]	axial dispersion coefficient of continuous phase
d_m	[mm]	mean droplet size
d_{Sh}	[m]	shaft diameter
g	[$m\ s^{-2}$]	gravity (9.81)
H	[m]	active column height
n	[$1\ s^{-1}$]	rate of rotation
t	[s]	time
$\bar{t}$	[s]	mean residence time
V	[m^3]	volume
w	[$rad\ s^{-1}$]	angular velocity
Z	[-]	$=(w^2 d_{Sh})/(2g)$ = centrifugation number

Greek symbols

ρ	[$kg\ m^{-3}$]	density
ν	[$m^2\ s^{-1}$]	kinematic viscosity
ϕ	[-]	holdup

Subscripts

c	continuous phase
d	dispersed phase
s	solid phase

Abbreviations

AA	Acetic acid
EtAc	Ethyl acetate
EtOH	Ethanol
FAME	Fatty acid methyl ester (biodiesel)
LL	Liquid-liquid flow
LLS	Liquid-liquid-solid flow
MeAc	Methyl acetate
MeOH	Methanol
RTD	residence time distribution
SL	Solid-liquid flow
SST	ShellSol-T
TCDC	Taylor-Couette Disc Contactor

References

[1] M. Hundt, Ph.D. Thesis, Cottbus-Senftenberg, 2015.

[2] B.Saha, S.P.Chopade, and S.M.Mahajani, Catal. Today, 2000, 60, 147. .

[3] H. T. R. Teo and B. Saha, J. Catal., 2004, 228 (1), 174. DOI: 10.1016/j.jcat.2004.08.018.

[4] Y. Liu, E. Lotero, and J. G. Goodwin, J. Catal., 2006, 242 (2), 278. DOI: 10.1016/j.jcat.2006.05.026.

[5] T. F. Dossin, M. F. Reyniers, and G. B. Marin, Appl. Catal. B Environ., 2006, 62 (1–2), 35. DOI: 10.1016/j.apcatb.2005.04.005.

[6] D. B. Keyes, Ind. Eng. Chem., 1932, 24 (10), 1096. DOI: 10.1021/ie50274a003.

[7] T. Pöpken, L. Götze, and J. Gmehling, Ind. Eng. Chem. Res., 2000, 39 (7), 2601. DOI: 10.1021/ie000063q.

[8] Berthelot and Saint-Gilles, Recherches sur les affinités de la formation et de la décomposition des éthers. Paris: Mallet-Bachelier, 1890.

[9] E. C. L. De Silva, B. A. N. N. Bamunusingha, and M. Y. Gunasekera, Eng. J. Inst. Eng. Sri Lanka, 2014, 47 (1), 9. DOI: 10.4038/engineer.v47i1.6855.

[10] S. I. KIRBASLAR, Z. B. BAYKAL, and U. DRAMUR, Turk J Engin Env. Sci, 2001, 25 (837), 569. .

[11] N. S. Ahmed, Al-Khwarizmi Eng. J., 2010, 6 (2), 33. .

[12] E. VAN DE STEENE, J. DE CLERCQ, and J. W. THYBAUT, J. Ion Exch., 2014, 25 (4), 234. DOI: 10.5182/jaie.25.234.

[13] K. D. Patil and B. D. Kulkarni, Int. J. Eng. Res., 2015, 3 (8), 488. DOI: 10.17950/ijer/v3s8/803.

[14] A. N. Al-Saadi and G. V. Jeffreys, AIChE J., 1981, 27 (5), 768. .

[15] A. Chakrabarti and M. M. Sharma, React. Polym., 1993, 20 (1–2), 1. .

[16] E. Aksamija, Ph.D. Thesis, Graz University of Technology, 2015.

[17] E. Aksamija, C. Weinländer, R. Sarzio, and M. Siebenhofer, Sep. Sci. Technol., 2015, 50 (18), 2844. DOI: 10.1080/01496395.2015.1085406.

[18] A. Grafschafter, E. Aksamija, and M. Siebenhofer, Chem. Eng. Technol., 2016, 39 (11), 2087. DOI: 10.1002/ceat.201600191.

[19] A. Grafschafter and M. Siebenhofer, Chemie Ing. Tech., 2017, 4, DOI: 10.1002/cite.201600142.

[20] A. Grafschafter, G. Rudelstorfer, and M. Siebenhofer, Chemie-Ingenieur-Technik, 2018, DOI: 10.1002/cite.201800031.

[21] O. Levenspiel, Chemical Reaction Engineering. Wiley, 1999.

[22] A. Grafschafter and M. Siebenhofer, Chemie-Ingenieur-Technik, 2017, 89 (4), DOI: 10.1002/cite.201600142.

Chapter 8

Summary & Future Prospects

8. Summary & Future Prospects

Liquid-liquid extraction has grown over the last decades to a powerful separation technique with applications covering a wide range of the chemical process industry. A variety of different extraction devices have been developed until now, but due to the change of fossil to biogenic raw material, requirements for reliable operation have changed. At the very beginning of this thesis, the question raised whether it is necessary to develop new extraction equipment, and if so, what are the driving forces for the improvement of design and performance? Since the answer is supposed to be yes, results of the detailed investigation of a novel two-phase extractor design, called the Taylor-Couette Disc Contactor (TCDC) are summarized in this thesis.

Since the Taylor-Couette Disc Contactor results from a modified Taylor-Couette reactor (TCR) design, the effect of decreasing shaft diameter on the hydraulics of a TCR was examined with the aim to improve the hydraulic capacity. For hydrodynamic characterization, the dispersed phase holdup, the residence time distribution of the continuous phase as well as the mean droplet size for varying hydraulic load and centrifugation number of the shaft were determined. With decreasing rotor shaft diameter (d_{Sh}=0.5*D), the hydraulic capacity could be increased up to 40 $m^3m^{-2}h^{-1}$ with holdup values of approximately 8 %. The rather low dispersed phase holdup and high axial dispersion lead to further optimization by installing rotor discs along the shaft, resulting in the TCDC design.

The effect of different rotor disc diameter on the hydrodynamics was investigated subsequently. Compared to the data obtained without rotor discs and shaft diameter of d_{Sh}=0.5*D, the axial dispersion of the continuous phase could be decreased by ~50 % for the hydraulic load of 40 $m^3m^{-2}h^{-1}$ when the rotor disc diameter is increased to the suggested [1] value of d_R = 0.86*D. With this design specification, the dispersed phase holdup could be increased up to 18 % for operation with stable flow pattern. Further investigations of the hydraulic performance of TCDC were thus carried out with the rotor disc diameter of d_R = 0.86*D.

Another part of this PhD-thesis concerned the appropriate design of the TCDC i.a. by development of empirical correlations for the prediction of hydrodynamic parameters.

Mass transfer experiments and residence time distribution confirm applicability of the CSTR cascade model for column design. Mass transfer was investigated with the system n-butanol/kerosene/water. Through interpretation of mass transfer experiments, an overall mass transfer coefficient for n-butanol of $k''_{CSTR} = (1.4*10^{-4} \pm 0.1*10^{-4})$ $m*s^{-1}$ was determined. Results of the dispersed phase holdup and the Sauter mean diameter predicted by several empirical correlations that were originally developed for the Rotating Disc Contactor were compared with experimental data. By modification of the model parameters, the predicted data fit well with experimental data.

Subsequently, empirical correlations for the prediction of the drop size distribution, the Sauter mean diameter and dispersed phase holdup in the TCDC were developed by dimensional analysis. The hydrodynamic investigation of an up-scaled TCDC confirmed applicability of the correlations.

The implementation and investigation of continuous multiphase flow demonstrates the flexibility of the TCDC. In the column with 50 mm column diameter, dispersed phase holdup values up to 45 % and solid phase holdup values of 8 % could be realized for continuous liquid-liquid-solid flow. This hydraulic setup provides access to heterogeneously catalyzed liquid-phase reaction with transfer of products into the solvent phase, as suggested for successful isolation of dilute constituents from biorefinery broths.

The outcome of this thesis provides a simple tool for the basic design of the TCDC. Performance and operation range of the TCDC design were investigated and design rules are developed. The next steps will include investigations of the hydraulics for different test systems besides the applied system kerosene/water and biodiesel/water. Mass transfer experiments in the up-scaled TCDC with 300 mm column diameter will be necessary to confirm the separation efficiency determined for 50 mm and 100 mm column diameter. Finally, extension of apparatus design to gas-liquid-liquid contact has to be seriously considered.

Appendix

APPENDIX

PUBLICATIONS

Articles:

Grafschafter, A; Aksamija, E; Siebenhofer, M; (2016), 'The Taylor-Couette Disc Contactor' *Chemical engineering & technology*, DOI: 10.1002/ceat.201600191

Grafschafter, A; Siebenhofer, M; (2017), 'Design Rules for the Taylor-Couette Disc Contactor' *Chemie-Ingenieur-Technik*, DOI: 10.1002/cite.201600142

Grafschafter, A; Rudelstorfer, G; Siebenhofer, M; (2018), 'Hydraulics and Operation Performance of TCDC-Extractors' *Chemie-Ingenieur-Technik*, DOI: 10.1002/cite.201800031

Grafschafter, A; Siebenhofer, M; (2018), 'Effect of rotor disc diameter on holdup, axial dispersion and droplet size in a Taylor-Couette Disc Contactor' *Chemie-Ingenieur-Technik*, submitted

Grafschafter, A; Siebenhofer, M; (2018), 'Two-phase Taylor-Couette contactors: Holdup, axial dispersion and droplet size' *Separation Since and Technology*, DOI: 10.1080/01496395.2019.1595650

Painer, D; Lux, S; Grafschafter, A; Toth, A; Siebenhofer, M; (2017), 'Isolation of carboxylic acids from biobased feedstock' *Chemie-Ingenieur-Technik*, DOI: 10.1002/cite.201600090

Grafschafter, A; Siebenhofer, M; (2016), 'Taylor-Couette Disc Contactors' *CEET-Konkret TU Graz*.

Grafschafter, A; Siebenhofer, M; (2017), 'Design of Taylor-Couette Disc Contactors for application in biosepratıons' *CEET-Konkret TU Graz*.

Grafschafter, A; Siebenhofer, M; (2018), 'Residence time distribution and drop size distribution in Taylor-Couette Disc Contactors' *CEET-Konkret TU Graz*.

Siebenhofer, M; Grafschafter, A; (2019), 'The role of single droplet mass transfer experiments in solvent design for acetic acid extraction with triisooctylamine based solvents' *Chemie-Ingenieur-Technik*, submitted

Presentations:

Siebenhofer, M; Grafschafter, A; Toth, A; Painer, D; Lux, S; Kienberger, M; Aksamija, E; (2016) 'TCDC-Reaktoren' Jahrestreffen Reaktionstechnik 2016, Würzburg, Germany.

Grafschafter, A; Siebenhofer, M; (2016) 'Hydrodynamic Modeling of Taylor-Couette Disc Contactors' 19th Symposium on Separations Science and Technology for Energy Applications, Gatlinburg, USA.

Grafschafter, A; Siebenhofer, M; (2016) 'Hydrodynamic Modeling of Taylor-Couette Disc Contactors' 19th Symposium on Separations Science and Technology for Energy Applications, Gatlinburg, USA.

Grafschafter, A; Siebenhofer, M; (2016), 'Design of Taylor-Couette Disc Contactors' AIChE Annual Meeting 2016, San Francisco, USA.

Grafschafter, A; Siebenhofer, M; (2016) 'Modeling of Taylor-Couette Disc Contactors' AIChE Annual Meeting 2016, San Francisco, USA.

Grafschafter, A; Siebenhofer, M; (2017) 'Design of Taylor-Couette Disc contactors for application in bioseparations' The 7th International TIChE conference, Bangkok, Thailand.

Grafschafter, A; Siebenhofer, M; (2017) 'Scale-Up rules of Taylor-Couette Disc Contactors' AIChE Annual Meeting 2017, Minneapolis, USA.

Grafschafter, A; Painer, D; Siebenhofer M; (2017) 'Apparatus design for liquid-liquid extraction combined with heterogeneously catalyzed esterification' AIChE Annual Meeting 2017, Minneapolis, USA.

Grafschafter, A; Siebenhofer, M; (2017) 'Design and Scale Up of the Taylor-Couette Disc Contactor' 21st International Solvent Extraction Conference, Miyazaki, Japan.

Grafschafter, A; Siebenhofer, M; (2018) 'The Taylor-Couette Disc Contactor: heterogeneously catalyzed reaction with liquid-liquid extraction' ACHEMA 2018, Frankfurt, Germany.

Grafschafter, A; Siebenhofer, M; (2018) 'Heterogeneously catalyzed conversion combined with solvent extraction: An inventive approach for isolating dilute constituents' ProcessNet-Jahrestagung und 33. DECHEMA-Jahrestagung der Biotechnologen 2018, Aachen, Germany.

Grafschafter, A; Siebenhofer, M; (2018) 'Hydraulics of Taylor-Couette Disc Contactors' AIChE Annual Meeting 2018, Pittsburg, USA.

Siebenhofer, M; Grafschafter, A; (2018) 'Taylor-Couette' AIChE Annual Meeting 2018, Pittsburg, USA.

Grafschafter, A; Siebenhofer, M; (2018) 'The Taylor-Couette Disc Contactor: heterogeneously catalyzed reaction with liquid-liquid extraction' 8th International Thai Institute of Chemical Engineering Conference and Applied Chemistry Conference, Pattaya, Thailand.

Siebenhofer, M; Grafschafter, A; (2018) 'Fascinating Two-Phase Taylor-Couette Flow' 8th International Thai Institute of Chemical Engineering Conference and Applied Chemistry Conference, Pattaya, Thailand.

Grafschafter, A; Siebenhofer, M; (2019) 'Dreiphasenströmung im Taylor-Couette Disc Contactor (TCDC)' Tief-Temperatur-Thermodynamik-Kolloquium, Canazei, Italy.

Siebenhofer, M; Grafschafter, A; (2019) 'Taylor-Couette Zweiphasenströmung' Tief-Temperatur-Thermodynamik-Kolloquium, Canazei, Italy.

Grafschafter, A; Siebenhofer, M; (2019) 'Implementation of continuous multiphase flow for heterogeneously catalyzed reactions with liquid-liquid extraction in the Taylor-Couette Disc Contactor' 46th International Conference of the Slovak Society of Chemical Engineering, Tatranské Matliare, Slovakia.

Siebenhofer, M; Grafschafter, A; (2019) 'Taylor-Couette Two Phase Contactors' 46th International Conference of the Slovak Society of Chemical Engineering, Tatranské Matliare, Slovakia.

Grafschafter, A; Siebenhofer, M; (2019) 'Continuous multiphase flow: heterogeneously catalyzed reactions combined with liquid-liquid extraction' Jahrestreffen Reaktionstechnik 2019, Würzburg, Germany.

Poster:

Grafschafter, A; Aksamija, E; Siebenhofer, M; (2016) 'TCDC, design and validation' Minisymposium Verfahrenstechnik, Graz, Austria.

Grafschafter, A; Siebenhofer, M; (2017) 'TCDC reactors for isolation of biobased products' COST Meeting FP1306, Torremolinos, Spain.

Grafschafter, A; Siebenhofer, M; (2017) 'Taylor-Couette Disc Contactor for application in bioseparations' Jahrestreffen Reaktionstechnik 2017, Würzburg, Germany.

Grafschafter, A; Siebenhofer, M; (2017) 'Taylor-Couette Disc Contactor for application in bioseparations' 10th World Congress of Chemical Engineering, Barcelona, Spain.

Grafschafter, A; Painer, D; Siebenhofer, M; (2018) 'Multiphase flow for heterogeneously catalyzed reaction with liquid-liquid extraction in the Taylor-Couette Disc Contactor', Jahrestreffen der ProcessNet-Fachgruppen Fluidverfahrenstechnik, Membrantechnik und Mischvorgänge, Munich, Germany.

Grafschafter, A; Siebenhofer, M; (2018) 'Taylor-Couette Disc Contactor for heterogeneously catalyzed reaction with liquid-liquid extraction' Jahrestreffen der ProcessNet Fachgruppen Extraktion und Rohstoffe, Frankfurt, Germany.

Grafschafter, A; Painer, D; Siebenhofer, M; (2018) 'An innovative approach to isolate constituents from dilute aqueous effluents' COST Action 2018, Thessaloniki, Greece.

Grafschafter, A; Painer, D; Siebenhofer, M; (2018) 'An innovative approach to isolate constituents from dilute aqueous effluents' Minisymposium Verfahrenstechnik 2018, Linz, Graz.

Grafschafter, A; Painer, D; Siebenhofer, M; (2018) 'Taylor-Couette Disc Contactors for liquid-liquid extraction combined with heterogeneously catalysed reaction' Jahrestreffen Reaktionstechnik 2018, Würzburg, Germany.

Grafschafter, A; Siebenhofer, M; (2018) 'An inventive approach for multiphase reactors' 20th Symposium on Separation Science and Technology for Energy Applications, Gatlinburg, USA.

Grafschafter, A; Siebenhofer, M; (2019) 'Challenging continuous multiphase operation: Hete. catalyzed reactions with solvent extraction' Minisymposium Verfahrenstechnik, Leoben, Austria.

PRICES

Best Presentation Award (2017) at the 7th International TIChE conference, Bangkok, Thailand.

Best Poster Award (2018) at 20th Symposium on Separation Science and Technology for Energy Applications, Gatlinburg, USA.

Best Presentation Award (2019) at the Jahrestreffen Reaktionstechnik 2019 gemeinsam mit der Fachgruppe Mehrphasenströmungen, Würzburg, Deutschland.

SUPERVISED and CO-SUPERVISED THESES

Master Theses:

'Construction and scale up of a Taylor-Couette Disc Contactor: including installation, placing in operation, holdup measurements and determination of drop size distribution'
Georg Rudelstorfer

'Hydraulic investigation and process validation of the Taylor-Couette Disc Contactor'
Jonathan Shaw

'Heterogeneously Esterification of Acetic Acid in the TCDC'
Tobias Maier (in progress)

Bachelor Theses:

'Holdup und Stoffaustausch in einem Taylor-Couette Disc Contactor'
Bettina Rauchdobler

'Mehrphasenströumg im Taylor-Couette Disc Contactor'
Sebastian Dohr (in progress)

'Verweilzeitverteilungsmessungen in einem Taylor-Couette Disc Contactor im Scale-Up'
Sebastian Pickl (in progress)

'Hydrodynamischer Einfluss des Wellendurchmessers in Taylor-Couette Reaktoren'
Georg Wimmer (in progress)

'Einfluss der Rotorscheibendurchmesser in einem Taylor-Couette Disc Contactor auf die Hydrodynamik'
Maximilian Hübner (in progress)

Cover Picture Chem. Ing. Tech.
6/2018

Juni 2018
90. Jahrgang

CITAH 90 (6)
745-908 (2018)
ISSN 0009-286 X

www.CIT-journal.com

Chemie Ingenieur Technik

CIT 90 Jahre

Verfahrenstechnik · Technische Chemie · Apparatewesen · Biotechnologie

6 | 2018

Fokusheft:
Abgas-
nachbehandlung

Gastherausgeber:
Olaf Deutschmann
Ulrich Nieken

Fokusheft:
ACHEMA 2018

Herausgeber:
DECHEMA
GDCh
VDI-GVC

WILEY-VCH